

## ABSTRACT

Title of Thesis: THE EFFECT OF SUMMER STORM  
EVENTS AS A DISTURBANCE ON THE  
MOVEMENT BEHAVIORS OF BLACK SEA  
BASS IN THE SOUTHERN MID-ATLANTIC  
BIGHT

Caroline Jane Wiernicki, Master of Science,  
2019

Thesis Directed By: Professor David H. Secor  
Marine Estuarine Environmental Sciences

Storm events are a key disturbance in the Middle Atlantic Bight (MAB), driving thermal, hydrodynamic, and acoustic perturbations on demersal fish communities. Black sea bass are a model MAB species as their sedentary behavior exposes them to storm disturbances. I coupled biotelemetry with an oceanographic model, monitoring black sea bass movement behaviors during the summer-fall of 2016-2018. Storm-driven changes in bottom temperature (associated with rapid destratification) had the greatest effects on fish movement and evacuation rates, while the cumulative effects of consecutive storms had little to no observed effect. Storms also generate substantial noise, but the hearing frequencies of black sea bass are currently unknown. I conducted a quantitative literature analysis on fish hearing based on swim bladder elaboration, successfully classifying detected sound frequency

ranges among fishes, including black sea bass. Climate change will likely alter the intensity of MAB storms, prioritizing research on their impacts to fish communities.

THE EFFECT OF SUMMER STORM EVENTS AS A DISTURBANCE ON THE  
MOVEMENT BEHAVIORS OF BLACK SEA BASS IN THE SOUTHERN MID-  
ATLANTIC BIGHT

by

Caroline Jane Wiernicki

Thesis submitted to the Faculty of the Graduate School of the  
University of Maryland, College Park, in partial fulfillment  
of the requirements for the degree of  
Master of Science  
2019

Advisory Committee:  
Professor David H. Secor, Chair  
Associate Research Professor Helen Bailey  
Professor Ming Li

© Copyright by  
Caroline Jane Wiernicki  
2019



## Acknowledgements

I would like to thank my advisor, Dr. David Secor for his guidance, support, and sense of humor over the past three years. Ever since he took me on as a faculty research assistant, then as a graduate student, Dave has never failed to challenge me to become a better scientist. He has also never failed to encourage and advocate for me along the way. It was a pleasure and a privilege to work on this project under his direction. He was, and remains, a brilliant mentor.

I must also thank the Secor lab—Michael O’Brien, Ella Rothermel, Alex Carroll, Kohma Arai, and Benjamin Frey—for their assistance through all of the speed bumps along the way with this project. I would like to particularly thank Mike O’Brien and Ellie Rothermel. When I arrived at CBL Mike taught me everything on the ground, particularly the importance of thinking on your feet and the importance of thinking creatively. He never turned away any of the many, many questions I had from across the lab, and he is an exceptional scientist that I am grateful to consider a colleague and friend. I would also like to give special thanks to Ellie, for being my number one go-to in the trenches as we navigated our theses together. I could always count on Ellie for support, whether it was walking through a statistics assignment, critiquing a presentation the week before the conference, or lending an ear to one of many good rants on the ups and downs of graduate school. I’m thankful to have gone through this process with her. Special thanks are also due to Alexandra Carroll and Amber Fandel, for taking the time out of their own very busy schedules to answer my never-ending questions on bioacoustics and sound physics. They were my crash

course in an exceptionally fascinating—and complex—field, and this project would not have the depth it does without their patience.

Many thanks are also due to the member of my committee, Drs. Helen Bailey and Ming Li, for encouraging me to step out of my comfort zone and into the worlds of bioacoustics and physical oceanography. Their experience and their enthusiasm to share said experience has been infectious, and it has shaped and expanded the questions in fisheries science I sought with this project and continue to think about today. I must also thank the various people at CBL and beyond who made this project possible. Not only did Dr. Fan Zhang compile and run the FVCOM used in this project, but he also went above and beyond in familiarizing me with both the model and the MATLAB code used to interpret it. His patience and his positivity were limitless. I am grateful for his time and efforts, which ultimately afforded this project another valuable dimension. Drs. Dong Liang and Vyacheslav Lyubchich also provided invaluable support and technical skill in developing the statistical analyses used in this study. Their knowledge, creativity, and patience in both developing the analyses and teaching me how to use them spanned many hours of meetings, and I'm immensely grateful to them for it. Skyler Golt and Ben Frey slogged through over 100 frozen black sea bass samples with me for this study's diet analysis, and I am grateful to them for their help and enthusiasm at a time when the project quite literally took a sticky (and smelly) turn. Nicole Barbour and Reed Brodnik assisted with the deployment of acoustic receivers as well as the sampling of black sea bass in the field; a special thanks is due to Reed Brodnik for his willingness to help (as well as his humor) during the many times I invaded the Miller lab to borrow equipment.

Lastly, Dr. Art Popper provided invaluable knowledge and guidance on navigating the complex topic of fish hearing, and graciously reviewed the third chapter of this thesis. His constructive criticism and unwavering encouragement were invaluable.

I would also like to thank the family members and friends whose unwavering support ultimately saw me through this project. To my parents, Peter and Kathy Wiernicki, who have always encouraged me to pursue my passion and career goals in science. To Spencer Sallee, who always had a word of motivation and an ear for yet another rant on the day's obstacle. To Christina Goethel, Isabel Sanchez-Viruet, Erin Reilly, and Casey Hodgkins, for the 7am runs, the 2pm walks, and the kitchen counter conversations. To Billy Bartlett, who never hesitated to support me as I struggled to navigate the balance between my project and personal life, and never hesitated to listen and talk through whatever theoretical question I was ruminating on, regardless of the place or time. Lastly, I would like to thank my sister, Caitlin Wiernicki, for quite literally being my rock during these past three years and beyond.

# Table of Contents

Acknowledgements .....	ii
Table of Contents .....	v
List of Tables .....	viii
List of Figures .....	x
Chapter 1. Introduction .....	1
Storm disturbance .....	1
Study system .....	2
Goals and objectives .....	4
Thesis contents .....	5
Implications and future work .....	7
References .....	8
Chapter 2. The recurring role of storm disturbance on black sea bass movement behaviors in the Mid-Atlantic Bight. ....	13
Introduction .....	13
Materials and methods .....	18
Study site .....	18
Acoustic telemetry data collection .....	19
Oceanographic model outputs .....	21
Storm identification .....	22
Data analysis: Movement behavior .....	23
Results .....	26
Storm events and destratification .....	26
Storm characterization: Modeled variables .....	28
Movement analysis: Observed activity and evacuation behavior .....	30
Movement analysis: Coupled telemetry-FVCOM mixed effects model .....	31
Discussion .....	33
References .....	44
Tables .....	53

Figures.....	60
Chapter 3. The effect of swim bladder presence and morphology on sound sensitivity for marine and freshwater fishes.....	75
Introduction.....	75
Materials and methods .....	79
Literature Review.....	79
Data analysis.....	81
Results.....	83
Discussion.....	86
References.....	91
Tables.....	100
Figures.....	118
Appendix A. Supplemental Figures to Chapter 2: FVCOM performance, spatiotemporal estimates of current velocity and turbulent kinetic energy, and GAMLSS movement model diagnostics. ....	130
Methods.....	130
FVCOM model performance .....	130
FVCOM current velocity and TKE output .....	130
Movement model sex-length interaction .....	130
Movement model diagnostics .....	131
Results.....	131
FVCOM model performance .....	131
FVCOM current velocity and TKE output .....	131
Movement model sex-length interaction .....	134
Movement model diagnostics .....	134
Figures.....	136
Appendix B. Temporal and spectral characterization of sound data obtained from a single Mid-Atlantic Bight storm event, 2018. ....	147
Methods.....	147
Results.....	148
Tables.....	151
Figures.....	153

Appendix C. Body condition and feeding ecology of black sea bass sampled from the Middle-Atlantic Bight 2018.....	157
Methods.....	157
Results.....	158
References.....	161
Tables.....	162
Figures.....	165
Bibliography .....	172

## List of Tables

**Table 2.1.** Receiver site, mooring position, deployment location, and deployment duration information for 2016-2018 study periods. Note that the Northern site SW receiver was not recovered in 2017.

**Table 2.2.** Receiver site, mooring position, and depth for 2016-2018 study periods. Note that the Northern site SW receiver was not recovered in 2017.

**Table 2.3.** Year, location, and size for black sea bass tagged and released during the summers of 2016-2018.

**Table 2.4.** Description of variables utilized in black sea bass movement GAMLSS model.

**Table 2.5.** Year and names of identified Mid-Atlantic Bight storm events detected between June-October of 2016-2018, presented along dates and times of storm arrival, departure, and maximum windspeed, as well as calculations of storm duration (hr), maximum wind speed ( $\text{m s}^{-1}$ ), mean wind speed ( $\text{m s}^{-1} \pm \text{SD}$ ), and minimum windspeed ( $\text{m s}^{-1}$ ). A storm was considered present in the area when wind speeds consistently increased over  $5 \text{ m s}^{-1}$ . Windspeeds refer to average velocity vectors.

**Table 2.6.** Slope and adjusted R-square values for black sea bass transmitter loss time series data, fit to exponential curves for all sites and years. Absolute loss rate, calculated as the average percent decrease in transmitter presence per day, is also presented for each site for 2016-2018.

**Table 2.7.** Mu estimates (the direction and magnitude of the fitted response), standard error, t-values, and p-values for numerical and categorical predictors used in the GAMLSS model for black sea bass movements. Note that all numerical predictors were centered and scaled prior to incorporation in the model, allowing cross-comparisons of both the direction and magnitude of mu.

**Table 3.1.** Detected frequency benchmarks, associated metadata, and sourced study for each species-, method-, and sound form-specific audiogram experiment identified. Experiments are listed in alphabetical order of the source studies.

**Table 3.2.** Counts of available unique studies, experimental method (BEH, AEP), sound form (SPL, PAL), mean number of replicates per experiment  $\pm$  standard deviation (SD), and number of taxonomic orders across hearing type (types 1-4).

**Table 3.3.** Orders of species included in this literature review categorized by broader phylogenetic subgroups, based on common morphological characteristics.

**Table 3.4.** Model structures, predictor variables, degrees of freedom, and absolute AIC values for both maximum and optimal hearing frequency benchmarks.

Generalized least squares (GLS) and linear mixed effect (LME) models were constructed and compared.

**Table 3.5.** Spearman correlation coefficients ( $r$ ) measuring the correlation between maximum and optimum frequency benchmarks for individual hearing types and phylogenetic groups.

**Table B.1.** Moorings, locations, deployment duration, and recording settings for each hydrophone deployed in the summer of 2018.

**Table B.2.** Moorings, calibration sensitivities, and gain values for each deployed hydrophone.

**Table C.1.** Distribution of individuals sampled for diet study, across site and season of sampling. Summer refers to the months of June-July, whereas Fall refers to October. No fish were sampled at the Middle site during the Fall season because of inclement weather and sea state conditions on site.

**Table C.2.** Counts of sampled stomachs, categorized by stomachs found containing prey, empty, or inverted, across site and season.

**Table C.3.** Calculations of percent number (%N), percent weight (%W), and percent frequency of occurrence (%FO), alongside respective counts, for each phylum of prey type.



## List of Figures

**Figure 2.1.** Experimental study sites. Map of three reef sites east of the Maryland coast, consistent for the 2016-2018 study seasons. Colored points refer to receiver deployment locations, while black points refer to approximate tagging locations. The black line depicts the selected 38.73 km transect for cross-sectional FVCOM estimates. The black asterisk refers to the location of National Data Buoy Center Station 44009.

**Figure 2.2.** Observed hourly bottom water temperature ( $^{\circ}\text{C}$ ), averaged across each study site for each year. Black dashed lines refer to dates of observed maximum windspeed for identified storm events (see Table 2.5).

**Figure 2.3.** Time series of hourly directional wind vectors for 2016, 2017, and 2018. Wind vectors are observed for the Middle site of each year, and are measured in  $\text{m s}^{-1}$ . Wind direction corresponds to compass direction, and dashed red lines refer to the date and time (month-day hour) of peak wind speeds for each storm event (see Table 2.5).

**Figure 2.4.a-c.** Modeled hourly time series estimates of bottom water temperature ( $^{\circ}\text{C}$ ), averaged for each site for (a) August-September 2016, (b) June-October 2017, and (c) June-October 2018. Dashed red lines refer to modeled maximum wind speeds occurring during each of the six identified storm events (see Table 2.5).

**Figure 2.5.** Modeled bottom water temperature cross-sectional profiles predicted by the FVCOM for storm events in 2016 and 2018. The left column predicts temperatures related to TS Hermine (2016); the right column predicts temperatures related to the unnamed wind event (2018). Vertical black dashed lines in each pane refer to the transmitter release locations central to each study site (Southern, Northern, and Middle, for both years in increasing depth and distance from coastline). Cross sections are taken along a transect spanning the Middle site (Figure 1), and depict snapshot predictions at 00:00 for each given day.

**Figure 2.6.** Modeled bottom water temperature in the southern MAB predicted by the FVCOM for single storm events occurring in 2016 (left column) and 2018 (right column). Black asterisks refer to the location of transmitter release, central to each study site.

**Figure 2.7.** Modeled bottom water temperature cross-sectional profiles predicted by the FVCOM for storm events in 2017. The left column predicts temperatures related to the July nor'easter; the middle column predicts temperatures related to PTC10; and the right column predicts temperatures related to TS Jose (see Table 2.5). Vertical black dashed lines in each pane refer to the transmitter release locations central to each study site (Southern, Northern, and Middle, increasing depth and distance from coastline). Cross sections are taken along a transect spanning the Middle site (Figure 1), and depict snapshot predictions at 00:00 for each given day.

**Figure 2.8.** Modeled bottom water temperature in the southern MAB predicted by the FVCOM for storm events occurring in 2017. The left column predicts temperatures related to the July nor'easter; the middle column predicts temperatures related to PTC10; and the right column predicts temperatures related to TS Jose (see Table 2.5). Black asterisks refer to the location of transmitter release, central to each study site.

**Figure 2.9.** Hourly black sea bass activity index across study sites for each year before and after storm events (see Table 2.5). Box and whisker plots are shown where the black horizontal line central to each plot defines the median activity index value; the horizontal lines above and below the median value (completing the box) describe the range of the upper and lower quartile values; the vertical lines extending above and below each box provide upper and lower extremes, respectively; and the black dots provide outliers.

**Figure 2.10.** Black sea bass tag loss time series across sites, 2016-2018. The colored lines refer to site-specific time series of the last day a unique tag was detected within a given site, across years. Dashed black lines refer to the day of maximum windspeed associated with a given storm event (Table 2.5).

**Figure 2.11.** ARIMA intervention analysis output for 2016 study sites. The black and blue lines in the upper pane refer to the observed transmitter loss time series and modeled ARIMA output, respectively. The red lines in the lower panes refers to the model's identified interventions, where step-wise declines indicate permanent level shifts and sharp curvatures that dip and recover indicate temporary shifts. Note that the model failed to converge and achieve stationarity at the Southern site, thus no identifiable interventions were detected at that reef. The vertical dashed black lines refer to the date of maximum wind speed associated with TS Hermine.

**Figure 2.12.** ARIMA intervention analysis output for 2017 study sites. The black and blue lines in the upper panes refer to the observed transmitter loss time series and modeled ARIMA output, respectively. The red line in the lower panes refers to the model's identified interventions, where step-wise declines indicate permanent level shifts and sharp curvatures that dip and recover indicate temporary shifts. The vertical dashed black lines refer to the date of maximum wind speed associated with the July nor'easter, PTC10, TS Jose, and TS Maria.

**Figure 2.13.** ARIMA intervention analysis output for 2018 study sites. The black and blue lines in the upper panes refer to the observed transmitter loss time series and modeled ARIMA output, respectively. The red line in the lower panes refers to the model's identified interventions, where step-wise declines indicate permanent level shifts and sharp curvatures that dip and recover indicate temporary shifts. Note that the model failed to converge and achieve stationarity at the Middle site and failed to identify ARIMA model components in the time series for the Northern site. Thus, no identifiable interventions were detected at those reefs, and no model fit or intervention visualizations were provided for the Northern site. The vertical dashed

black lines refer to the date of maximum wind speed associated with the unnamed wind event in early September.

**Figure 3.1.** Distribution of fish hearing sensitivity studies over time, categorized by sound form type used: particle acceleration (PAL) or sound pressure level (SPL).

**Figure 3.2.** Distribution of fish hearing sensitivity studies over time, categorized by method of sound detection used: auditory-evoked potential (AEP) or behavioral (BEH).

**Figure 3.3.** An example audiogram, showing frequency benchmarks. Maximum and minimum frequency benchmarks refer to the maximum and minimum frequencies detected (the endpoint frequency values of the audiogram). The optimal frequency benchmark refers to the frequency detected with the greatest sensitivity to sound and at the lowest sound level (here, the frequency value corresponding to the sound pressure minimum.)

**Figure 3.4.** Distributions of log<sub>10</sub>-transformed frequency benchmarks detected for each hearing type under all study conditions included in the literature review. Box and whisker plots are shown where the black horizontal line central to each plot defines the median; the horizontal lines above and below the median (completing the box) describe the range of the upper and lower quartile values; the vertical lines extending above and below each box provide upper and lower extremes, respectively; and the black dots provide outliers.

**Figure 3.5.** Log<sub>10</sub>-transformed least square means and 0.95 confidence intervals across hearing type for maximum detected frequency benchmarks. Hearing types with significantly different numbers next to their means were significantly different at  $p < 0.05$ .

**Figure 3.6.** Log<sub>10</sub>-transformed least square means and 0.95 confidence intervals across hearing type for optimal detected frequency benchmarks. Hearing types with significantly different numbers next to their means were significantly different at  $p < 0.05$ .

**Figure 3.7.** Log<sub>10</sub>-transformed values for maximum frequencies detected across hearing types, broken down by the method of identifying sound detection used in the study. Box and whisker plots are shown where the black horizontal line central to each plot defines the median; the horizontal lines above and below the median (completing the box) describe the range of the upper and lower quartile values; the vertical lines extending above and below each box provide upper and lower extremes, respectively; and the black dots provide outliers.

**Figure 3.8.** Log<sub>10</sub>-transformed values for optimal frequencies detected across hearing types, broken down by the method of identifying sound detection used in the study. Box and whisker plots are shown where the black horizontal line central to

each plot defines the median; the horizontal lines above and below the median (completing the box) describe the range of the upper and lower quartile values; the vertical lines extending above and below each box provide upper and lower extremes, respectively; and the black dots provide outliers.

**Figure 3.9.** Log10-transformed values for maximum frequencies detected across hearing types, broken down by the sound form measured in the study. Box and whisker plots are shown where the black horizontal line central to each plot defines the median; the horizontal lines above and below the median (completing the box) describe the range of the upper and lower quartile values; the vertical lines extending above and below each box provide upper and lower extremes, respectively; and the black dots provide outliers.

**Figure 3.10.** Log10-transformed values for optimal frequencies detected across hearing types, broken down by the sound form measured in the study. Box and whisker plots are shown where the black horizontal line central to each plot defines the median; the horizontal lines above and below the median (completing the box) describe the range of the upper and lower quartile values; the vertical lines extending above and below each box provide upper and lower extremes, respectively; and the black dots provide outliers.

**Figure 3.11.** Log10 optimum frequency benchmarks v. log10 maximum benchmarks from same experiments. Colors refer to hearing types (T1-T4), with shapes referring to sound forms measured: particle acceleration (PAL) and pressure waves (SPL).

**Figure 3.12.** Log10 optimum frequency benchmarks v. log10 maximum benchmarks from same experiments. Colors refer to groups of similar phylogenetic characteristics, with shapes referring to sound forms measured: particle acceleration (PAL) and pressure waves (SPL).

**Figure A.1.a-c.** Modeled and observed hourly bottom water temperature values across sites for 2016-2018. Vertical black dashed lines refer to maximum wind speed dates for identified storm events.

**Figure A.2.** Modeled current velocity cross-sectional profiles predicted by the FVCOM for storm events in 2016 and 2018. The left column predicts current speed and direction related to TS Hermine (2016); the right column predicts current speed and direction related to the unnamed wind event (2018). Red colors refer to offshore current movement, and blue colors refer to inshore current movement. Vertical black dashed lines in each pane refer to the transmitter release locations central to each study site (Southern, Northern, and Middle, for both years in increasing depth and distance from coastline). Cross sections are taken along a transect spanning the Middle site (Figure 2.1), and depict snapshot predictions at 00:00 for each given day.

**Figure A.3.** Modeled current velocity cross-sectional profiles predicted by the FVCOM for storm events in 2017. The left column predicts current direction and

speed related to the July nor'easter; the middle column predicts current direction and speed related to PTC10; and the right column predicts current and speed related to TS Jose. Red colors refer to offshore current movement, and blue colors refer to inshore current movement. Vertical black dashed lines in each pane refer to the transmitter release locations central to each study site (Southern, Northern, and Middle, increasing depth and distance from coastline). Cross sections are taken along a transect spanning the Middle site (Figure 2.1), and depict snapshot predictions at 00:00 for each given day.

**Figure A.4.** Modeled turbulent kinetic energy (TKE) cross-sectional profiles predicted by the FVCOM for storm events in 2016 and 2018. The left column predicts TKE values related to TS Hermine (2016); the right column predicts TKE values related to the unnamed wind event (2018). Vertical black dashed lines in each pane refer to the transmitter release locations central to each study site (Southern, Northern, Middle, for both years in increasing depth and distance from coastline). Cross sections are taken along a transect spanning the Middle site (Figure 2.1), and depict snapshot predictions at 00:00 for each given day.

**Figure A.5.** Modeled turbulent kinetic energy (TKE) profiles predicted by the FVCOM for storm events in 2017. The left column predicts TKE values related to the July nor'easter; the middle column predicts TKE values related to PTC10; and the right column predicts temperatures related to TS Jose. Vertical black dashed lines in each pane refer to the transmitter release locations central to each study site (Southern, Northern, and Middle, increasing depth and distance from coastline). Cross sections are taken along a transect spanning the Middle site (Figure 2.1), and depict snapshot predictions at 00:00 for each given day.

**Figure A.6.** Modeled turbulent kinetic energy (TKE) in the southern MAB predicted by the FVCOM for single storm events occurring in 2016 (left column) and 2018 (right column). Black asterisks refer to the location of transmitter release, central to each study site.

**Figure A.7.** Modeled turbulent kinetic energy (TKE) in the southern MAB predicted by the FVCOM for storm events occurring in 2017. The left column predicts TKE values related to the July nor'easter; the middle column predicts TKE values related to PTC10; and the right column predicts TKE values related to TS Jose. Black asterisks refer to the location of the transmitter release, central to each site.

**Figure A.8.** Distributions of log-transformed movement index across individual tagged fish in 2017, ordered by increasing length and color-coded by sex; F, M, and U refer to female, male, and unidentified fish, respectively. X-axis labels refer to the tag number, as well as the length of the individual (mm). Box and whisker plots are shown where the black horizontal line central to each plot defines the median; the horizontal lines above and below the median (completing the box) describe the range of the upper and lower quartile values; the vertical lines extending above and below

each box provide upper and lower extremes, respectively; and the black dots provide outliers.

**Figure A.9.** Quantile residual summary plots for the final fitted Generalized Additive Model for Location, Shape, and Scale (GAMLSS) model.

**Figure B.1.** Experimental study sites, including locations of receiver sites, tagging sites, and hydrophone deployments. Colored points refer to receiver deployment locations, while black points refer to approximate tagging locations. Black asterisks refer to hydrophone deployment locations at each receiver site.

**Figure B.2.** Root mean square (RMS) sound pressure levels (SPL) calculated from sound voltage measurements taken at each site during 2018. The black dotted line refers to the date of maximum wind speed associated with the 2018 unnamed wind event.

**Figure B.3.** Sound pressure levels calculated during the week of storm activity, September 6 – September 11, 2018, calculated across third octave bands and a predefined low frequency band (0-100 Hz). The black dotted line refers to the date of maximum wind speed associated with the 2018 unnamed wind event.

**Figure B.4.** Hourly power spectral density values calculated across detected frequencies for September 6, 9, 10, and 11 of September, 2018. Warmer colors indicate higher power values.

**Figure C.1.** Distributions of Fulton's K (K) for sampled fish, calculated across sampling site and season. K assumes an allometric relationship where weight (g) = length (cm)<sup>3</sup>. Here K was thus determined by dividing observed weight (g) by cubed observed length (cm) and multiplying the quotient by 100.

**Figure C.2.** Distribution of GSI calculations for sampled fish, across site and season of sampling. GSI was calculated as the percent contribution of gonad weight (g) relative to total body weight (g) per individual.

**Figure C.3.** Distribution of HSI calculations for sampled fish, across site and season of sampling. HSI was calculated as the percent contribution of liver weight (g) relative to total body weight (g) per individual.

**Figure C.4.** Log-transformed measurements of weight plotted as a function of log-transformed measurements of length for individuals sampled. The black line refers to log length-weight regression model predictions of weight based on input observed length. The color and shape of the plotted points refer to the site of sampling and the sampling season, respectively.

**Figure C.5.** Distribution of weights across sampling site and season. Site and sampling season interacted significantly (ANOVA,  $p < 0.01$ ). Weights taken from the

Middle and Southern sites, during the summer, were significantly different from other distributions (Tukey HSD,  $p < 0.05$ ).

**Figure C.6.** Distributions of percent gut fullness of sampled individuals, across sampling site and season. Gut fullness was calculated as the percent weight of stomach contents (stomach weight minus the weight of stomach lining; (g)) relative to total body weight (g).

**Figure C.7.** Percent number (%N) and percent weight (%W) of each identified prey phylum, plotted against respective prey percent frequency of occurrence (%FO).

## Chapter 1. Introduction

### Storm disturbance

Ecological disturbances are discrete temporal events that alter ecosystem function through changes to physical and biological features (White and Jentsch 2001), and thus play key roles in defining ecosystem function and stability (Sousa 1984; Petraitis 1989; White and Jentsch 2001). Fire disturbance shapes diversity and productivity in forest and grassland communities, while also shaping heterogeneity (Heinselman 1973; Collins and Barber 1986; Rood et al. 2007). In marine communities, hurricanes positively influence kelp propagation (Dayton 1984) and succession (Witman 1987; Kennelly 1987). Hurricanes also influence community membership of coral and fish assemblages in reef habitats (Walsh 1983; Bythell et al. 2000; Gardner et al. 2005), and can also increase the vulnerability of coral reef habitat to human degradation (Gardner et al. 2005; Mumby 1999). Therefore, in order to fully describes the function and stability of an ecosystem, one must also integrate the effects of natural and anthropogenic perturbations (Holling 1973; Sousa 1984).

Storm events, such as tropical storms and hurricanes, are a powerful source of natural disturbance to marine communities. In addition to coral reef and kelp forest communities, systems impacted by storm disturbance include benthic invertebrate communities (Underwood 1999; Dernie et al. 2003), individual coastal fish and shellfish species (Onuf and Quammen 1983; Bailey and Secor 2016; Biggs et al. 2018), and entire coastal fisheries (Pettersen et al. 2006; Binn et al. 2007; Solís et al. 2013). The impacts of storm disturbance on the movement behavior of marine fishes has been the focus of a few recent studies (Bailey and Secor 2016; Bachelier et al.



2019; Secor et al. 2019). However, the vast majority of these studies focus on storms as a stochastic event evoking an isolated behavioral response, rather than a recurring source of natural disturbance shaping the species' baseline movement behavior. Subsequently, there is a gap in the literature on storm disturbance as a recurring effect. This study seeks to inform this gap, investigating the effect of storm events as a regular disturbance to black sea bass (*Centropristis striata*) in the Middle Atlantic Bight (MAB).

### Study system

The MAB is the region of the continental shelf extending from the southern flank of George Bank to Cape Hatteras. It regularly experiences high-energy storm activity during the summer and fall months, and it is characterized by a prominent oceanographic feature—the cold pool—that preconditions the water column to large threshold changes in response to storm disturbance. The cold pool is a denser layer of bottom water formed from the vernal heating of surface waters during the spring-summer, and subsequent trapping of colder, saltier winter water below (Bigelow 1933; Chen et al. 2018). This seasonal, differential heating forms a highly stratified temperature gradient in the MAB water column, which are rapidly destratified during severe storms through wind-driven mixing and cross-shelf advection (Beardsley et al. 1985; Lentz et al. 2003). Summer storms in the MAB pose a potentially formidable source of physiological disturbance to its demersal fishes, as storm-driven destratification can increase bottom temperatures by as much as 10°C over 24 hrs (Secor et al. 2019). Physical wind-driven disturbances during storms also include increases in surface and seafloor turbulence (Ginis 2002; McPhaden et al. 2009;

Huang et al. 2009) and increases in current velocity gradients at the surface and mixed layers (Ginis 2002; Li and Xue 2002). These changes in flow regime might be expected to influence station-keeping and movements of exposed fishes.

In addition to causing rapid thermal destratification storm events in the MAB and elsewhere may be considered a source of disturbance to the ambient sound field. Storms generate high-energy low frequency sound (approximately <1000 Hz), within the hearing range of most fishes (see Appendix B); sound pressure levels increase proportionally to the cube of the local wind speed during storms (Wenz 1962; Sutton and Barstow 1990; Wilson and Makris 2008) and can increase ambient noise levels by as much as 25 dB re: 1  $\mu$ Pa within the frequency range of fish hearing sensitivity (400 Hz) (Wilson and Makris 2006). Storms also increase high frequency sound (approximately 3000-10000 Hz) with increased wind speed, caused by the forced attenuation of sea surface bubbles (Wenz 1962; Wilson and Makris 2006). While the effects of storm-forced flow and water quality changes on fish movements have been explored (Bailey and Secor 2016; Bacheler et al. 2019; Secor et al. 2019), less is known about how storm sound might serve as a natural disturbance to marine fish communities. This knowledge gap is deepened by the slowly growing understanding of how fish perceive underwater sound (Popper and Hawkins 2019), with advances in the topic limited by expensive equipment and time-consuming research practices as well as inconsistencies in methodology (Sisneros et al. 2015; Popper and Hawkins 2018).

As a model species for examining the impacts of storms on movement ecology, black sea bass (*Centropristis striata*) are a demersal, structure-oriented

species whose distribution ranges from Cape Cod, MA to Cape Canaveral, FL, and supports commercial and recreational fisheries in the MAB (Cape Cod, MA to Cape Hatteras, NC) (Musick and Mercer 1977; Mercer and Moran 1989). MAB populations undertake a cross-shelf seasonal migration, moving on-shelf into structured reef habitats during the spring and off-shelf into deeper, warmer water during the fall (Mercer et al. 1989; Colvorcoresses and Musick 1984; Shepherd and Terceiro 1994). Black sea bass demonstrate high fidelity to reef habitats during the spring-summer, with observed home ranges of approximately 0.137-7.364 km<sup>2</sup> (Fabrizio et al. 2014). This mostly sedentary behavior and affinity for structured demersal habitats renders black sea bass a model species for examining the recurring effects of storm disturbance on the movement behaviors of a marine fish species.

#### Goals and objectives

The overall goal of this thesis is to monitor the recurring effects of storm events on the movement behavior of black sea bass, focusing on oceanographic drivers as well as local and broad-scale movement responses. Specific objectives are to explore how storms cause changes to the temperature structure of the water column and to ambient flow dynamics. Because published measurements of black sea bass hearing sensitivities are not currently available, an additional objective of this thesis is to quantify hearing sensitivities for black sea bass and other fish species based on morphological characteristics of the fish. Meeting this objective ultimately provides a reference point for understanding how vulnerable black sea bass might be to sound perturbations generated by storms. Thesis objectives were thus organized into two chapters focused on (1) characterizing and modeling black sea bass movements in

response to storms over a three-year period, and (2) undertaking a comprehensive review of the literature to frame initial expectations on hearing sensitivity of black sea bass and other fishes for which hearing sensitivity is unknown. Appendices support both of these chapters.

The opportunity to conduct this study, exploring storm effects over three field seasons of telemetry data, was provided by grants through the Maryland Department of Natural Resources (DNR) and Maryland Energy Administration. The original project goal of this grant was to evaluate the effect of pile driving on black sea bass owing to the construction of a 100 m high meteorological tower, sited in the Bureau of Ocean Energy (BOEM)-leased Wind Energy Area off Maryland. This tower would precede > 200 m high wind turbines slated for construction by the US Wind Company and provide an opportunity to evaluate wind energy impacts on demersal fishes (Secor et al. 2019). Despite plans during each of the summers, 2016-2018, the meteorological tower has not yet been erected. My study design of three replicate sites reflects the goal of the Maryland DNR study, but has been repurposed to examine the effects of storm disturbance to black sea bass movement behaviors.

### Thesis contents

Chapter 2 addresses individual and cumulative effects of multiple seasons of storm disturbance on black sea bass movement behaviors. Coupling observing system and a numerical ocean model (FVCOM) data, this chapter evaluates the differences between seasons with single and multiple storms, and the effects of storms on water column characteristics. An explanatory statistical model evaluated how these characteristics influenced local activity and evacuations of black sea bass across the

experimental reef sites. This research represents a collaboration with Drs. Ming Li and Fan Zhang (UMCES), who assisted with running FVCOM. Dr. Vyacheslav Lyubchich (UMCES) assisted with the explanatory model on movement activity. No manuscript has yet resulted from this chapter.

Chapter 3 comprises the first-ever literature review of the published data for hearing sensitivity across a number of marine and freshwater species and creates a statistical framework for predicting hearing sensitivity based on swim bladder morphology. This framework may then be used to estimate hearing sensitivities of fish species not yet rigorously tested, such as black sea bass, but for which information is needed to predict vulnerability to both natural and anthropogenic disturbance. This research has been prepared as a manuscript for publication and shared with fish hearing authority Dr. Arthur Popper (UMCP) and committee member Dr. Helen Bailey (UMCES), who provided helpful comments. Dr. Dong Liang (UMCES) assisted with the statistical analysis attached with the literature review.

Appendices A-C provide supplemental analyses I performed to support the Chapters 2 and 3. Appendix A assesses the detailed structure and relative intensities of changes in turbulent kinetic energy and current velocity during storm events, focusing on patterns of change throughout the vertical water column and across the continental shelf. Appendix B provides a detailed characterization of sound signals occurring during a 2018 storm event, analyzing signal strength over time as well as breakdowns of signal energy across frequency bands. Appendix C provides comparisons of various condition metrics for fish sampled across the study area over

the study period, as well as a breakdown of diet composition and the relative abundance of selected prey items.

### Implications and future work

Understanding the role of storms in shaping local movement and residence of black sea bass in the MAB will be critical for understanding both the ecology and management of the species in light of a future shaped by the increased presence of higher intensity storms (Knutson et al. 1998; Holland and Bruyère 2014) as well as increased ocean use and development. Multiple areas along the US East Coast are leased for future wind development (ESS 2016; BOEM 2018), and successful management of both black sea bass and other demersal fish species in the region is contingent upon understanding the impacts of both natural and anthropogenic disturbances. This study can inform management of potential disturbances on demersal fish species by supplying a baseline understanding how black sea bass as a model species respond to storms in the MAB. The study can also inform management by providing a coarse tool to predict hearing sensitivities of fish species based on physical morphology, which may be useful when considering acoustic disturbances related to offshore development.

Future telemetry studies should focus on increasing the spatial and temporal resolution and capture movement behaviors across a broader range of habitat types and locations using improved receiver array designs. Future work should also improve the scale of measured behavioral response to storms by coupling telemetry data with data on the physiology of individual fish, as well as by exploring changes in fishes' depth behavior during and after storms.

## References

- Bacheler, N. M., Shertzer, K. W., Cheshire, R. T., & MacMahan, J. H. (2019). Tropical storms influence the movement behavior of a demersal oceanic fish species. *Scientific Reports*, *9*(1481), 1-13. <https://doi.org/10.1038/s41598-018-37527-1>
- Bailey, H., & Secor, D. H. (2016). Coastal evacuations by fish during extreme weather events. *Scientific Reports*, 1-9. <https://doi.org/10.1038/srep30280>
- Beardsley, R. C., Chapman, D. C., Brink, K. H., Ramp, S. R., & Schlitz, R. (1985). The Nantucket Shoals Flux Experiment (NSFE79). Part I: A basic description of the current and temperature variability. *Journal of Physical Oceanography*, *15*, 713-748.
- Bigelow, H. B. (1933). Studies of the waters on the continental shelf, Cape Cod to Chesapeake Bay, I, The cycle of temperature. *Papers in Physical Oceanography and Meteorology*, *11*(4), 1-134.
- Biggs, C. R., Lowerre-Barbieri, S. K., & Erisman, B. (2018). Reproductive resilience of an estuarine fish in the eye of a hurricane. *Biology Letters*, *14*, 1-5. <https://doi.org/10.1098/rsbl.2018.0579>
- Bin, O., Dumas, C., Poulter, B., & Whitehead, J. (2007, March). *Measuring the impacts of climate change on North Carolina coastal resources*. Washington DC, USA: National Commission on Energy Policy.
- Bureau of Ocean Energy Management, Office of Renewable Energy Programs. (2012, January). *Commercial wind lease issuance and site assessment activities on the Atlantic outer continental shelf offshore New Jersey, Delaware, Maryland, and Virginia* (OCS EIS/EA BOEM No. 2012-003). U.S. Department of the Interior.
- Bureau of Ocean Energy Management. (2018, August). *Outer continental shelf renewable energy leases map book*.
- Bythell, J. C., Hillis-Starr, Z. M., & Rogers, C. S. (2000). Local variability but landscape stability in coral reef communities following repeated hurricane impacts. *Marine Ecological Progress Series*, *204*, 93-100.
- Chen, Z., Curchitser, E., Chant, R., & Kang, D. (2018). Seasonal variability of the cold pool over the Mid-Atlantic Bight continental shelf. *Journal of Geophysical Research: Oceans*, *123*, 8203-8226. <https://doi.org/10.1029/2018JC014148>

- Collins, S. L., & Barber, S. C. (1986). Effects of disturbance on diversity in a mixed-grass prairie. *Plant Ecology*, 64, 87-94. <https://doi.org/10.1007/BF00044784>
- Colvocoresses, J. A., & Musick, J. A. (1984). Species associations and community composition of Middle Atlantic Bight continental shelf demersal fishes. *Fishery Bulletin*, 82(2), 295-313.
- Dayton, P. K., Currie, V., Gerrodette, T., Keller, B. D., Rosenthal, R., & Ven Tresca, D. (1984). Patch dynamics and stability of some California kelp communities. *Ecological Monographs*, 54(3), 253-289.
- Dernie, K. M., Kaiser, M. J., & Warwick, R. M. (2003). Recovery rates of benthic communities following physical disturbance. *Journal of Animal Ecology*, 72, 1043-1056.
- ESS Group Inc. (2016, April). *Site assessment plan, Maryland offshore wind project* (ESS Project No. U167).
- Fabrizio, M. C., Manderson, J. P., & Pessutti, J. P. (2014). Habitat associations and dispersal of black sea bass from a mid-Atlantic Bight reef. *Marine Ecological Progress Series*, 482, 241-253. <https://doi.org/10.3354/meps10302>
- Gardner, T. A., Côté, I. M., Gill, J. A., Grant, A., & Watkinson, A. R. (2005). Hurricanes and Caribbean coral reefs: Impacts, recovery patterns, and role in long-term decline. *Ecology*, 86(1), 174-184.
- Ginis, I. (2002). Tropical cyclone-ocean interactions. *Atmosphere-Ocean Interactions, Advances in Fluid Mechanics Series*, 33, 83-114.
- Heinselman, M. L. (1973). Fire in the virgin forests of the Boundary Waters Canoe Area, Minnesota. *Quaternary Research*, 3, 329-382. [https://doi.org/10.1016/0033-5894\(73\)90003-3](https://doi.org/10.1016/0033-5894(73)90003-3)
- Holland, G., & Bruyère, C. L. (2014). Recent intense hurricane response to global climate change. *Climate Dynamics*, 42, 617-627. <https://doi.org/10.1007/200382-013-1713-0>
- Holling, C. S. (1973). Resilience and stability of ecological systems. *Annual Review of Ecology and Systematics*, 4, 1-23.
- Huang, P., Sanford, T. B., & Imberger, J. (2009). Heat and turbulent kinetic energy budgets for surface layer cooling induced by the passage of Hurricane Frances (2004). *Journal of Geophysical Research*, 114(C12023), 1-14. <https://doi.org/10.1029/2009JC005603>



- Kennelly, S. J. (1987). Physical disturbances in an Australian kelp community. I. Temporal effects. *Marine Ecology Progress Series*, 40, 145-153.
- Knutson, T. R., Tuleya, R. E., & Kurihara, Y. (1998). Simulated increase of hurricane intensities in a CO<sub>2</sub>-warmed climate. *Science*, 279, 1018-1020.
- Lentz, S., Shearman, K., Anderson, S., Plueddemann, A., & Edson, J. (2003). Evolution of stratification over the New England shelf during the coastal mixing and optics study, August 1996-June 1997. *Journal of Geophysical Research*, 108(C1), 1-14. <https://doi.org/10.1029/2001JC001121>
- Li, Y., & Xue, H. (2002). Air-sea interactions during the passage of a winter storm over the Gulf Stream: A three-dimensional coupled atmosphere-ocean model study. *Journal of Geophysical Research*, 107(C11), 1-13. <https://doi.org/10.1029/2001JC001161>
- McPhaden, M. J., Foltz, G. R., Lee, T., Murty, and 5 others (2009). Ocean-atmosphere interactions during Cyclone Nargis. *EOS Transactions American Geophysical Union*, 90(7), 53-60.
- Mercer, L. P., & Moran, D. (1989). *Species profile: Life histories and environmental requirements of coastal fishes and invertebrates (South Atlantic)* Biological Report No. 82 11.99.
- Mumby, P. J. (1999). Bleaching and hurricane disturbances to populations of coral recruits in Belize. *Marine Ecology Progress Series*, 190, 27-35.
- Musick, J. A., & Mercer, L. P. (1977). Seasonal distribution of black sea bass (*Centropristis striata*), in the Middle Atlantic Bight with comments on the ecology and fisheries of the species. *Transactions of the American Fisheries Society*, 106(1), 12-25.
- Onuf, C. P., & Quammen, M. L. (1983). Fishes in a California coastal lagoon: Effects of major storms on distribution and abundance. *Marine Ecology Progress Series*, 12, 1-14.
- Petraitis, P. S., Latham, R. E., & Niesenbaum, R. A. (1989). The maintenance of species diversity by disturbance. *The Quarterly Review of Biology*, 64(4), 393-418.
- Petterson, J. S., Stanley, L. D., Glazier, E., & Philipp, J. (2006). A preliminary assessment of social and economic impacts associated with Hurricane Katrina. *American Anthropologist*, 108(4), 643-670.

- Popper, A. N., & Hawkins, A. D. (2018). The importance of particle motion to fishes and invertebrates. *The Journal of the Acoustical Society of America*, *143*(1), 470-488. <https://doi.org/10.1121/1.5021594>
- Popper, A. N., & Hawkins, A. D. (2019). An overview of fish bioacoustics and the impacts of anthropogenic sounds on fishes. *Journal of Fish Biology*, *94*, 692-713. <https://doi.org/10.1111/jfb.13948>
- Rood, S. B., Goater, L. A., Mahoney, J. M., Pearce, C. M., & Smith, D. G. (2007). Floods, fire, and ice: Disturbance ecology of riparian cottonwoods. *Canadian Journal of Botany*, *85*, 1019-1032. <https://doi.org/10.1139/B07-073>
- Secor, D. H., Zhang, F., O'Brien, M. H.P., & Li, M. (2019). Ocean destratification and fish evacuation caused by a Mid-Atlantic tropical storm. *ICES Journal of Marine Science*, 1-12. <https://doi.org/10.1093/icesjms/fsx241>
- Shepherd, G. R., & Terceiro, M. (1994, August). *The summer flounder, scup, and black sea bass fishery of the Middle Atlantic Bight and Southern New England waters* (NOAA Technical Report NMFS No. 122). Seattle, WA: US Department of Commerce.
- Sisneros, J. S., Popper, A. N., Hawkins, A. D., & Fay, R. (2015). Audio evoked potential audiograms compared with behavioral audiograms in aquatic animals. *Advances in Experimental Medicine and Biology*, *875*, 1049-1056.
- Solis, D., Perruso, L., del Corral, J., Stoffle, B., & Letson, D. (2013). Measuring the initial economic effects of hurricanes on commercial fish production: the US Gulf of Mexico grouper (Serranidae) fishery. *Natural Hazards*, *66*, 271-289. <https://doi.org/10.1007/s11069-012-0476-y>
- Sousa, W. P. (1984). The role of disturbance in natural communities. *Annual Review of Ecology, Evolution, and Systematics*, *15*, 353-391.
- Sutton, G. H., & Barstow, N. (1990). Ocean-bottom ultralow frequency (ULF) seismo-acoustic ambient noise: 0.002 to 0.4 Hz. *The Journal of the Acoustical Society of America*, *87*, 2005-2012. <https://doi.org/10.1121/1.399328>
- Underwood, A. J. (1999). Physical disturbances and their direct effect on an indirect effect: Responses of an intertidal assemblage to a severe storm. *Journal of Experimental Marine Biology and Ecology*, *232*, 125-140.
- Walsh, W. J. (1983). Stability of a coral reef fish community following a catastrophic storm. *Coral Reefs*, *2*, 49-63.

- Wenz, G. M. (1962). Acoustic ambient noise in the ocean: Spectra and sources. *The Journal of the Acoustical Society of America*, 34(12), 1936-1956.
- White, P. S., & Jentsch, A. (2001). The search for generality in studies of disturbance and ecosystem dynamics. *Progress in Botany*, 62, 399-450.
- Wilson, J. D., & Makris, N. C. (2006). Ocean acoustic hurricane classification. *The Journal of the Acoustical Society of America*, 119(1), 168-181.  
<https://doi.org/10.1121/1.2130961>
- Wilson, J. D., & Makris, N. C. (2008). Quantifying hurricane destructive power, wind speed, and air-sea material exchange with natural undersea sound. *Geophysical Research Letters*, 35, 1-5.  
<https://doi.org/10.1029/2008GL033200>
- Witman, J. D. (1987). Subtidal coexistence: Storms, grazing, mutualism, and the zonation of kelps and mussels. *Ecological Monographs*, 57(2), 167-187.

## Chapter 2. The recurring role of storm disturbance on black sea bass movement behaviors in the Mid-Atlantic Bight.

### *Introduction*

Disturbance is a key structuring force in coastal marine ecosystems, affecting population and community dynamics, as well as the habitats upon which they depend (Sousa 1984; White and Jentsch 2001). Such impacts are well-described for shallow, physical habitats such as reefs and marshes (Jackson and Hughes 1985; Dollar and Tribble 1993; Michener 1997). In shallow reef fish communities, storms have been associated with increased mortality (Robins 1957; Araga and Tanase 1966; Lassig 1983; Harmelin-Vivien 1994) as well as causing net changes in species abundance and density (Kaufman 1983; Lassig 1983; Walsh 1983; Harmelin-Vivien 1994; Fenner 1991). Storms caused significant shifts in species composition and abundance for fish communities inhabiting shallow mangrove habitats (Bouchon 1994), and increased frequency of high-intensity storms has been linked to decreased fish abundance and changes in trophic structure in kelp forests (Ebeling et al. 1985; Byrnes et al. 2011). However, impacts of storm disturbance on fish communities in comparatively remote marine ecosystems with less physical structure—systems that may still be subject to hurricane-forcing—are less well known.

The Mid-Atlantic Bight (MAB)—the continental shelf extending from the southern flank of Georges Bank to Cape Hatteras—is a region regularly susceptible to significant storm disturbance during the summer and fall months. Storm-driven perturbations are catalyzed by a number of wind-driven hydrodynamic forces, such as changes in sea surface temperature due to vertical mixing (Ginis 2002; Li and Xue 2002; Huang et al. 2009; McPhaden et al. 2009); increased turbulence at surface and

bottom-boundary layers, either due to wind-driven shear or stirring (Ginis 2002; McPhaden et al. 2009; Huang et al. 2009); and increased current velocity gradients in the oceanic surface and mixed layers (Ginis 2002; Li and Xue 2002). The MAB is also uniquely vulnerable to storm-driven disturbance due to the overlapping presence of an oceanographic feature known as the “cold pool”. The cold pool is an isolated layer of relatively colder, saltier—and subsequently denser—bottom water within the MAB, receiving winter waters formed at Nantucket Shoals (Houghton et al. 1982; Chen et al. 2018). It forms seasonally with the vernal heating of surface waters, related to increases in air temperature, and resulting in the stratification of the water column (Bigelow 1933; Houghton et al. 1982). This stratification and associated bottom-layer cold pool can be rapidly “destroyed” through cross-shelf advection, wind-driven overturn, and current-driven longitudinal transport (Rasmussen et al. 2005; Lentz 2007); which are commonly caused by storms (Beardsley et al. 1985; Lentz et al. 2003).

Summer and fall storm events, such as hurricanes, tropical storms, and nor’easters, contribute to the seasonal deterioration of the cold pool through wind-driven forcing and advection. In this capacity, summer storms in the MAB act as a significant source of natural disturbance, driving rapid partial destratification of the cold pool due to mixing and forcing bottom water temperatures to increase as much as 10°C over 24 hr (Secor et al. 2019). For many fish species, physiological tolerance to extreme temperature shifts depends on acclimation (Atwood et al. 2001; Pörtner 2001; Pörtner 2002). Therefore, the rapid changes in bottom water temperature in the MAB are likely a significant source of disturbance and physiological stress to

demersal fish communities. The rapid increase in bottom water temperatures co-occurs with rapid changes in current velocity, turbulent kinetic energy, and noise. Thus, storms in the MAB expose demersal fish communities to multiple physical and physiological stressors. Because several storm systems can affect destratification each year, cumulative impacts caused by these storm-driven stressors could represent a disturbance regime unique to the MAB and its demersal fish communities.

A small but growing pool of research has emerged emphasizing the role of storms as singular, extreme disturbances driving changed movement behaviors by marine fishes. Biotelemetry studies off the coasts of Florida and North Carolina observed storm-driven evacuation by tagged juvenile blacktip sharks, *Carcharhinus limbatus*, (Heupel et al. 2003) and gray triggerfish, *Balistes capriscus* (Bacheler et al. 2019); movement behaviors were respectively associated with decreased barometric pressure and increased wave orbital velocity. Storm-driven decreases in temperature, dissolved oxygen, and salinity were observed to drive emigration of striped bass, *Morone saxatilis*, from the Hudson River Estuary to coastal habitats (Bailey and Secor 2016). In the Great Bay Estuary, New Hampshire, increased migration of American lobster, *Homarus americanus*, towards coastal waters was observed in the wake of a major hurricane (Jury et al. 1995). Summer flounder, *Paralichthys dentatus*, and black sea bass, *Centropristis striatus*, evacuations occurred following severe storm events in the MAB (Sackett et al. 2007; Secor et al. 2019). Thus, the literature supports that storms can be disruptive events to demersal communities. Still, the concept of storm events collectively representing a recurring source of natural disturbance each year has not been fully explored.

Here, I investigate the effect of storm events as a recurring source of disturbance to a common member of the demersal MAB shelf assemblage: black sea bass. Black sea bass exhibit range behaviors centered on artificial and natural structure (Cullen and Stevens 2017), which makes them amenable to biotelemetry studies on their movement behaviors. They are a mostly sedentary, reef-associated species, particularly from the spring to fall (Musick and Mercer 1977; Mercer and Moran 1989; Moser and Shepherd 2009; Fabrizio et al. 2014). Black sea bass are often a dominant member of reef-associated demersal fish communities in the MAB (Musick and Mercer 1977; Colvocoresses and Musick 1984; Sedberry and Van Dolah 1984). Demersal fish assemblages in the MAB characteristically occur throughout the summer and early fall months and then species undertake cross-shelf seasonal migrations to deeper waters during the fall, typically throughout mid-September to late October (Mercer and Moran 1989; Colvocoresses and Musick 1984; Musick and Mercer 1977). These migrations are understood to coincide with seasonal shifts in water temperature, with demersal species transiting by late fall from cooling bottom waters to relatively warmer, deeper outer shelf waters, where they remain for the winter (Colvocoresses and Musick 1984; Sedberry and Van Dolah 1985; Fabrizio et al. 2005). This broad transit period of off-shelf movement overlaps spatially and temporally with the arrival of hurricanes and tropical storms in the western Atlantic. Secor et al. (2019) hypothesized that cumulative storm impacts during this period could cue offshore seasonal migration during fall-early winter.

Should storms have a recurring, if increasing, impact on demersal fish behaviors, such baseline behaviors will be important to evaluate against

anthropogenic impacts such as increased vessel traffic and emplacement of wind towers. Higher intensity storm disturbances in the MAB, forecasted owing to climate change (Knutson et al. 1998; Lin et al. 2012; Vermaire et al. 2013; Holland and Bruyère 2014), could alter the phenology (aka seasonal timing) of regional migrations. Offshore wind energy development throughout the MAB is anticipated in the near future, yet its influence on demersal fishes remains poorly known (BOEM 2012). Both recreational and commercial fishermen have expressed concerns regarding the potential impacts of windfarm construction on fished species within the MAB (ESS Group 2016). Concerns have been raised particularly over construction noise related to both pile-driving and increased vessel activity (Hildebrand 2009); both of which can cause significant disturbance to demersal marine fish communities (Vabø et al. 2002; Popper and Hastings et al. 2009; Slabbekoorn et al. 2010). Windfarm impact studies will be confounded if they do not take into account the effects of potentially co-occurring natural disturbance features, such as storms.

The goal of this study is to better characterize the recurrence of summer storm events in the MAB, their impact on the local oceanography, and their impact on movement and evacuations by black sea bass. More specifically, I hypothesized that: (1) storm events are a recurring feature that impact black sea bass habitat variables: temperature, bottom current velocity, and turbulent kinetic energy; (2) changes in movement behavior are caused by both individual and cumulative storm-driven environmental changes; and (3) storm-related movement behaviors are driven chiefly by rapid (<1 d) mixing and increased bottom temperature. I addressed these hypotheses for three summer-fall seasons (2016-2018), measuring evacuation and



movement behaviors through biotelemetry and coupling these behaviors with predicted storm-driven changes in water column conditions provided by a coastal ocean model. Cumulative storm impact was modeled separately for 2017, when a series of storm events occurred with sequential impacts on the water column, using a Generalized Additive Model to evaluate the influence of cumulative storm days and other habitat variables.

### Materials and methods

#### *Study site*

Study sites for this project included three reef sites located 16-46 km east and southeast of Ocean City, Maryland: The Twin Wrecks Reef, the Great Eastern Reef, and the African Queen Wreck (Figure 2.1; Tables 2.1, 2.2). Study sites were identified in cooperation with a recreational charter boat captain and based on the presence of both black sea bass and structured habitat.

The Twin Wrecks reef is comprised of the 1914 and 1918 wrecks of the sunken tanker (the *Oklahoma*) and sunken steam freighter (the *Saetia*) (A. Carroll, University of Maryland Center for environmental Science pers. comm.; Loftus and Stone, 2007); the *Saetia* is approximately 98 m in length and 15 m at its widest, with the *Oklahoma* comparable in size. Both rest on an area of sandy substrate, at a distance of 585 m apart. (A.Carroll, pers. comm.; Loftus and Stone, 2007; Aquaventureonline.com) The Great Eastern Reef, is an artificial reef comprise primarily of opportunistic materials (such as concrete units and cable mounds), resting on sandy substrate (coastalfisherman.net; Loftus and Stone, 2007). The reef is approximately 1.62 km<sup>2</sup> in area, and is located 29.1 km from the Ocean City Inlet

([https://dnr.maryland.gov/fisheries/Documents/MARIOC04209postersize\\_with\\_coordinates\\_web.pdf](https://dnr.maryland.gov/fisheries/Documents/MARIOC04209postersize_with_coordinates_web.pdf)). Lastly, the *African Queen* reef is the site of a 1958 wreck, and covers a surface area of ~3.21 km<sup>2</sup> over sandy substrate 19.5 km miles from the Ocean City Inlet (Loftus and Stone, 2007; [dnr.maryland.gov](http://dnr.maryland.gov)). The wreck consists of the remains of a freighter, which sank in the 1950s, and rests on the seafloor in two nearby sections ([coastalfisherman.net](http://coastalfisherman.net)); additional structures were added to the reef site until 2005, and include concrete units, cable mounds, and several additional smaller sunken vessels ([coastalfisherman.net](http://coastalfisherman.net); Loftus and Stone, 2007).

These reefs—the Twin Wrecks, Great Eastern, and *African Queen* Reefs—corresponded to the three study sites utilized for the duration of the experiment—the Northern, Middle, and Southern sites, respectively. All study sites were exposed to the persistent presence of the cold pool for approximately 7-8 months of the year (spring-late summer), and spanned a gradient of depths (Table 2.2), although the shallower Southern site exhibiting a less stable pattern of summer-fall stratification than the other two deeper sites (see Results).

#### *Acoustic telemetry data collection*

A total of nine VEMCO VR2AR acoustic-release receivers were deployed across study sites during June-October, 2016-2018 (Table 2.1). For each year of deployment, three receivers were positioned to capture movement behaviors associated with each reef. Receivers were deployed 800 m away and at 0°, 120°, and 240° degree angles from tagging locations at each reef; the 800 m distance was set based on detection ranges observed in a range test study using the same model of acoustic receivers under similar conditions off the coast of New Jersey (Fabrizio et al.

2014). Receivers were moored to the seabed with two 20.4 kg weight plates and positioned in the water column with one 10.8 kg positive buoyancy buoy each, with a vertical profile of approximately 2 m above the seafloor. Receivers continuously recorded data on unique transmitter detections, recorded bottom water temperature (°C), and ambient noise (mV) every 600 seconds.

During June 2016-2018 and at each site, 8-17 black sea bass were surgically implanted with VEMCO V9-2H acoustic transmitters (Table 2.3). Animal collection, surgical, and release procedures were approved by the UMCES Institutional Animal Care and Use Committee (IACUC-Secor-F-CBL-160-10). Transmitters were 26 mm long, 9 mm in diameter, and weighed 3.7 g; transmitters also emitted a 69 kHz signal at randomized 90-second intervals, with an estimated battery life of 346 days. Fish were captured at reef sites using rod-and-reel on a chartered recreational fishing boat, and immediately placed in a 57-liter tank containing ambient seawater until surgery. Sublegal ( $\leq 32$  cm) individuals were selected for tagging in an effort to reduce transmitter loss from fishing mortality, as the reef sites selected are heavily fished by recreational anglers throughout the summer months. Fish selected for surgery were transferred from the holding tank to a surgery tank containing a mixture of sea water and Aqui-S anesthetic ( $20 \text{ mg L}^{-1}$ ; active ingredient clove oil). Fish were deemed sufficiently anesthetized when pectoral fin and operculum movement slowed and individuals could no longer maintain equilibrium. Once sufficiently anesthetized, individuals were transferred to a sling, lined with synthetic foam to minimize damage to fins and epithelium, and while the head and gills remained immersed, a 1-cm incision was made cranial to the vent, and just lateral to the midline. One V-9 2H

acoustic transmitter was inserted through the incision and was closed with 1-2 single surgical-knot sutures. Post-surgery fish were transferred back to the holding tank to monitor for recovery, which was identified when regular operculum movement and equilibrium resumed. At the Middle and Northern sites, barotrauma was observed owing to greater depths. To promote recovery and reduce the risk of surface depredation by birds and large fishes, recovered fish were descended to half depth (~15 m) using a pressure-release device (Seaqualizer ©) at the site of their capture.

#### *Oceanographic model outputs*

Oceanographic variables associated with storms were predicted from the Finite Volume Community Ocean Model (FVCOM). The FVCOM is a three-dimensional unstructured grid hydrographic model, that consists of momentum, continuity, temperature, salinity, and density equations (Chen et al. 2003; Lee et al. 2016). The model is physically and mathematically closed and utilizes sigma-coordinate transformations and unstructured triangular cells to maximize the quality of estimates over irregular coastlines, such as those prevalent in coastal shelf or estuarine systems like the Mid-Atlantic Bight (Chen and Liu. 2003; Lee et al. 2016; Zhang et al. 2017). The model was configured for the MAB region, with the eastern boundary located approximately at 70 W, and the northern and southern boundaries located at approximately 42 N and 34 N, respectively. Initial conditions of salinity and temperature for the FVCOM were based on predictions from the Regional Ocean Modeling System (ROMS) Experimental System for Predicting Shelf and Slope Optics (ESPreSSO) model. The FVCOM was run from August 25 to December 31, 2016, and from January 1 to December 31 for 2017 and 2018. The model was

configured, optimized, and executed by the Li lab (M. Li and F. Zhang; Horn Point Laboratory, Cambridge, MD; Zhang et al. 2017). During summer 2019, I worked with this laboratory to develop simulations and evaluate model output.

Time series data on modeled bottom water temperature, current velocity, and turbulent kinetic energy (TKE) were extracted at hourly time-steps, for the duration of receiver deployment during each year of study for each site. Bottom water temperature was selected as an indication of cold pool destruction/recovery and potential physiological stress; current velocity was selected as an indication of physical hydrodynamic forcing and potential physical stress owing to the need for increased energy devoted to station-keeping; and TKE was selected as an indication of both destratification and physical shear between water parcels, as well as an additional potential physical stress. Time series of all three variables were predicted at each receiver location (Table 2.1) at hourly intervals, then averaged to yield mean hourly predictions per site. Time series data on modeled wind speed and direction were extracted at three-hour time-steps. Cross sectional and bottom (1 m from sea bed) measurements of triangulated grid-point estimates of bottom water temperature, current velocity, and TKE were also obtained. Estimated lateral measurement dimensions extended across the shelf in the DelMarVa region of the MAB; estimated cross-sectional measurements were taken along a 39 km transect that bisected the Middle study site (Figure 2.1). The model's precision was evaluated through comparisons to observed bottom water temperatures obtained through this study's acoustic receiver array (Appendix A).

*Storm identification*

Storms were initially identified through observations of rapid increases in observed bottom water temperature from acoustic receiver measurements, as well as from rapid, sustained increases in wind speed identified from observed wind fields. Peak winds, which are often used in storm warnings, varied substantially and do not convey information on storm duration. Therefore, storm presence and duration was subsequently defined as hours during which observed wind speeds occurred at sustained, consecutive magnitudes  $> 5 \text{ m s}^{-1}$ . Both named and unnamed events were considered, as well as those storms formally tracked by weather services (such as NOAA National Hurricane Center, or Ocean City WeatherUnderground) and those storms that were not formally tracked but still demonstrating threshold wind speeds. Following identification of storm presence and duration, modeled cross-sectional and lateral estimates of bottom water temperature, current velocity, and TKE were plotted and compared across the days before, during, and after each storm event.

*Data analysis: Movement behavior*

Telemetry data were analyzed for changes in local and broad-scale movement behaviors relative to dates of storm presence and maximum modeled wind speeds observed during each storm event. Analysis of local movement behaviors included the calculation of movement indices from logged detection data per individual fish, where the hourly movement index is equal to the average number of movements detected by consecutive unique receivers per hour. These movement indices were then aggregated across tagged fish within each site to provide a site activity index. Activity indices across sites were evaluated for each year, using an analysis of variance (ANOVA) test comparing activity indices across storm periods and nested

by site. Each year an initial baseline period (no storm) was compared to subsequent storm periods, defined as the period between onset of a particular storm and terminating prior to the onset of any ensuing storm. Post hoc multiple comparisons of activity indices across storm periods were conducted using Tukey contrasts. Individual movement and site-wide activity indices were calculated using the *TelemetryR* (O'Brien 2018) package in R; ANOVA tests and multiple comparisons were accomplished using the *car* (Fox and Weisberg 2019), *lme4* (Bates et al. 2015), and *multcomp* (Hothorn et al. 2008) packages in R.

Broad-scale movements and subsequent departures from study sites (aka evacuations) were evaluated by calculating instantaneous tag loss rates, and by using an autoregressive integrated moving average (ARIMA) time series intervention analysis (Secor et al. 2019). The percent absolute loss rate was calculated as the back-transformed percentage of the instantaneous tag loss rate. The ARIMA intervention analysis was selected as it facilitates the identification of an intervention, or of a single point within a time series that significantly alters the behavior of the rest of the time series, using a statistical t-test. This approach allows discrimination of “false” evacuations caused by acoustic interference caused by storms. Strong coastal storm events are capable of generating substantial noise owing to wind, wave action, or cavitation (Wenz 1962; Appendix B), which can diminish reception of transmitter signals. For this study, the intervention analysis was applied to a time series of transmitter presence, or the last day a unique transmitter was detected at its respective study site. The analysis tested for the presence of two types of interventions: (1) temporary shift interventions: points in the time series after which pre-intervention

time series behavior resumed; and (2) permanent level shifts: points in the time series after which the time series behavior was permanently altered. Intervention analyses were applied to transmitter loss time series for each site, across all years, and compared. Where the ARIMA model was able to converge, the modeled time series achieve stationarity. Here, permanent level shifts (stepped declines) are indicative of fish evacuation—interventions that fundamentally and permanently changed the remaining time series. Temporary shift are those interventions that altered the time series temporarily and appear as nonlinear returns to the previous detection level (see Figure 2.12). When the ARIMA model did not converge on stationarity, departures owing to permanent or temporary shifts could not be accurately discriminated. This occurred for three out of the nine time series. This analysis was carried out in R, using the *tsoutliers* package (López de Lacalle 2019).

The explanatory relationship between local activity levels and individual storm variables (Table 2.4) was explored using a Generalized Additive Model for Location, Scale, and Shape (GAMLSS). Telemetry data and predicted FVCOM output for 2017 supported analysis of the effects of multiple storm events and their cumulative impact as consecutive events (only a single storm event was identified in 2016 and 2018). Daily average movement index was the response variable, with predictors: daily average TKE, observed daily average bottom water temperature, and differenced modeled daily average current velocity, accumulated number of storm days (ANSD: the time series of total unique storm days throughout the study period), the sex of the tagged individual, and the length of the tagged individual. Due to a paucity of data points over time, site was excluded from the GAMLSS model, and



tested separately in a nested ANOVA. Unique transmitter code (individual fish) was incorporated as a random effect, and lagged response variables were incorporated to account for temporal autocorrelation of the response. The model was fit with a log mu link function—or an inherent transformation built into the model that exponentiates linear predictors—and with a generalized gamma distribution, then run for 400 iteration cycles. Prior to fitting the final model, numerical variables were iteratively incorporated and compared in various model structures containing raw, lagged, or differenced forms (i.e., TKE, bottom temperature, and current velocity) to assist with the detection and minimization of collinearity. Although these parameters are necessarily related—particularly the FVCOM-derived current velocity and TKE variables—substituting and comparing lagged, differences, and raw forms allowed greater differentiation of independence across these processes. Lagged, differenced, and raw variables were subsequently tested for collinearity by calculation and comparison of variable inflation factors and comparison of additional correlation matrices. All final, non-collinear numerical response variables were centered and scaled prior to incorporation in the final model. Model selection was based on lowest Akaike information criterion (AIC). All analysis for model development was completed in R, using the *car* (Fox and Weisberg 2019), *lme4* (Bates et al. 2015), *gamlss* (Rigby and Stasinopoulos 2005) and *forecast* (Hyndman and Khandakar 2008; Hyndman et al. 2019) packages.

## Results

### *Storm events and destratification*

Six storm events varying in timing, duration (33-87 hr), and intensity (maximum windspeed 13.4-16.6 m s<sup>-1</sup>) occurred between June-October of 2016-2018 (Table 2.5). The six storms were identified as (1) Tropical Storm Hermine, with peak windspeeds on September 3, 2016; (2) a Nor'easter, with peak windspeeds on July 29, 2017; (3) Potential Tropical Cyclone 10 (PTC10), with peak windspeeds on August 30, 2017; (4) Tropical Storm Jose, with peak windspeeds on September 19, 2017; (5) Tropical Storm Maria, with peak windspeeds on September 27, 2017; and (6) an unnamed wind event, with peak windspeeds on September 9, 2018. Observed bottom water temperature showed rapid increases over the course of the first several hours following storm arrivals, indicative of wind-driven mixing and destratification of the water column (Figure 2.2).

Patterns in observed bottom water temperatures showed a differential impact of storm-driven destratification across years and sites. In both 2016 and 2018, one significant storm disturbance was identified (Figure 2.2). During both years, prior to storm-induced increases in windspeed, cold pool temperatures remained relatively stable at 12.5-16.9 °C, particularly evident at the Northern and Middle sites. Moderate excursions occurred prior to large destratification events observed in September of both years. Associated storm events, TS Hermine in 2016 and the unnamed wind event in 2018, precipitated permanent destratification and increases in temperatures that ranged from 5.7 to 10.9°C ( $8.9 \pm 1.6^\circ\text{C}$ ) between sites and years. During 2017, multiple storm events occurred, with a destratification event during August, recovery of stratification at two sites, then subsequent cycles of destratification and restratification during September. Note that this pattern of

decreasing bottom water temperature and restratification of the water column did not occur at the Southern site, which was also the shallowest (approximately 21.06 m across years) and warmest site. Here, following August destratification, water temperatures remained elevated and the cold pool did not recover.

*Storm characterization: Modeled variables*

Based on average wind vectors, the observed storms were categorized in terms of intensity and duration, yielding two classes of comparatively stronger storms vs. more moderate storms. The more intense storms occurred in 2016 and 2017, while 2018 experienced a comparatively milder storm event. In 2016 and 2017, TS Jose, PTC10, and TS Hermine brought in the highest gusting windspeeds (16.6, 16.3, and 15.3 m s<sup>-1</sup>, respectively), while TS Maria, PTC10, and TS Hermine exhibited the longest duration (87, 81, and 81 hr, respectively) (Figure 2.3; Table 2.5). Conversely, the July nor'easter that occurred in 2017 reached a maximum windspeed of 14.8 m s<sup>-1</sup>, lasting for only 33 hr; similarly, in 2018, the unnamed wind event reached peak windspeeds of 14.3 m s<sup>-1</sup> and continued 45 hr (Figure 2.3; Table 2.5). Across all years, however, modeled storm directional wind vectors indicated a predominance of northwesterly winds directed along shore.

Modeled time series estimates of bottom water temperature, current velocity, and TKE peaked rapidly around periods of storm arrival and maximum storm-induced wind speed (Figure 2.4a-c). The model successfully captured permanent destratification owing to storm events in 2016 (Figure 2.4a) and 2018 (Figure 2.4c), as well as the recovery and gradual increase in temperatures following repeated storm events in 2017 (Figure 2.4b). Storm-driven excursions for current velocity and TKE,

on the other hand, were relatively high (velocity: 0.1-0.2 m s<sup>-1</sup>; TKE: 0.0005-0.003 m<sup>2</sup> s<sup>-2</sup>); and short-lived (10-25 hr), across all years, with little difference in baseline levels before and after storm events. Observed noise indices also showed short-term increases in power (dB re:  $\mu\text{Pa}^2/\text{Hz}$ ) and sound pressure level (dB re: 1  $\mu\text{Pa}$ ) associated with storm events, within the expected optimal hearing range of black sea bass (50-800 Hz; Chapter 3; Appendix B).

Storm destratification events encompassed major portions of the shelf environment (Figures 2.5-2.8). Spatial depictions of FVCOM outputs captured a range of destratification responses to storms across the shelf's spatial extent and depth range. In years when single events caused permanent destratification (2016 and 2018), mixing lagged approximately 1-2 days after peak wind speeds were reached (Figure 2.5); days after the storm passed, the cold pool remained intact farther offshore, with inshore bottom waters increased by 10-15 °C. Modeled bottom temperature for these single-storm years showed destratification extending towards mid-shelf waters (~30-35 m depth; Figure 2.6). The cold pool shifted offshore, where it remained for the rest of the summer-fall season. Stratification during 2017 (Figure 2.7) exhibited a complex cycle of cold pool restratification. After the July nor'easter, the cold pool recovered. Following PTC10, the cold pool recovered more slowly and to a lesser extent. The third storm—TS Jose—caused permanent destratification. Similarly, bottom water temperatures for 2017 showed a gradual retreat by the cold pool farther from shore, with permanent destratification occurring after TS Jose (Figure 2.8). Storm-driven spatiotemporal estimates of current velocity and TKE were ephemeral (see additional figures in Appendix A).

*Movement analysis: Observed activity and evacuation behavior*

During all years, significant changes in local activity and evacuation rates from reef sites were observed in the wake of storm events. Local activity indices were significantly different across all sites before and after single storm events for each year (Figure 2.9). In 2016 and 2018, activity at all sites was significantly lower, by approximately 50%, during the periods of time following TS Hermine and the unnamed wind event, respectively, than during the periods before these storms (ANOVA,  $p < 0.001$ ; Tukey,  $p < 0.001$ ). During 2017, activity indices were significantly different across all sites during combined periods of time before and after PTC10, with activity declining persistently across sites and during the time following that storm (ANOVA,  $p < 0.01$ ; Tukey,  $p < 0.01$ ). Again, activity was reduced by approximately 50%.

Observations of transmitter loss over time indicated a steady decline in the number of unique tags present at each site over each year of study, modeled through exponential decay (Table 2.6). During 2016 and 2018, the Southern site had the lowest loss rates ( $< 1\% \text{ d}^{-1}$ ), while during 2017 the instantaneous loss rate was higher ( $2\% \text{ d}^{-1}$ ) than either the Middle or Northern sites ( $1.5\% \text{ d}^{-1}$ ). Instantaneous loss rates at the Middle site were highest during all years except for 2017, when the rate was equal to that at the Northern site. Averaged across years, 2018 had the lowest loss rate ( $1\% \text{ d}^{-1}$ ), followed by 2016 ( $1.3\% \text{ d}^{-1}$ ) then 2017 ( $1.7\% \text{ d}^{-1}$ ).

Significant increases in the number of fish evacuating reef sites were identified during days of peak storm wind speed for storm events during all years. Rapid declines were noted for some but not all storm events (Figure 2.10). In 2016

and 2018, the highest incremental rates of transmitter loss overlapped directly with September storm events. In 2017, the Northern site exhibited sharp declines in unique transmitter detections associated with the second and third storm events. Results of the more formal ARIMA intervention analysis indicated event-driven, permanent declines in fish presence at all sites during all years (Figures 2.11-2.13). Permanent level shifts were identified at the Northern and Middle sites during 2016, with the time series changing significantly the day after TS Hermine's wind speeds peaked (Figure 2.11). In 2017, permanent level shifts were also identified during the July nor'easter (at the Middle and Southern sites), the PTC10 (at all sites), and immediately before peak winds arrived for TS Jose (at the Northern site) (Figure 2.12). Lastly, a permanent level shift at the Southern site was identified during the date of maximum wind speed associated with 2018's unnamed wind event (Figure 2.13). The ARIMA intervention analysis was unable to converge for the tag loss time series taken from the Southern site during 2016 and the Middle site during 2018; inferences related to evacuation were thus not possible for these events (Figure 2.11, 2.13). For the Northern 2018 time series, the *forecast* function utilized to detect ARIMA components failed to detect significant interventions, which again precluded inferences related to storm-driven evacuations. Still, in the case of the Southern site during 2016 and the Middle site during 2018 cases, large excursions in the raw time series coincided with storm events.

*Movement analysis: Coupled telemetry-FVCOM mixed effects model*

As predicted, changes in bottom water temperature had the greatest and most significant negative impact on movement index ( $\mu=-0.217$ ;  $p < 0.01$ ; where  $\mu$  is the

direction and magnitude of the fitted response), but, contrary to expectations the model failed to detect a significant effect of consecutive cumulative storm impacts, ANSD ( $\mu=0.002$ ;  $p=0.84$ ) (Table 2.7). Modeled TKE ( $\mu=-0.168$ ;  $p<0.01$ ) was also influential in the model, with modeled current velocity showing a modest influence ( $\mu=-0.099$ ;  $p<0.01$ ). A significant negative effect was also identified for fish length ( $\mu=-0.19$ ;  $p<0.01$ ), although it did not directly relate to storm influence on movement. Both males ( $\mu=0.617$ ;  $p<0.01$ ) and unidentified individuals ( $\mu=0.683$ ;  $p<0.01$ ) were predicted by the model to have higher movement indices than females. While the model did not directly test for the presence and magnitude of interactions between sex and size, the distributions of movement indices across tagged individuals suggested an interaction, where males had higher movement rates for their size than females (Appendix A, Figure A.8: 2017 data only). Males only occurred at lengths  $> 270$  mm but many females also occurred at this size. Still, an overall negative effect of length on movement holds across the entire sample.

Autoregressive moving average components analysis indicated the presence of autocorrelation within the response variable, lagged by 1 and 2 days. These components were incorporated as additional numerical predictors, and both were found to be statistically significant (Table 2.7). Table and figure summaries of the model quantile residuals can be found in Appendix A.

Results of an ANOVA testing the fixed effect of site on movement index, with transmitter incorporated as a random effect, found a significant effect of site on movement (ANOVA;  $p<0.01$ ). The Middle site exhibited lower movement indices

than the other sites (Tukey contrasts;  $p < 0.01$ ). Contrasts between the Northern and Southern sites were not significant ( $p = 0.97$ ).

### Discussion

By coupling fine-scale telemetry and oceanography, this study demonstrated that storm disturbance was a key driver of seasonal movement behaviors by black sea bass in the shelf waters of the MAB. My results indicate that the series of summer storms observed in 2016-2018 varied in intensity, duration, and timing; and had significant, recurring effects on black sea bass habitat conditions, which often caused large changes in their movement ecology.

Results supported my initial hypotheses that storms impact black sea bass habitat through shifts in temperature, current velocity, and turbulent kinetic energy; that these storm-driven environmental changes are associated with changes in movement behavior; and that these storm-driven changes in movement are caused primarily through rapid increases in bottom water temperature. In the multi-storm year, 2017, I failed to detect a relationship between cumulative consecutive storm days (ANSD) and depressed movements, but rather observed that depressed movement occurred as a threshold response to a late season storm, similar to what occurred in other study years. This effect of late season storm disturbance occurred across all the three sites and resulted in an approximately 50% decreased activity level, which in most instances was also associated with incomplete evacuations. Movement patterns also covaried by length and sex variables. Males had higher movement levels (independent to storm effects), a result previously reported in the NY Bight by Fabrizio et al. (2014).



Rapid change in bottom water temperature associated with destratification was the predominant driver of shifted movement behaviors during storm events. Storm disturbances incurred significant changes in local and broadscale movement behavior that depended on the timing of the storm during that year's season, as well as the relative stability of the cold pool. Early summer storms (such as the July nor'easter of 2017) did not incur permanent stratification, nor were they associated with changes in movement metrics or evacuations across sites. Storms that occurred later in the year, however, (such as TS Hermine in 2016, PTC10 in 2017, and the unnamed wind event in 2018), triggered permanent breakdowns of the cold pool and destratification of the water column. As such, these storms caused significant declines in activity levels as well as higher numbers of fish evacuating reef habitats across sites. The mechanism driving the impact of these later-season storms on stratification—and subsequently fish movement—was not identified during this study. Higher degrees of surface heating, and thus higher magnitudes of water column instability, however, might occur during late summer and early fall, preconditioning cold pool destruction (Beardsley et al. 1985; Lentz et al. 2003).

Evacuations are an extreme faunal response to catastrophic change (Gunn and Crocker 1951; Waide 1991; Wauer and Wunderle 1992; Secor 2015), yet occurred in each year of my study. Biotelemetry detections can be biased low during storm events when ambient noise interferes with detection of transmitted signals. Across years, I conducted analyses robust to this source of bias through an ARIMA intervention analysis, and observed that in all years, late season storms were associated with permanent evacuations. However, in 2017, where multiple storm disturbances

occurred, no evacuations were observed during storms that followed the permanent destruction of the cold pool. The number of evacuations across sites peaked with PTC10 in August (when permanent destratification occurred), with a smaller level of evacuations associated with TS Jose in early September (when destratified bottom water temperatures increased and plateaued). Evacuations were not observed during storm activity following cold pool destratification, with the passage of TS Maria. This suggests a disturbance threshold to black sea bass was met with the permanent destruction of the cold pool and sustained elevation of bottom water temperature—despite the later season Maria incurring similar increases in TKE and current velocity, and having the longest duration observed out of all of the 2016-2018 storms (87 hr). The observed patterns in evacuation rates and the 2017 ARIMA intervention analysis complement the results of the explanatory GAMLSS analysis, which also identified temperature as the dominant variable negatively impacting local movements and did not identify ANSD as significantly impacting movement. Such carryover effects of one storm disturbance mitigating—or preconditioning—the water column impacts of next has also been showed for the North Pacific Ocean. In a numerical model, Baranowski et al. (2014) showed how a mid-September typhoon dampened the destratification potential of a later mid-October typhoon in the Western North Pacific.

Site differences in water column stability were apparent and related to depth and proximity of the cold pool front, similar to findings by Lentz et al. (2003), who examined cold pool thermal structure in the MAB over repeated wind stress events. The cold pool front, which separates offshore-stratified water from inshore-mixed water, extends along the continental shelf in waters ranging between 30 m and 100 m

deep (Houghton et al. 1982; Chen et al. 2018). The front is bound in the north by Nantucket Shoals and the southern perimeter of Georges Bank, and meets mixed inner shelf waters at the 40 m isobath; the front is bound in the south towards the mouth of Chesapeake Bay and Cape Hatteras at the 30 m isobath (Houghton et al. 1982; Lentz 2017). The Southern site was located in the shallowest waters and on the fringe of the front, and thus showed the highest level of bottom water temperature variance and associated water column instability. The Middle site was located in the deepest waters; the Northern site was also located in deeper water, and showed temperature changes more similar to the Middle site in comparison to the Southern site. In accordance with proximity to the cold pool front, I observed the smallest storm-driven change in bottom water temperatures at the Southern site, and the greatest change at the Middle site.

Our results may suggest that fish inhabiting reefs with more stable temperature dynamics are less likely to change residency time or local movement patterns than fish inhabiting reefs with less stable temperature dynamics. The lowest rates of transmitter loss and the lowest number of evacuations occurred at the Southern site for all years. I argue that these patterns were driven by the Southern site's comparatively shallow depth and location on the fringe of the cold pool; these features caused this site to demonstrate a less severe temperature gradient and subsequent lower magnitude of destratification than that occurring at the deeper Northern and Middle sites. Similarly, the ANOVA results comparing 2017 movement indices across sites identified the greatest difference in movement between the Middle vs. Northern and Southern site. Again, this difference is likely related to the

interaction of depth with cold pool presence. As the Middle site is located at the deepest depths and farthest beyond the cold pool front, it experiences the highest magnitude temperature difference following cold pool destruction. It also experiences the least stable recurring oscillation in bottom water temperature between cold pool destruction and recovery with each storm event, until permanent destratification occurs.

A similar pattern of storm-driven destratification impacting the local activity of a demersal fish species was observed by Fabrizio et al. (2005), Fabrizio et al. (2013), and Fabrizio et al. (2014) in the NY Bight, where the authors conducted a large acoustic telemetry study on a proposed refuse site, evaluating habitat use of black sea bass and summer flounder. Although not the focus of their study, data summaries of that research permits some inferences on the effects of storms on evacuations and movement behaviors. During this study, Hurricane Isabel passed through the receiver array on September 19, 2003, with peak windspeeds of  $20.1 \text{ m s}^{-1}$  observed at Sandy Hook, NJ, which triggered permanent destratification and increased bottom water temperatures (approximately  $13^{\circ}\text{C}$  in 12 hr) (Beven and Cobb, 2004; Fabrizio et al. 2005, their Figure 15). This storm also caused a rapid and prolonged depression in bottom salinity (indicative of mixing) as well as short-lived peaks in wave orbital velocity (shear scaled to the effect of wave energy on fluid particle oscillation). Estimates of evacuation probabilities estimated through Kaplan Meier hazard analysis by Fabrizio et al. (2005) did not exhibit the same strong episodic losses associated with storm events as I detected. Rather, evacuations by black sea bass occurred in later pulses, principally in October. In contrast, summer

flounder did show evidence of a particularly strong loss in tagged fish from the site coincident with Isabel. A large majority of fish (8/11) departed during the September 2-20 period. In a separate analysis examining home range and movement levels at the same site, Fabrizio et al. (2014) reported large declines in late season movement activities. The authors defined movement indices as a binary metric of 0 or 1, indicating whether or not a fish moved between adjacent receivers during a three-hr period, a measure with similar intent to that used in my analysis. Whether seasonal changes in movement were associated with cooling bottom temperature, seasonal migratory cues, or Hurricane Isabel (the latter not deliberately considered in their analysis) cannot be clearly distinguished from their analysis.

Storm-driven changes in movement and evacuation behaviors by black sea bass likely have broader ecological consequences. Here and elsewhere, storms have been shown to impact the movement behaviors of coastal fish species across diverse taxa (Heupel et al. 2003; Bailey and Secor 2016; Secor et al. 2019; Bachelier et al. 2019). Reduced movement behavior has been linked to short term reductions in feeding rate and encounter rates with optimal foraging habitats, as well as long term decreases in growth and fecundity (Werner and Peacor 2003; Preisser and Bolnick 2008; Strobbe et al. 2011). Black sea bass are known to show small home ranges on structured habitats (0.137-7.364 km<sup>2</sup>, Fabrizio et al. 2014), where they feed on reef associated prey items (Sedberry et al. 1988; Mercer and Moran 1989; Appendix C), although Steimle and Figley (1996) observed that black sea bass likely foraged on sandy bottom areas adjacent to reef habitat (Cullen and Stevens 2017). Reproduction has been observed to occur during September-October (Mercer and Moran 1989),

which could cause storms to disrupt spawning activity as fish are induced to become less active. However, no gonadosomatic indices of fish sampled during October indicated a capacity to spawn (Appendix C), suggesting that storms during 2018 occurred after reproduction occurred.

Longer-term carryover effects owing to disruptions to activity and site fidelity caused by storm-induced destratification include changed timing in fall-winter migrations and regional shifts in summer habitats. These longer-term consequences are relevant in the context of a changing climate, which predicts an increased frequency of high-energy storm events in the NW Atlantic Ocean (Knutson et al. 1998; Lin et al. 2012; Vermaire et al. 2013; Holland and Bruyère 2014). A possible outcome of increased high-energy storms in the MAB, depending on their timing and tracks, could be long-term changes to the timing, location, and stability of the cold pool (Houghton et al. 1982; Chen et al 2018). This in turn could influence range shifts and seasonal timing of offshore migrations of black sea bass and other demersal species in the MAB. As an initial expectation, one might predict that the cold pool will shift northward and towards deeper waters with increased frequency of high-intensity storms; these storms can be predicted to permanently destratify the water column earlier in the summer-fall season and perhaps prompt earlier winter migrations by MAB black sea bass. That these dynamics might occur elsewhere and affect other species is suggested by the impacts of Hurricane Isabel on the early dispersal of winter flounder in the NY Bight (Fabrizio et al. 2005).

Beyond the direct influences of storms on demersal fish ecology, storms also impact fisheries and assessment activities on those same species. Storms in the Gulf

of Mexico have negatively impacted commercial harvest of grouper (Solís et al. 2013), shrimp, and oyster (Pettersen et al. 2006) fisheries through destruction of fishing infrastructure and habitat. Increased freshwater input in North Carolina during Hurricane Floyd led to dense blue crab aggregations, which rendered the population susceptible to subsequent overfishing, as well as increased loss of bay scallop yield to the fishery (Bin et al. 2007). Assessment of species abundance for management can also be impacted when survey vessels cannot operate in high seas during fall storms (B. Frey, CBL, pers. comm.).

A priority assessment focus in shelf ecosystems is evaluating the impacts of wind farm development. Wind tower construction and maintenance impacts will likely concur with natural storm disturbances. Stresses related to wind tower construction can include sound caused by piledriving or vessel operation (Wahlberg and Westerberg 2005; Thomsen et al. 2006; Casper et al. 2013), alterations to local electromagnetic fields (Öhman et al. 2007; Gill et al. 2012); or, altered distribution of local benthic and demersal species through the emplacement of additional structured habitat (Andersson and Öhman 2010; Bergström et al. 2013; Stenberg et al. 2015 ). Each of these stresses can interact with storm disturbance, obscuring or enhancing impacts associated with wind tower construction alone. Likely responses to pile driving include changes in local (on-reef) and broad-scale (off-reef) movements (Popper and Hastings 2009). Increased vessel noise has also been identified as a potential source of physical and behavioral disturbance (Slabbekoorn et al. 2010), with studies demonstrating avoidance of areas with high vessel activity by herring (Vabø et al. 2006) and disruption of schooling behavior in response to vessel activity

by bluefin tuna (Sarà et al. 2007). In summary, offshore wind farm baseline and impact monitoring should include the effect of storms as a dominant source of year-to-year disturbance.

Key limitations to my findings relate to study design, including assumptions that (1) the three-receiver array sufficiently overlapped with the distribution of black sea bass at each reef site; and (2) that movement rates were realistically indexed as unique movements between receivers. The study design did not adjust for site differences in reef dimensions and how the different sites may have functioned different as habitats for refuge, forage, and reproduction (Steimle and Figley 1996; Steimle and Zetlin 2000; Fabrizio et al 2014). Where fish were caught and released may have also caused differences in how well their home ranges were represented across sites and years. Importantly, this study did not account for changes in vertical movement behaviors in response to storm disturbances. A strong expectation in the literature is that disturbed reef fishes become more tightly coupled to structure (Lassig 1983; Williams 1984; Syms and Jones 1999) Unpublished data from a 2019 biotelemetry study at the Northern site did indeed show that black sea bass implanted with depth-pressure transmitters used deeper habitats and showed less vertical movements following an August storm-destratification event (D. Secor, CBL, pers. comm.).

A key assumption was that daily synchrony between peaks in storm winds and tag losses were evidence for storm-driven evacuations, while slower decays in tag presence resulted from seasonal departures or predation. Despite the episodic losses associated with storm events, these cannot definitively distinguish evacuation from



seasonal emigration into deeper shelf habitat. Additional sources of uncertainty include tag loss unrelated to storm-driven evacuation, such as predation or capture of tagged individuals by anglers. Tagged fish were vulnerable to predation immediately following their surgery and release, but by releasing them at depth, risk of surface depredation by birds and fishes (e.g., sharks) was eliminated. Although I targeted sublegal fish for tagging, larger individuals likely grew into the legal size limit during each year's study period; additionally, anglers may have incidentally retained some sublegal fish.

Future research can address the integral role of storm disturbance in shaping demersal fish species' movement ecology in the MAB by incorporating more fine-scaled measures of movement behaviors, which occur during high energy wind events. Improvements to account for 3D motion could include the use of multiple strategically placed receivers that triangulate transmitter position in the water column, as well as by deploying depth-recording transmitters. Additional efforts should also be made to better characterize reef habitats in greater detail, so as to better understand the use of such habitats during storm response, and how certain habitats might be more prone to evacuation behaviors. These differences in reef structure—and how these differences impact habitat use and movement behavior—may then also be accounted for by better telemetry receiver array designs. Improved designs might incorporate a larger number of receivers over habitat gradients, thus facilitating census counts of tagged fish at a finer spatial resolution (similar to the array design employed by Fabrizio et al. 2014).

Future research would also be improved by examining storm variables and movement behaviors of black sea bass at other regions in the Western Atlantic, across differing reef habitats and through deployment of replicate census-oriented receiver arrays; this replication of a common study design across differing habitat gradients would inform this study's expectation that storm disturbance is an integral feature to the movement ecology and habitat use of demersal fish species. Also important are longer term, multi-year telemetry studies that can capture how storms shape the full seasonal evolution of the cold pool in the MAB (Lentz et al. 2003), and related responses by demersal fish communities. Finally, natural cues to evacuation and migration warrant investigation. Valuable additional methods may include otolith stable isotope analysis (Sturrock et al. 2012) and hormone signals (Leatherland 1982). Both methods, with increased sampling over the summer-winter season, would provide an opportunity to compare chemical tracers of fish movement immediately prior to and following migration, as well as explore the relationship between internal migratory cues vs. external evacuation cues.

## References

- Andersson, M. H., & Öhman, M. C. (2010). Fish and sessile assemblages associated with wind-turbine constructions in the Baltic Sea. *Marine and Freshwater Research*, *61*, 642-650.
- Araga, C., & Tanase, H. (1966). Fish stranding caused by a typhoon in the vicinity of Seto. *Publications of the Seto Marine Biological Laboratory*, *14*(2), 155-160.
- Atwood, H. L., Young, S. P., Tomasso, J. R., Jr., & Smith, T. I. J. (2001). Salinity and temperature tolerances of black sea bass juveniles. *North American Journal of Aquaculture*, *63*, 285-288.
- Bacheler, N. M., Shertzer, K. W., Cheshire, R. T., & MacMahan, J. H. (2019). Tropical storms influence the movement behavior of a demersal oceanic fish species. *Scientific Reports*, *9*(1481), 1-13. <https://doi.org/10.1038/s41598-018-37527-1>
- Bailey, H., & Secor, D. H. (2016). Coastal evacuations by fish during extreme weather events. *Scientific Reports*, 1-9. <https://doi.org/10.1038/srep30280>
- Bates, D., Maechler, M., Bolker, B., Walker, S. (2015). Fitting Linear Mixed-Effects Models Using lme4. *Journal of Statistical Software*, *67*(1), 1-48. <[doi:10.18637/jss.v067.i01](https://doi.org/10.18637/jss.v067.i01)>.
- Baranowski, D. B., Flatau, P. J., Chen, S., & Black, P. G. (2014). Upper ocean response to the passage of two sequential typhoons. *Ocean Science*, *10*, 559-570. <https://doi.org/10.5194/os-10-559-2014>
- Beardsley, R. C., Chapman, D. C., Brink, K. H., Ramp, S. R., & Schlitz, R. (1985). The Nantucket Shoals Flux Experiment (NSFE79). Part I: A basic description of the current and temperature variability. *Journal of Physical Oceanography*, *15*, 713-748.
- Beven, J., & Cobb, H. (2004, July). *Tropical cyclone report: Hurricane Isabel*. National Hurricane Center.
- Bergström, L., Sundqvist, F., & Bergström, U. (2013). Effect of an offshore wind farm on temporal and spatial patterns in the demersal fish community. *Marine Ecology Progress Series*, *485*, 199-210. <https://doi.org/10.3354/meps10344>
- Bigelow, H. B. (1933). Studies of the waters on the continental shelf, Cape Cod to Chesapeake Bay, I, The cycle of temperature. *Papers in Physical Oceanography and Meteorology*, *11*(4), 1-134.

- Bin, O., Dumas, C., Poulter, B., & Whitehead, J. (2007, March). *Measuring the impacts of climate change on North Carolina coastal resources*. Washington DC, USA: National Commission on Energy Policy.
- Bouchon, C., Bouchon-Navaro, Y., & Louis, M. (1994). Changes in the coastal fish communities following Hurricane Hugo in Guadeloupe Island (French West Indies). *Atoll Research Bulletin*, (422), 1-19.
- Byrnes, J. E., Reed, D. C., Cardinale, B. J., Cavanaugh, K. C., Holbrook, S. J., & Schmitt, R. J. (2011). Climate-driven increases in storm frequency simplify kelp forest food webs. *Global Change Biology*, *17*, 2513-2524.  
<https://doi.org/10.1111/j.1365-2486.2011.02409.x>
- Casper, B. M., Smith, M. E., Halvorsen, M. B., Sun, H., Carlson, T. J., & Popper, A. N. (2013). Effects of exposure to pile driving sounds on fish inner ear tissues. *Comparative Biochemistry and Physiology, Part A*, *166*.  
<https://doi.org/10.1016/j.cbpa.2013.07.008>
- Chen, C., & Liu, H. (2003). An unstructured grid, finite-volume, three-dimensional, primitive equations ocean model: Application to coastal ocean and estuaries. *Journal of Atmospheric and Oceanic Technology*, *20*, 159-186.
- Chen, Z., Curchitser, E., Chant, R., & Kang, D. (2018). Seasonal variability of the cold pool over the Mid-Atlantic Bight continental shelf. *Journal of Geophysical Research: Oceans*, *123*, 8203-8226.  
<https://doi.org/10.1029/2018JC014148>
- Coastal Fisherman. (2012, September 19). Straight from the Maryland DNR fisheries service. Retrieved November 15, 2019, from Coastal Fisherman website:  
<https://coastalfisherman.net/issues.cfm?issue=8A13C17C-5056-9F21-090A10DE6EFB925B&story=B2C7507E-5056-9F21-0933D8A161BE1084>
- Colvocoresses, J. A., & Musick, J. A. (1984). Species associations and community composition of Middle Atlantic Bight continental shelf demersal fishes. *Fishery Bulletin*, *82*(2), 295-313.
- Cullen, D. W., & Stevens, B. G. (2017). Use of an underwater video system to record observations of black sea bass (*Centropristis striata*) in waters off the coast of Maryland. *Fishery Bulletin*, *115*(3), 408-418.  
<https://doi.org/10.7755/FB.115.3.10>
- Dollar, S. J., & Tribble, G. W. (1993). Recurrent storm disturbance and recovery: A long-term study of coral communities in Hawaii. *Coral Reefs*, *12*, 223-233.

- Ebeling, A. W., Laur, D. R., & Rowley, R. J. (1985). Sever storm disturbances and reversal of community structure in a southern California kelp forest. *Marine Biology*, 84, 287-294.
- ESS Group Inc. (2016). *Site assessment plan, Maryland offshore wind project* (ESS Project No. U167).
- Fabrizio, M.C., Pessutti, J.P., Manderson, J.P., Drohan, A.F., Phelan, B.A. (2005). Use of the Historic Area Remediation Site by black sea bass and summer flounder. U.S. Dep. Commer., Northeast Fish. Sci. Cent. Ref. Doc. 05-06; 95 p. Available from: National Marine Fisheries Service, 166 Water Street, Woods Hole, MA 02543-1026.
- Fabrizio, M. C., Manderson, J. P., & Pessutti, J. P. (2013). Habitat associations and dispersal of black sea bass from a mid-Atlantic Bight reef. *Marine Ecological Progress Series*, 482, 241-253. <https://doi.org/10.3354/meps10302>
- Fabrizio, M. C., Manderson, J. P., & Pessutti, J. P. (2014). Habitat associations and dispersal of black sea bass from a mid-Atlantic Bight reef. *Marine Ecological Progress Series*, 482, 241-253. <https://doi.org/10.3354/meps10302>
- Fenner, D. P. (1991). Effects of Hurricane Gilbert on coral reefs, fishes and sponges at Cozumel, Mexico. *Bulletin of Marine Science*, 48(3), 719-730.
- Fox, J. and Weisberg, S. (2019). An {R} Companion to Applied Regression, Third Edition. Thousand Oaks CA: Sage.  
URL: <https://socialsciences.mcmaster.ca/jfox/Books/Companion/>
- Gill, A., Huang, Y., Spencer, J., & Gloyne-Philips, I. (2012). *Electromagnetic Fields Emitted by High Voltage Alternating Current Offshore Wind Power Cables and Interactions with Marine Organisms*. Electromagnetics in Current and Emerging Energy Power Systems Seminar, London, UK.
- Ginis, I. (2002). Tropical cyclone-ocean interactions. *Atmosphere-Ocean Interactions, Advances in Fluid Mechanics Series*, 33, 83-114.
- Gunn, W. W. H., & Crocker, A. M. (1951). Analysis of unusual bird migration in North America during the storm of April 4-7, 1947. *The Auk*, 68(2), 139-163.
- Harmelin-Vivien, M. L. (n.d.). The effects of storms and cyclones on coral reefs: A review. *Journal of Coastal Research*, (12), 211-231.

- Heupel, M. R., Simpfendorfer, C. A., & Hueter, R. E. (2003). Running before the storm: Blacktip sharks respond to falling barometric pressure associated with Tropical Storm Gabrielle. *Journal of Fish Biology*, 63, 1357-1363. <https://doi.org/10.1046/j.1095-8649.2003.00250.x>, available online at <http://www.blackwell-synergy.com>
- Hildebrand, J. A. (2009). Anthropogenic and natural sources of ambient noise in the ocean. *Marine Ecology Progress Series*, 395, 5-20. <https://doi.org/10.3354/meps08353>
- Holland, G., & Bruyère, C. L. (2014). Recent intense hurricane response to global climate change. *Climate Dynamics*, 42, 617-627. <https://doi.org/10.1007/200382-013-1713-0>
- Hothorn, T., Bretz, F., and Westfall, P. (2008). Simultaneous Inference in General Parametric Models. *Biometrical Journal* 50(3), 346-363.
- Houghton, R. W., Schlitz, R., Beardsley, R. C., Butman, B., & Chamberlin, J. L. (1982). The Middle Atlantic Bight cold pool: Evolution of the temperature structure during summer 1979. *Journal of Physical Oceanography*, 12, 1019-1029.
- Huang, P., Sanford, T. B., & Imberger, J. (2009). Heat and turbulent kinetic energy budgets for surface layer cooling induced by the passage of Hurricane Frances (2004). *Journal of Geophysical Research*, 114(C12023), 1-14. <https://doi.org/10.1029/2009JC005603>
- Hyndman R. J., Khandakar Y. (2008). “Automatic time series forecasting: the forecast package for R.” *Journal of Statistical Software*, 26(3), 1-22. <http://www.jstatsoft.org/article/view/v027i03>.
- Hyndman R., Athanasopoulos G., Bergmeir C., Caceres G., Chhay L., O'Hara-Wild M., Petropoulos F., Razbash S., Wang E., Yasmeeen F. (2019). *forecast: Forecasting functions for time series and linear models*. R package version 8.9, <http://pkg.robjhyndman.com/forecast>.
- Jackson, J. B. C., & Hughes, T. P. (1985). Adaptive strategies of coral reef invertebrates: Coral reef environments that are regularly disturbed by storms and by predation often favor the very organisms most susceptible to damage by these processes. *American Scientist*, 73(3), 265-274.
- Jury, S. H., Howell, W. H., & Watson, W. H., III. (1995). Lobster movement in response to a hurricane. *Marine Ecology Progress Series*, 119, 305-310.
- Kaufman, L. S. (1983). Effects of Hurricane Allen on reef fish assemblages near Discovery Bay, Jamaica. *Coral Reefs*, (2), 43-47.

- Knutson, T. R., Tuleya, R. E., & Kurihara, Y. (1998). Simulated increase of hurricane intensities in a CO<sub>2</sub>-warmed climate. *Science*, 279, 1018-1020.
- Lassig, B. R. (1983). The effects of a cyclonic storm on coral reef fish assemblages. *Environmental Biology of Fishes*, 9(1), 55-63.
- Leatherland, J. F. (1982). Environmental physiology of the teleostean thyroid gland: A review. *Environmental Biology of Fishes*, 7(1), 83-110.
- Lee, S. B., M. Li, and F. Zhang (2017), Impact of sea level rise on tidal range in Chesapeake and Delaware Bays, *J. Geophys. Res. Oceans*, 122, 3917–3938, doi:10.1002/2016JC012597.
- Lentz, S., Shearman, K., Anderson, S., Plueddemann, A., & Edson, J. (2003). Evolution of stratification over the New England shelf during the coastal mixing and optics study, August 1996-June 1997. *Journal of Geophysical Research*, 108(C1), 1-14. <https://doi.org/10.1029/2001JC001121>
- Lentz, S. J. (2007). Seasonal variations in the circulation over the Middle Atlantic Bight Continental Shelf. *Journal of Physical Oceanography*, 38, 1486-1500.
- Lentz, S. J. (2017). Seasonal warming of the Middle Atlantic Bight Cold Pool. *Journal of Geophysical Research: Oceans*, 122, 941-954. <https://doi.org/10.1002/2016JC012201>
- Li, Y., & Xue, H. (2002). Air-sea interactions during the passage of a winter storm over the Gulf Stream: A three-dimensional coupled atmosphere-ocean model study. *Journal of Geophysical Research*, 107(C11), 1-13. <https://doi.org/10.1029/2001JC001161>
- Lin, N., Emanuel, K., Oppenheimer, M., & Vanmarcke, E. (2012). Physically based assessment of hurricane surge threat under climate change. *Nature Climate Change*, 2, 462-467. <https://doi.org/10.1038/NCLIMATE1389>
- Loftus, A. J., & Stone, R. B. (2007, June). *Artificial reef management plan for Maryland* (Maryland Environmental Service Contract No. 06-07-58).
- López de Lacalle, J. (2019). tsoutliers: Detection of outliers in time series. R package version 0.6-8. <https://CRAN.R-project.org/packages=tsoutliers>
- Maryland Department of Natural Resources. (n.d.). *MARI/Ocean City Reef Foundation Reefs*. Retrieved from [https://dnr.maryland.gov/fisheries/Documents/MARIOC04209postersize\\_with\\_coordinates\\_web.pdf](https://dnr.maryland.gov/fisheries/Documents/MARIOC04209postersize_with_coordinates_web.pdf)

- McPhaden, M. J., Foltz, G. R., Lee, T., Murty, and 5 others (2009). Ocean-atmosphere interactions during Cyclone Nargis. *EOS Transactions American Geophysical Union*, 90(7), 53-60.
- Mercer, L. P., & Moran, D. (1989). *Species profile: Life histories and environmental requirements of coastal fishes and invertebrates (South Atlantic)* (Biological Report No. 82 11.99).
- Michener, W. K., Blood, E. R., Bildstein, K. L., Brinson, M. M., & Gardner, L. R. (1997). Climate change, hurricanes and tropical storms, and rising sea level in coastal wetlands. *Ecological Applications*, 7(3), 770-801.
- Moser, J., & Shepherd, G. R. (2009). Seasonal distribution and movement of black sea bass (*Centropristis striata*) in the Northwest Atlantic as determined from a mark-recapture experiment. *Journal of Northwest Atlantic Fishery Science*, 40, 17-28.
- Musick, J. A., & Mercer, L. P. (1977). Seasonal distribution of black sea bass (*Centropristis striata*), in the Middle Atlantic Bight with comments on the ecology and fisheries of the species. *Transactions of the American Fisheries Society*, 106(1), 12-25. [https://doi.org/10.1577/1548-8659\(1977\)106<12:SDOBSB>2.0.CO;2](https://doi.org/10.1577/1548-8659(1977)106<12:SDOBSB>2.0.CO;2)
- O'Brien, M. H. P. (2019). TelemetryR. R package version 0.9.4. <https://rdrr.io/github/mhpob/TelemetryR/>
- Öhman, M. C., Sigray, P., & Westerberg, H. (2007). Offshore windmills and the effects of electromagnetic fields on fish. *Ambio*, 36(8), 630-633.
- Petterson, J. S., Stanley, L. D., Glazier, E., & Philipp, J. (2006). A preliminary assessment of social and economic impacts associated with Hurricane Katrina. *American Anthropologist*, 108(4), 643-670.
- Preisser, E. L., & Bolnick, D. I. (2008). The many faces of fear: Comparing the pathways and impacts of nonconsumptive predator effects on prey populations. *PLoS ONE*, 3(6), 1-9. <https://doi.org/10.1371/journal.pone.0002465>
- Popper, A. N., & Hastings, M. C. (2009). The effects of human-generated sound on fish. *Integrative Zoology*, 4, 43-52. <https://doi.org/10.1111/j.1749-4877.2008.00134.x>
- Popular wreck dives along our Delaware and Maryland coast. (n.d.). Retrieved from Aqua Ventures Online website: <http://www.aquaventuresonline.com/wrecks.html>



- Pörtner, H. O. (2001). Climate change and temperature-dependent biogeography: Oxygen limitation of thermal tolerance in animals. *Naturwissenschaften*, 88, 137-146. <https://doi.org/10.1007/s001140100216>
- Pörtner, H. O. (2002). Climate variations and the physiological basis of temperature dependent biogeography: Systemic to molecular hierarchy of thermal tolerance in animals. *Comparative Biochemistry and Physiology Part A*, 132, 739-761.
- Rasmussen, L. L., Gawarkiewicz, G., Owens, W. B., & Lozier, M. S. (2005). Slope water, Gulf Stream, and seasonal influences on southern Mid-Atlantic Bight circulation during the fall-winter transition. *Journal of Geophysical Research*, 110, 1-16. <https://doi.org/10.1029/2004JC002311>
- Rigby R. A., & Stasinopoulos D. M. (2005). Generalized additive models for location, scale and shape, (with discussion). *Applied Statistics*, 54, 507-554.
- Robins, C. R. (1957). Effects of storms on the shallow-water fish fauna of southern Florida with new records of fishes from Florida. *Bulletin of Marine Science in the Gulf and Caribbean*, 7(3), 266-275.
- Sackett, D. K., Able, K. W., & Grothues, T. M. (2007). Dynamics of summer flounder, *Parlichthys dentatus*, seasonal migrations based on ultrasonic telemetry. *Estuarine Coastal and Shelf Science*, 74, 119-130. <https://doi.org/10.1016/j.ecss.2007.03.027>
- Sarà, G., Dean, J. M., Amato, D. D., Buscaino, and 7 others (2007). Effect of boat noise on the behavior of bluefin tuna *Thunnus thynnus* in the Mediterranean Sea. *Marine Ecology Progress Series*, 331, 243-253.
- Secor, D. H. (2015). *Migration ecology of marine fishes*. Baltimore, MD: John Hopkins University Press.
- Secor, D. H., Zhang, F., O'Brien, M. H.P., & Li, M. (2019). Ocean destratification and fish evacuation caused by a Mid-Atlantic tropical storm. *ICES Journal of Marine Science*, 1-12. <https://doi.org/10.1093/icesjms/fsx241>
- Sedberry, G. R., & Van Dolah, R. F. (1984). Demersal fish assemblages associated with hard bottom habitat in the South Atlantic Bight of the USA. *Environmental Biology of Fishes*, 11(4), 241-258.
- Slabbekoorn, H., Bouton, N., van Opzeeland, I., Coers, A., ten Cate, C., & Popper, A. N. (2010). A noisy spring: The impact of globally rising underwater sound levels on fish. *Trends in Ecology and Evolution*, 25(7), 419-427. <https://doi.org/10.1016/j.tree.2010.04.005>

- Solís, D., Perruso, L., del Corral, J., Stoffle, B., & Letson, D. (2013). Measuring the initial economic effects of hurricanes on commercial fish production: the US Gulf of Mexico grouper (Serranidae) fishery. *Natural Hazards*, *66*, 271-289. <https://doi.org/10.1007/s11069-012-0476-y>
- Sousa, W. P. (1984). The role of disturbance in natural communities. *Annual Review of Ecology, Evolution, and Systematics*, *15*, 353-391.
- Steimle, F. W., & Figley, W. (1996). The importance of artificial reef epifauna to black sea bass diets in the Middle Atlantic Bight. *North American Journal of Fisheries Management*, *16*, 433-439.
- Steimle, F. W., & Zetlin, C. (2000). Reef habitats in the Middle Atlantic Bight: Abundance, distribution, associated biological communities, and fishery resource use. *Marine Fisheries Review*, *62*(2), 24-42.
- Stenberg, C., Støttrup, J. G., van Deurs, M., Berg, and 5 others (2015). Long-term effects of an offshore wind farm in the North Sea on fish communities. *Marine Ecology Progress Series*, *528*, 257-265. <https://doi.org/10.3354/meps11261>
- Strobbe, F., McPeck, M. A., De Block, M., & Stoks, R. (2011). Fish predation selects for reduced foraging activity. *Behavioral Ecology and Sociobiology*, *65*, 241-247. <https://doi.org/10.1007/s00265-010-1032-y>
- Sturrock, A. M., Trueman, C. N., Darnaude, A. M., & Hunter, E. (2012). Can otolith elemental chemistry retrospectively track migrations in fully marine fishes? *Journal of Fish Biology*, *81*, 766-795. <https://doi.org/10.1111/j.1095-8649.2012.03372.x>
- Syms, C., & Jones, G. P. (1999). Scale of disturbance and the structure of a temperate fish guild. *Ecology*, *80*(3), 921-940.
- Thomsen, F., Lüdemann, K., Kafemann, R., & Piper, W. (2006, July). *Effects of offshore wind farm noise on marine mammals and fish*. Hamburg, Germany: Cowrie.
- Vabø, R., Olsen, K., & Huse, I. (2002). The effect of vessel avoidance of wintering Norwegian spring spawning herring. *Fisheries Research*, *58*, 59-77.
- Vermaire, J. C., Pisaric, M. F. J., Thienpont, J. R., Mustaphi, C. J. C., Kokelj, S. V., & Smol, J. P. (2013). Arctic climate warming and sea ice declines lead to increased storm surge activity. *Geophysical Research Letters*, *40*, 1386-1390. <https://doi.org/10.1002/grl.50191,2013>

- Wahlberg, M., & Westerberg, H. (2005). Hearing in fish and their reaction to sounds from offshore wind farms. *Marine Ecology Progress Series*, 288, 295-309.
- Waide, R. B. (1991). Summary of the response of animal populations to hurricanes in the Caribbean. *Biotropica*, 23(4), 508-512.
- Walsh, W. J. (1983). Stability of a coral reef fish community following a catastrophic storm. *Coral Reefs*, 2, 49-63.
- Wauer, R. H., & Wunderle, J. M., Jr. (1992). The effect of Hurricane Hugo on bird populations on St. Croix, U.S. Virgin Islands. *The Wilson Bulletin*, 104(4), 656-673.
- Wenz, G. M. (1962). Acoustic ambient noise in the ocean: Spectra and sources. *The Journal of the Acoustical Society of America*, 34, 1936-1956.  
<https://doi.org/10.1121/1.1909155>
- Werner, E. E., & Peacor, S. D. (2003). A review of trait-mediated indirect interactions in ecological communities. *Ecology*, 84(5), 1083-1100.
- White, P. S., & Jentsch, A. (2001). The search for generality in studies of disturbance and ecosystem dynamics. *Progress in Botany*, 62, 399-450.
- Williams, A. H. (1984). The effects of Hurricane Allen on Back Reef populations of Discovery Bay, Jamaica. *Journal of Experimental Marine Biology and Ecology*, 75, 233-243.
- Zhang, F., Li, M., Ross, A. C., Lee, S. B., & Zhang, D.-L. (2017). Sensitivity analysis of Hurricane Arthur (2014) storm surge forecasts to WRF physics parameterizations and model configurations. *Weather and Forecasting*, 32, 1745-1764. <https://doi.org/10.1175/WAF-D-16-0218.1>

*Tables*

**Table 2.1.** Receiver site, mooring position, deployment location, and deployment duration information for 2016-2018 study periods. Note that the Northern site SW receiver was not recovered in 2017.

Site, Mooring	Location		Date Deployed			Date Retrieved			# Days Active		
	Latitude	Longitude	2016	2017	2018	2016	2017	2018	2016	2017	2018
Northern, N	38.4377	-74.7700	6/10	6/22	7/15	11/2	10/26	10/23	145	126	126
Northern, SE	38.4287	-74.7597	6/10	6/22	6/19	11/2	10/26	10/23	145	126	126
Northern, SW	38.4262	-74.7747	6/10	6/22	6/19	11/2	-	10/23	145	-	100
Middle, N	38.2307	-74.7581	6/12	6/22	7/15	11/1	10/26	10/23	142	126	100
Middle, SE	38.2212	-74.7472	6/12	6/22	7/15	11/1	10/26	10/23	142	126	100
Middle, SW	38.2186	-74.7630	6/12	6/22	7/15	11/1	10/26	10/23	142	126	100
Southern, N	38.1556	-74.9486	6/9	6/29	7/31	11/1	10/26	10/26	145	119	87
Southern, SE	38.1473	-74.9391	6/9	6/29	7/31	11/1	10/26	10/26	145	119	87
Southern, SW	38.1449	-74.954	6/9	6/29	7/31	11/1	10/26	10/26	145	119	87

**Table 2.2.** Receiver site, mooring position, and depth for 2016-2018 study periods. Note that the Northern site SW receiver was not recovered in 2017.

Site, Mooring	Depth (m)		
	2016	2017	2018
Northern, N	26.68	25.90	25.22
Northern, SE	26.08	25.64	26.66
Northern, SW	25.45	-	25.57
Middle, N	22.63	22.26	21.23
Middle, SE	32.33	32.47	30.74
Middle, SW	25.03	25.39	27.49
Southern, N	20.22	22.46	22.39
Southern, SE	19.85	22.38	19.01
Southern, SW	20.67	22.77	21.76

**Table 2.3.** Year, location, and size for black sea bass tagged and released during the summers of 2016-2018.

Site	Year	Latitude	Longitude	N	Size (mm)	Weight (g)
Northern	2016	38.4309	-74.7680	15	260 ± 25	200 ± 90
	2017	38.4307	-74.7677	15	262 ± 28	250 ± 70
	2018	38.43094	-74.76803	27	251 ± 38	240 ± 70
Middle	2016	38.2237	-74.7562	15	232 ± 30	260 ± 100
	2017	38.2234	-74.7558	15	283 ± 17	320 ± 60
	2018	38.223683	-74.756183	16	271 ± 37	280 ± 110
Southern	2016	38.1480	-74.9472	15	267 ± 24	270 ± 80
	2017	38.1589	-74.9439	8	256 ± 20	240 ± 50
	2018	38.148047	-74.947197	17	241 ± 30	190 ± 60

**Table 2.4.** Description of variables utilized in black sea bass movement GAMLSS model.

Variable	Type	Units	Source
Movement index	Numerical response	Average number of movements per unique receiver per hr	VEMCO VR2AR receiver array
Turbulent kinetic energy	Numerical predictor	Square meters per square second ( $m^2 s^{-2}$ )	FVCOM prediction
Bottom water temperature	Numerical predictor	Degrees Celsius ( $^{\circ}C$ )	VEMCO VR2AR receiver array
Current velocity, differenced	Numerical predictor	Meters per second ( $m s^{-1}$ )	FVCOM prediction
Accumulated number of storm days	Numerical predictor	Total number of days	FVCOM prediction
Tagged individual, length	Numerical predictor	Millimeters (mm)	Tagged black sea bass measurement
Tagged individual, sex	Categorical predictor	Male (M), Female (F), Unidentified (U)	Tagged black sea bass measurement
Transmitter	Random effect	No units	VEMCO V9-2x acoustic transmitter ID

**Table 2.5.** Year and names of identified Mid-Atlantic Bight storm events detected between June-October of 2016-2018, presented along dates and times of storm arrival, departure, and maximum windspeed, as well as calculations of storm duration (hr), maximum wind speed ( $\text{m s}^{-1}$ ), mean wind speed ( $\text{m s}^{-1} \pm \text{SD}$ ), and minimum windspeed ( $\text{m s}^{-1}$ ). A storm was considered present in the area when wind speeds consistently increased over  $5 \text{ m s}^{-1}$ . Windspeeds refer to average velocity vectors.

Year	Name	Arrival Date	Departure Date	Maximum Windspeed Date	Duration (hr)	Maximum Windspeed ( $\text{m s}^{-1}$ )	Mean Windspeed ( $\text{m s}^{-1} \pm \text{SD}$ )	Minimum Windspeed ( $\text{m s}^{-1}$ )
2016	Tropical Storm Hermine	Sep 2 09:00	Sep 5 18:00	Sep 3 21:00	81	15.25	$8.28 \pm 3.02$	5.02
	Nor'easter (unnamed) Potential	Jul 29 15:00	Jul 31 00:00	Jul 29 18:00	33	14.79	$10.25 \pm 2.88$	5.57
2017	Tropical Cyclone 10	Aug 26 15:00	Aug 30 12:00	Aug 30 00:00	81	16.28	$8.9 \pm 2.75$	5.1
	Tropical Storm Jose	Sep 17 12:00	Sep 20 15:00	Sep 19 12:00	75	16.6	$9.0 \pm 3.36$	5.23
	Tropical Storm Maria	Sep 25 15:00	Sep 29 06:00	Sep 27 18:00	87	13.44	$8.93 \pm 1.96$	5.23
2018	Wind event (unnamed)	Sep 8 15:00	Sep 10 12:00	Sep 9 18:00	45	14.3	$8.18 \pm 3.06$	5.05



**Table 2.6.** Slope and adjusted R-square values for black sea bass transmitter loss time series data, fit to exponential curves for all sites and years. Absolute loss rate, calculated as the average percent decrease in transmitter presence per day, is also presented for each site for 2016-2018.

Year	Site	Transmitter loss rates		
		Instantaneous loss rate		Absolute loss rate (%/day)
		Slope	R <sup>2</sup>	
2016	Northern	-0.013	0.811	0.013
	Middle	-0.021	0.822	0.021
	Southern	-0.005	0.870	0.005
2017	Northern	-0.015	0.771	0.015
	Middle	-0.015	0.965	0.015
	Southern	-0.021	0.793	0.021
2018	Northern	-0.011	0.919	0.011
	Middle	-0.012	0.773	0.012
	Southern	-0.004	0.843	0.004

**Table 2.7.** Mu estimates (the direction and magnitude of the fitted response), standard error, t-values, and p-values for numerical and categorical predictors used in the GAMLSS model for black sea bass movements. Note that all numerical predictors were centered and scaled prior to incorporation in the model, allowing cross-comparisons of both the direction and magnitude of mu.

	Mu estimate ( $\mu$ )	Standard error	T value	P value
Intercept	-0.4966	0.0601	-8.259	<0.001
TKE	-0.1680	0.0314	-5.328	<0.001
Temperature	-0.2173	0.0413	-5.260	<0.001
Current velocity, differenced	-0.0992	0.0309	-3.208	0.0014
Lag-1	0.2110	0.0165	12.767	<0.001
Lag-2	0.0780	0.0146	5.335	<0.001
ANSD	0.0016	0.0081	0.200	0.8413
Sex, male	0.6170	0.0692	8.913	<0.001
Sex, unidentified	0.6832	0.0662	10.321	<0.001
Length	-0.1904	0.0295	-6.459	<0.001

*Figures*

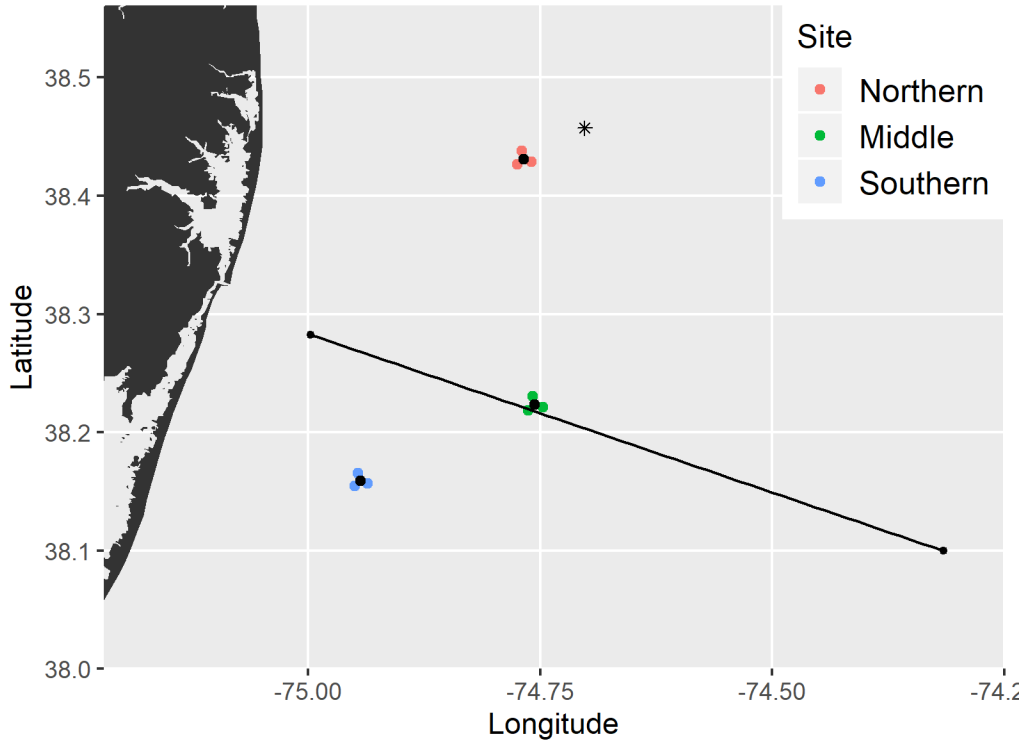


**Figure 2.1.** Experimental study sites. Map of three reef sites east of the Maryland coast, consistent for the 2016-2018 study seasons. Colored points refer to receiver deployment locations, while black points refer to approximate tagging locations. The black line depicts the selected 38.73 km transect for cross-sectional FVCOM estimates. The black asterisk refers to the location of National Data Buoy Center Station 44009.

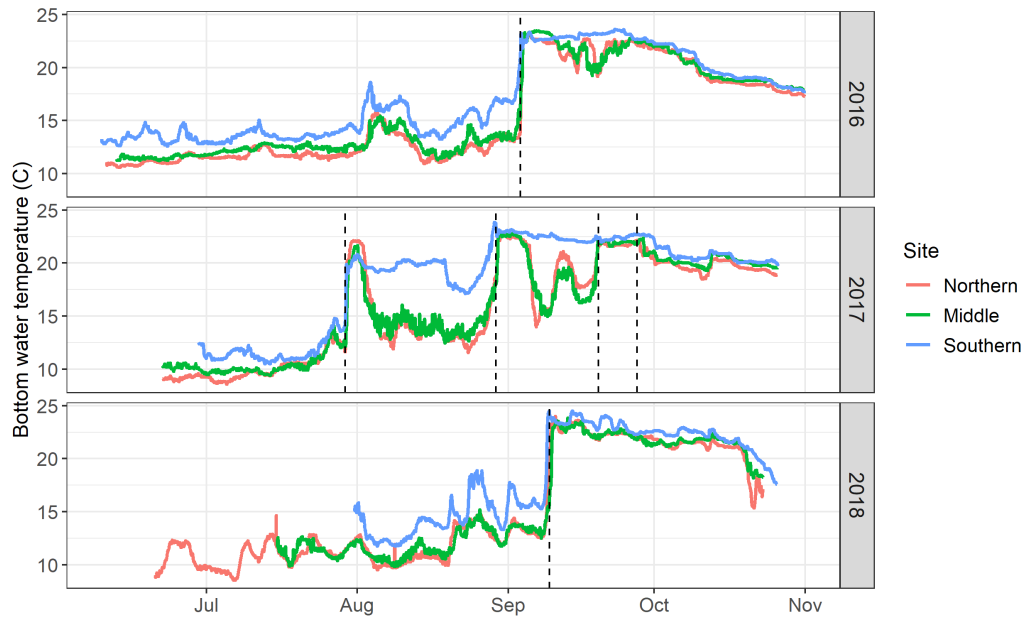


**Figure 2.2.** Observed hourly bottom water temperature ( $^{\circ}\text{C}$ ), averaged across each study site for each year. Black dashed lines refer to dates of observed maximum windspeed for identified storm events (see Table 2.5).

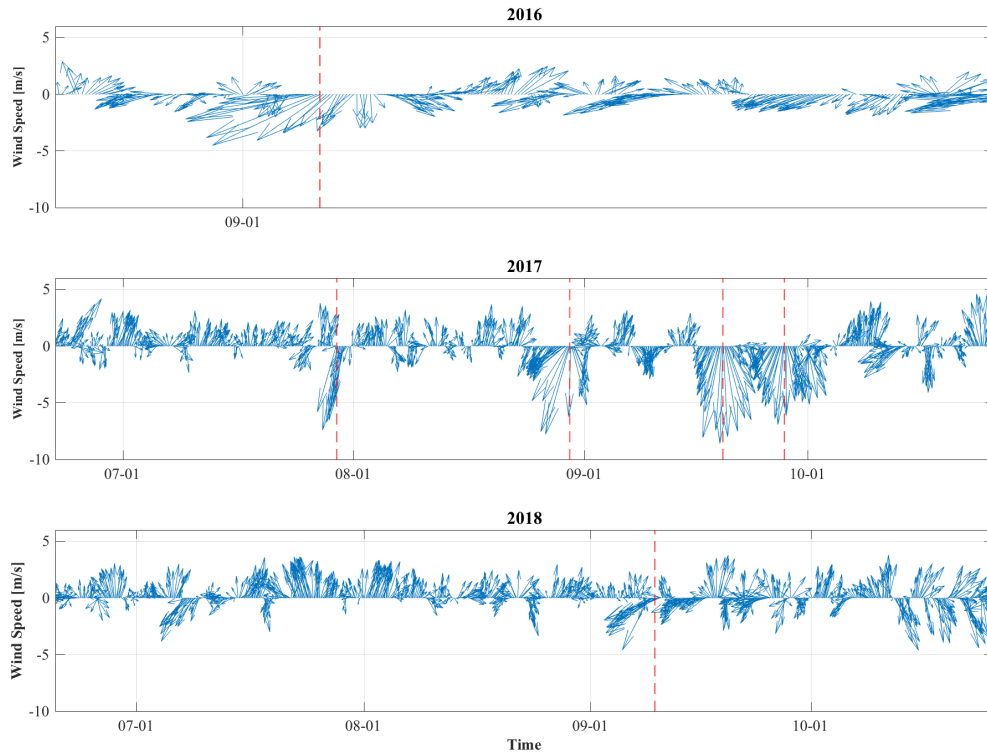
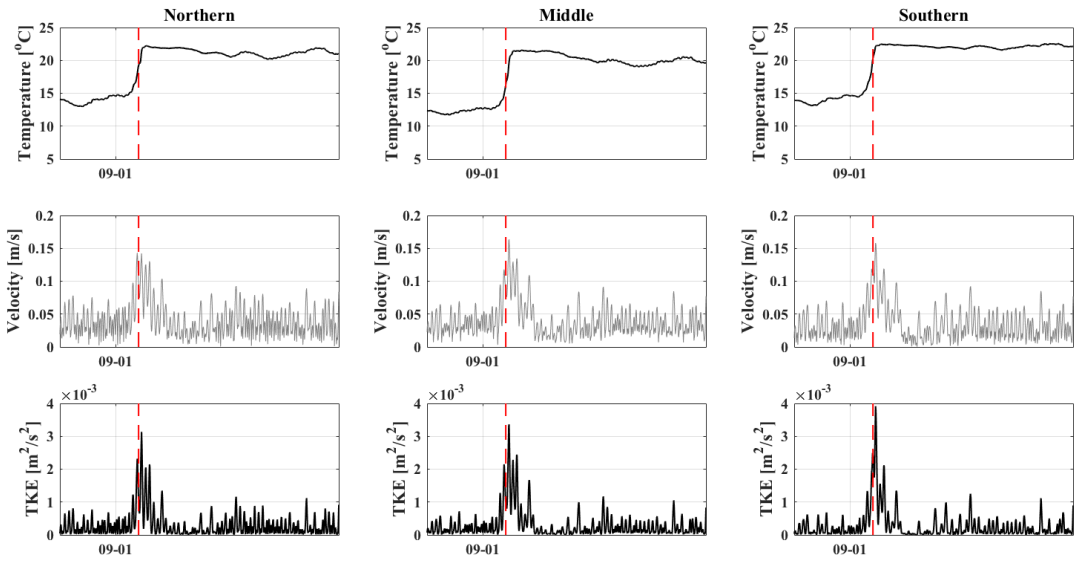
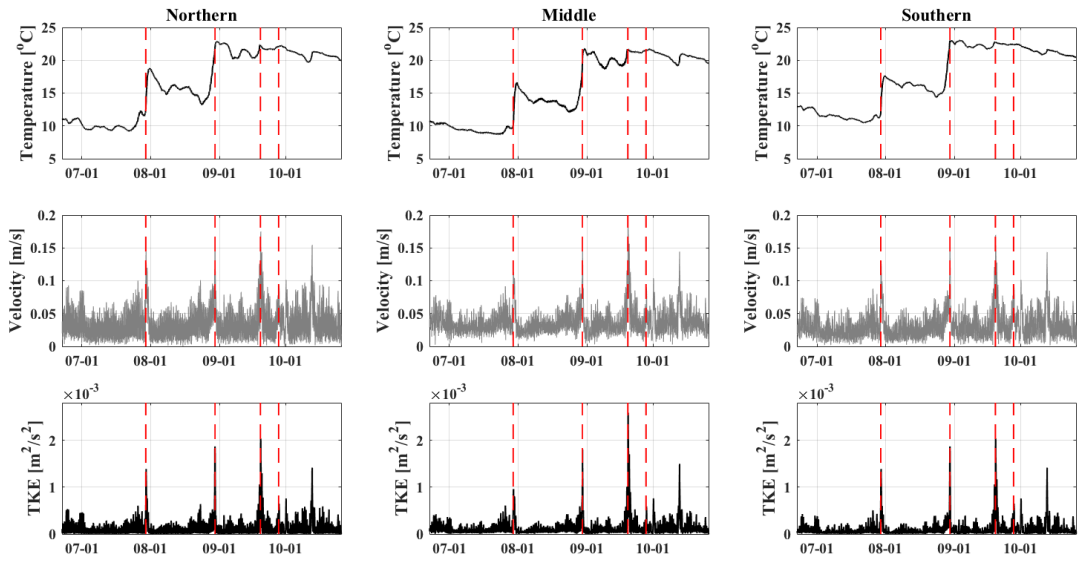


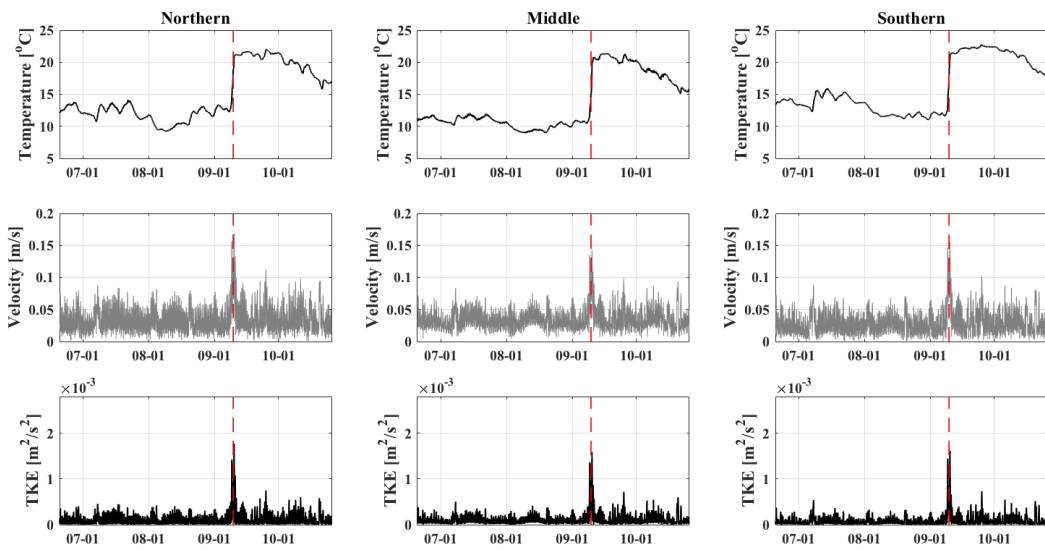
**Figure 2.3.** Time series of hourly directional wind vectors for 2016, 2017, and 2018. Wind vectors are observed for the Middle site of each year, and are measured in  $\text{m s}^{-1}$ . Wind direction corresponds to compass direction, and dashed red lines refer to the date and time (month-day hour) of peak wind speeds for each storm event (see Table 2.5).



2.4.a.



2.4.b.



### 2.4.c

**Figure 2.4.a-c.** Modeled hourly time series estimates of bottom water temperature ( $^{\circ}\text{C}$ ), averaged for each site for (a) August-September 2016, (b) June-October 2017, and (c) June-October 2018. Dashed red lines refer to modeled maximum wind speeds occurring during each of the six identified storm events (see Table 2.5).



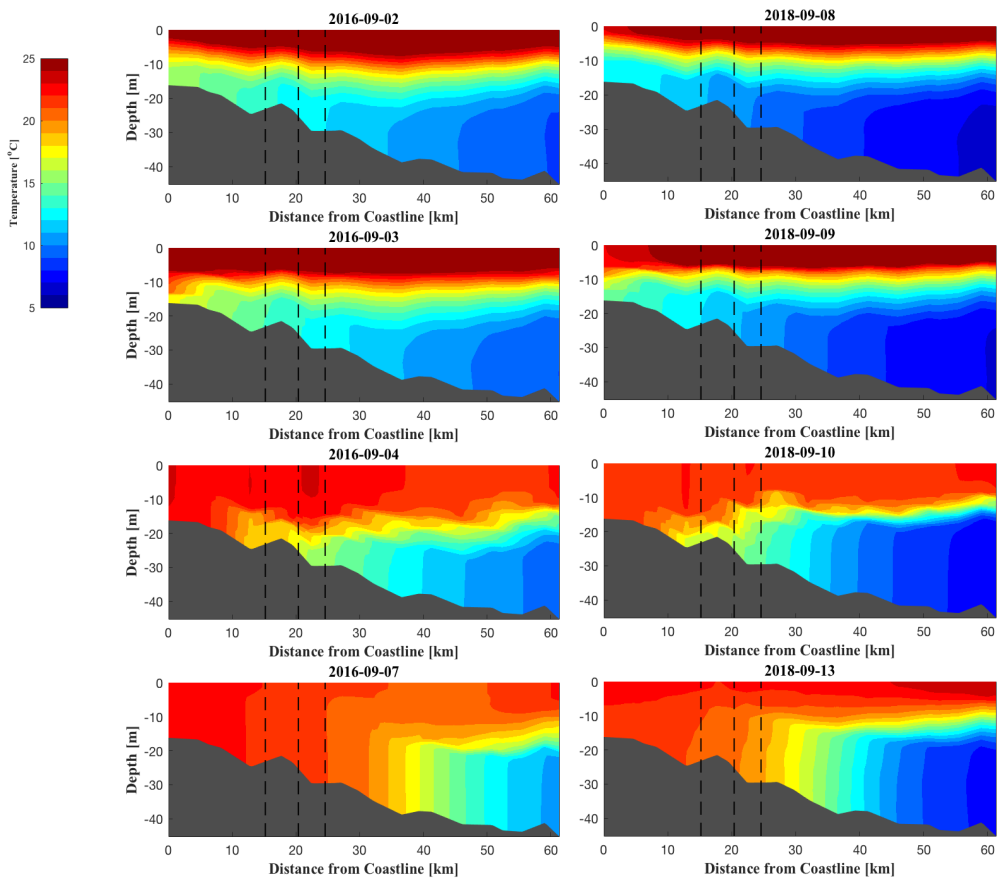


**Figure 2.5.** Modeled bottom water temperature cross-sectional profiles predicted by the FVCOM for storm events in 2016 and 2018. The left column predicts temperatures related to TS Hermine (2016); the right column predicts temperatures related to the unnamed wind event (2018). Vertical black dashed lines in each pane refer to the transmitter release locations central to each study site (Southern, Northern, and Middle, for both years in increasing depth and distance from coastline). Cross sections are taken along a transect spanning the Middle site (Figure 1), and depict snapshot predictions at 00:00 for each given day.

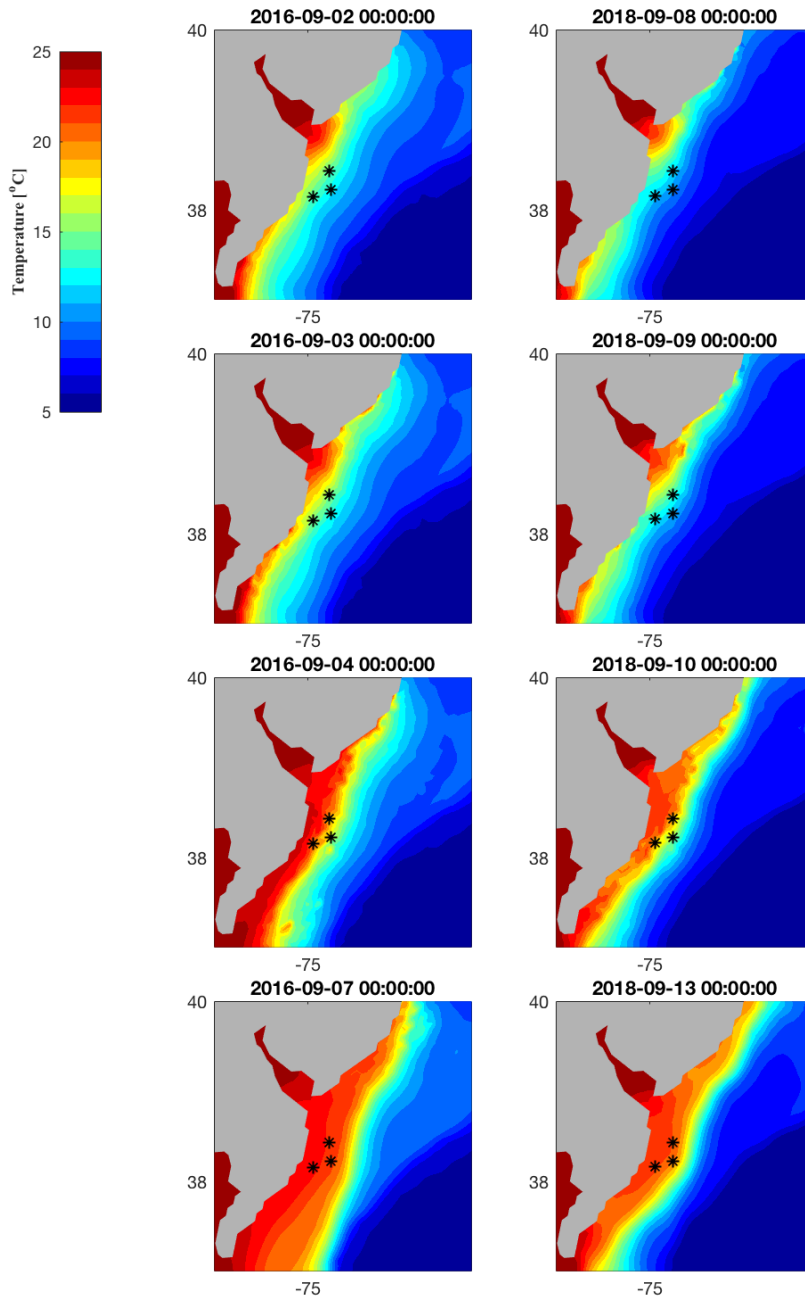


**Figure 2.6.** Modeled bottom water temperature in the southern MAB predicted by the FVCOM for single storm events occurring in 2016 (left column) and 2018 (right column). Black asterisks refer to the location of transmitter release, central to each study site.

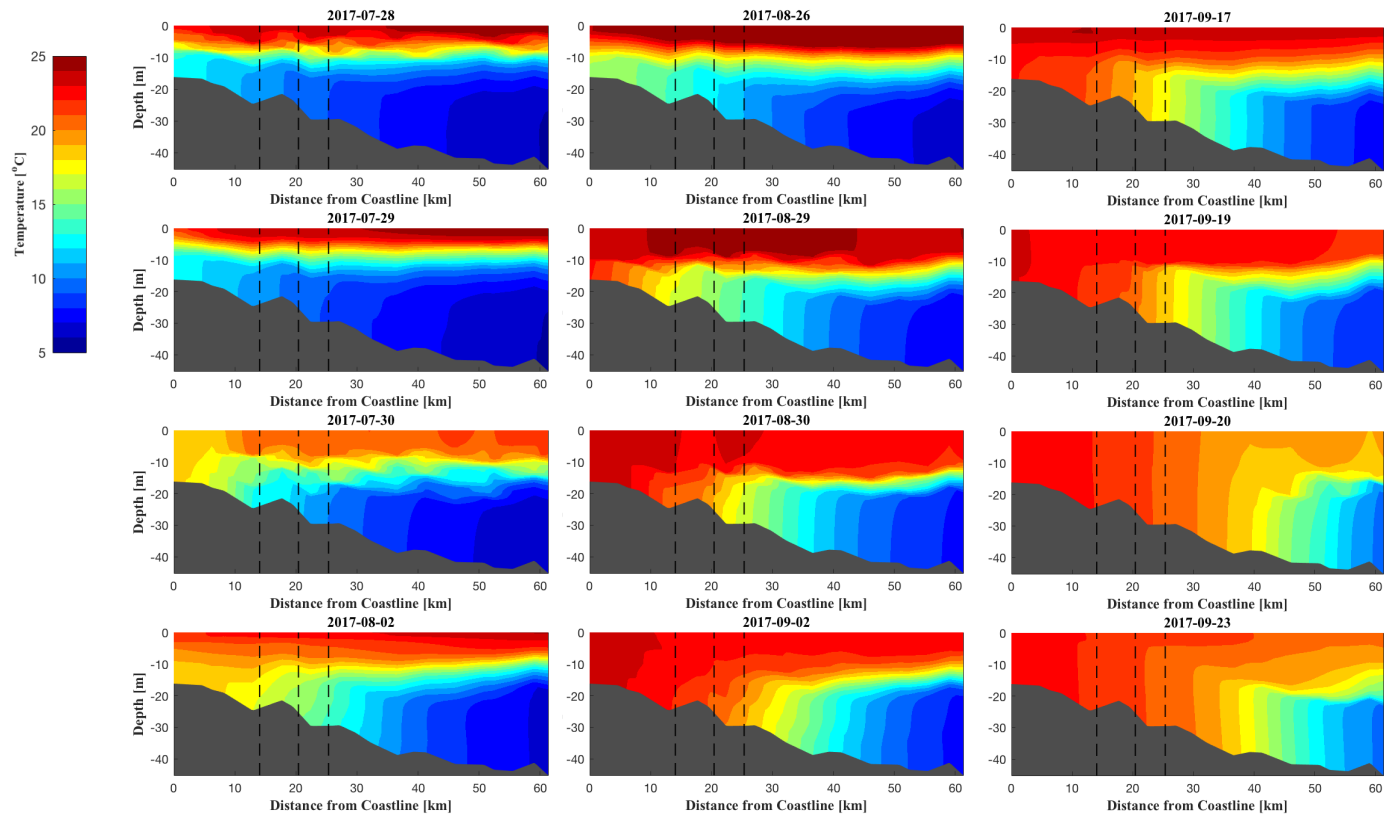


**Figure 2.7.** Modeled bottom water temperature cross-sectional profiles predicted by the FVCOM for storm events in 2017. The left column predicts temperatures related to the July nor'easter; the middle column predicts temperatures related to PTC10; and the right column predicts temperatures related to TS Jose (see Table 2.5). Vertical black dashed lines in each pane refer to the transmitter release locations central to each study site (Southern, Northern, and Middle, increasing depth and distance from coastline). Cross sections are taken along a transect spanning the Middle site (Figure 1), and depict snapshot predictions at 00:00 for each given day.

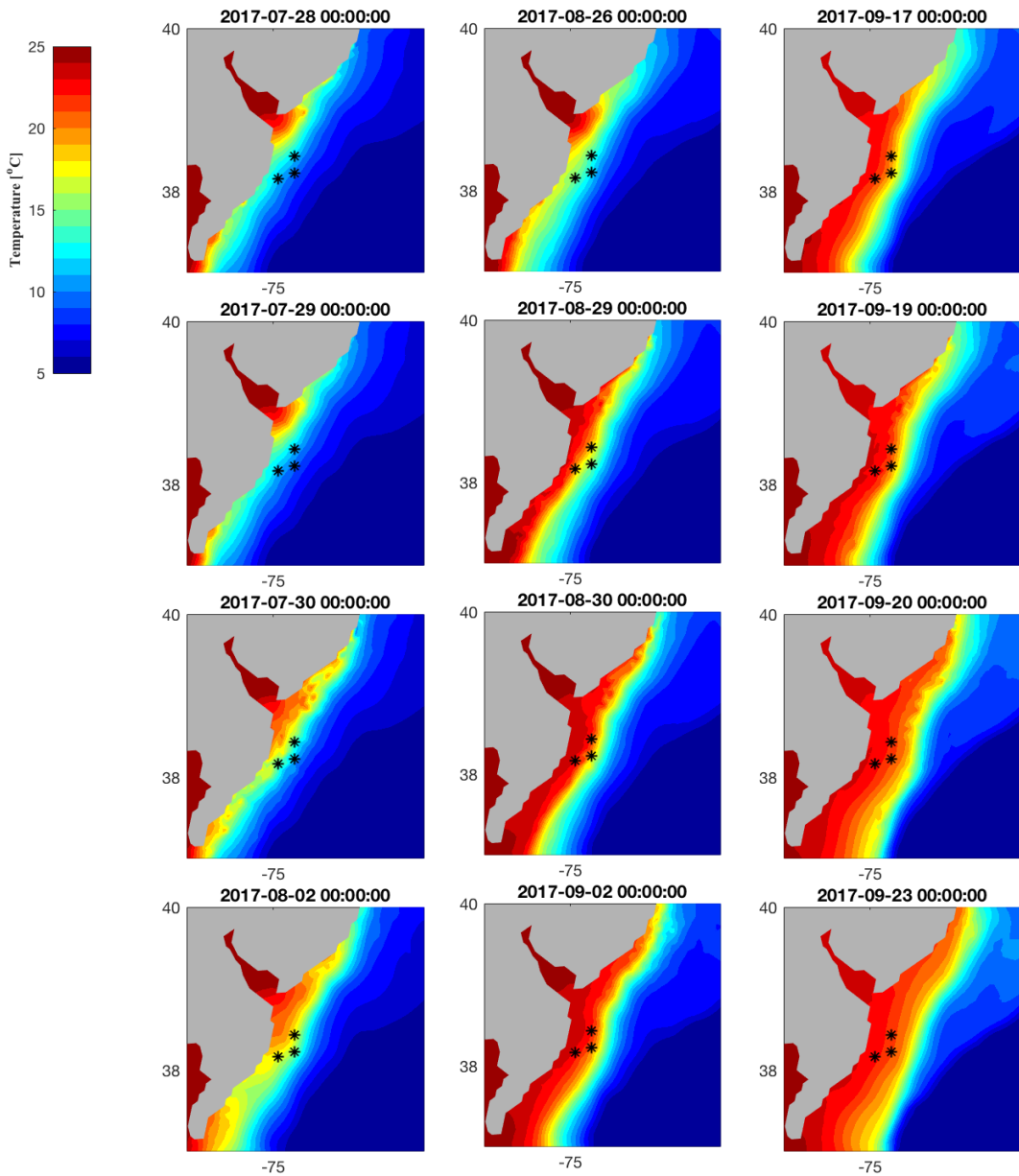


**Figure 2.8.** Modeled bottom water temperature in the southern MAB predicted by the FVCOM for storm events occurring in 2017. The left column predicts temperatures related to the July nor'easter; the middle column predicts temperatures related to PTC10; and the right column predicts temperatures related to TS Jose (see Table 2.5). Black asterisks refer to the location of transmitter release, central to each study site.

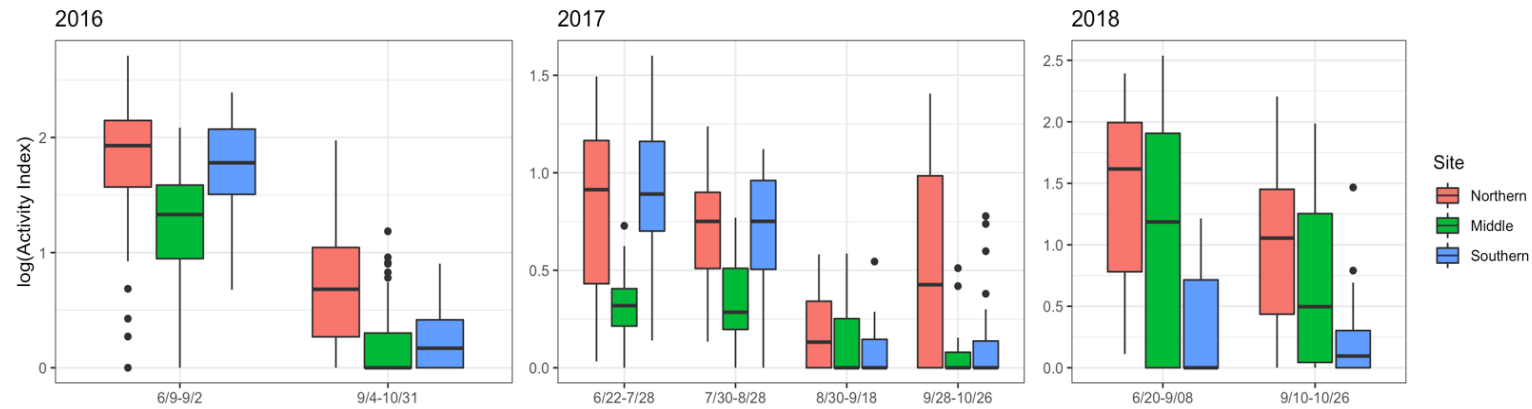


**Figure 2.9.** Hourly black sea bass activity index across study sites for each year before and after storm events (see Table 2.5). Box and whisker plots are shown where the black horizontal line central to each plot defines the median activity index value; the horizontal lines above and below the median value (completing the box) describe the range of the upper and lower quartile values; the vertical lines extending above and below each box provide upper and lower extremes, respectively; and the black dots provide outliers.

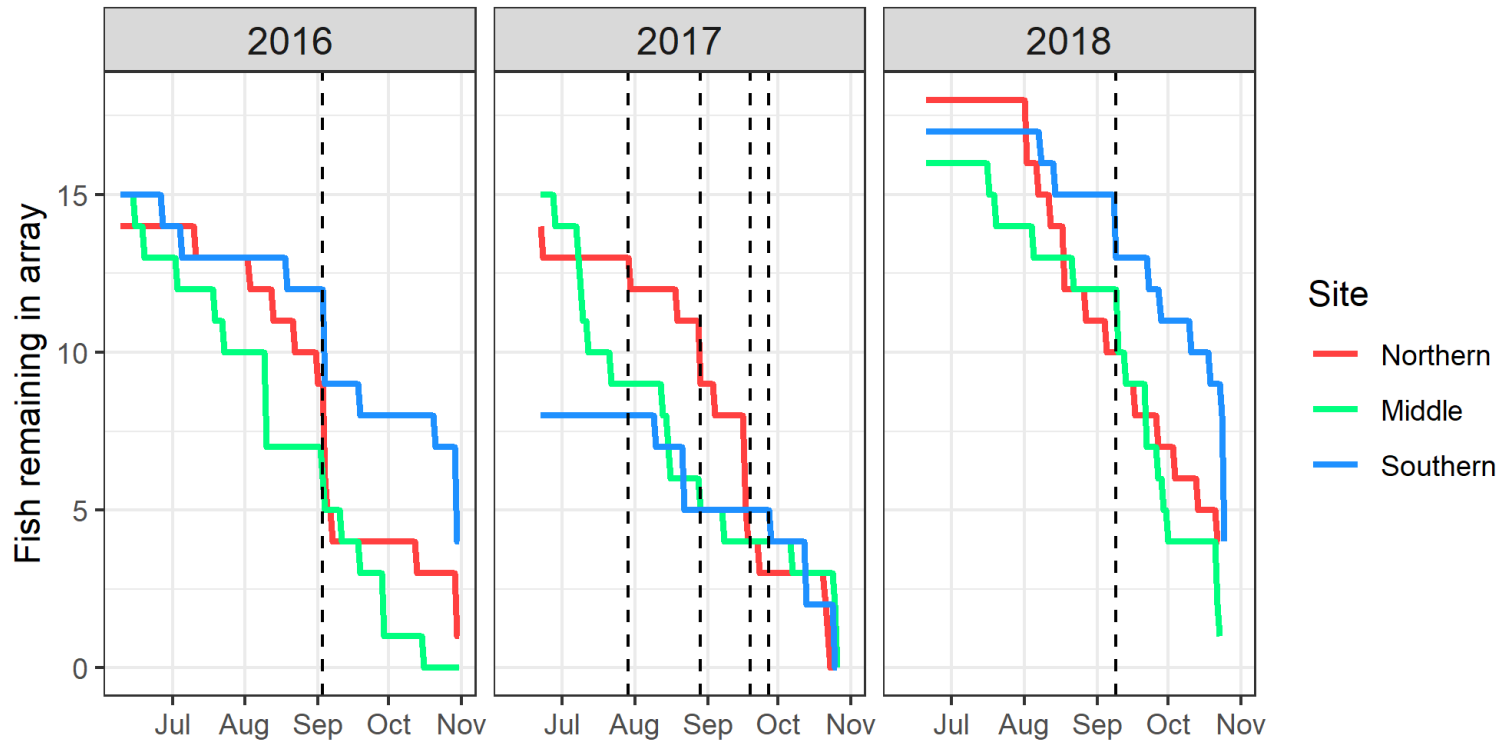


**Figure 2.10.** Black sea bass tag loss time series across sites, 2016-2018. The colored lines refer to site-specific time series of the last day a unique tag was detected within a given site, across years. Dashed black lines refer to the day of maximum windspeed associated with a given storm event (Table 2.5).

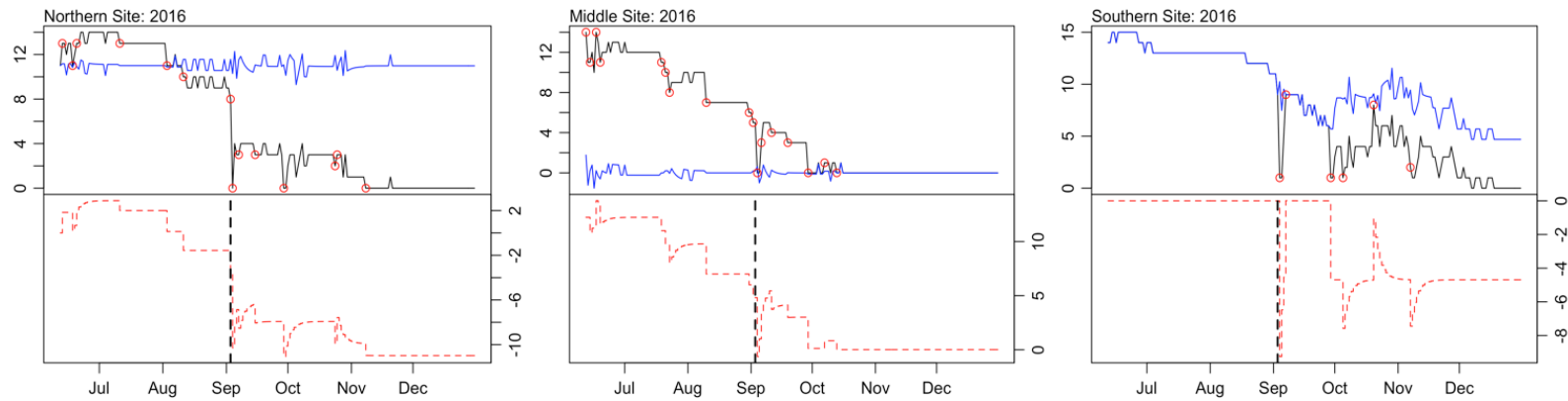


**Figure 2.11.** ARIMA intervention analysis output for 2016 study sites. The black and blue lines in the upper pane refer to the observed transmitter loss time series and modeled ARIMA output, respectively. The red lines in the lower panes refers to the model's identified interventions, where step-wise declines indicate permanent level shifts and sharp curvatures that dip and recover indicate temporary shifts. Note that the model failed to converge and achieve stationarity at the Southern site, thus no identifiable interventions were detected at that reef. The vertical dashed black lines refer to the date of maximum wind speed associated with TS Hermine.

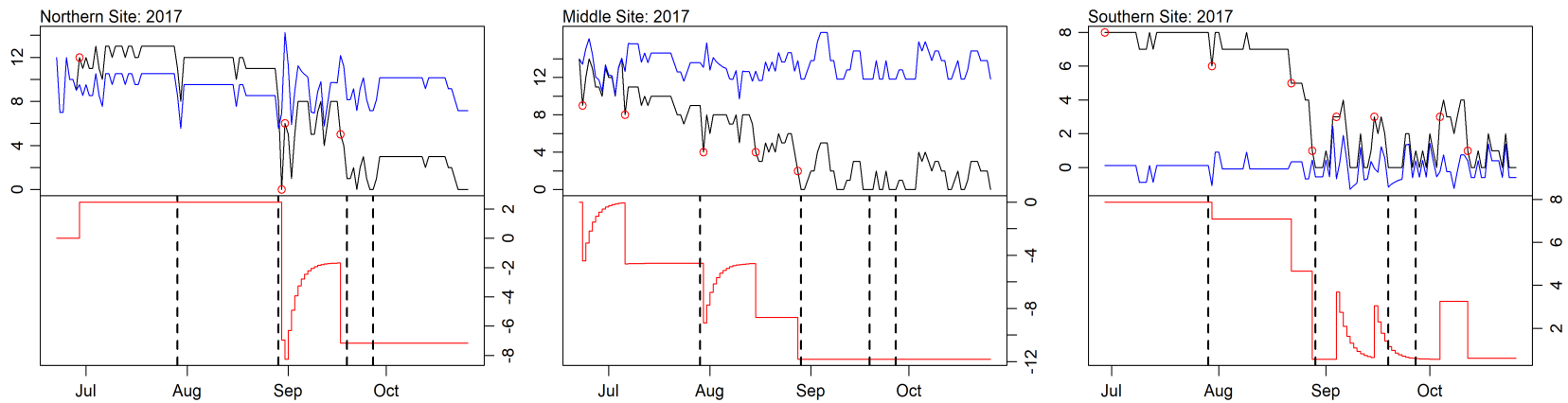


**Figure 2.12.** ARIMA intervention analysis output for 2017 study sites. The black and blue lines in the upper panes refer to the observed transmitter loss time series and modeled ARIMA output, respectively. The red line in the lower panes refers to the model's identified interventions, where step-wise declines indicate permanent level shifts and sharp curvatures that dip and recover indicate temporary shifts. The vertical dashed black lines refer to the date of maximum wind speed associated with the July nor'easter, PTC10, TS Jose, and TS Maria.



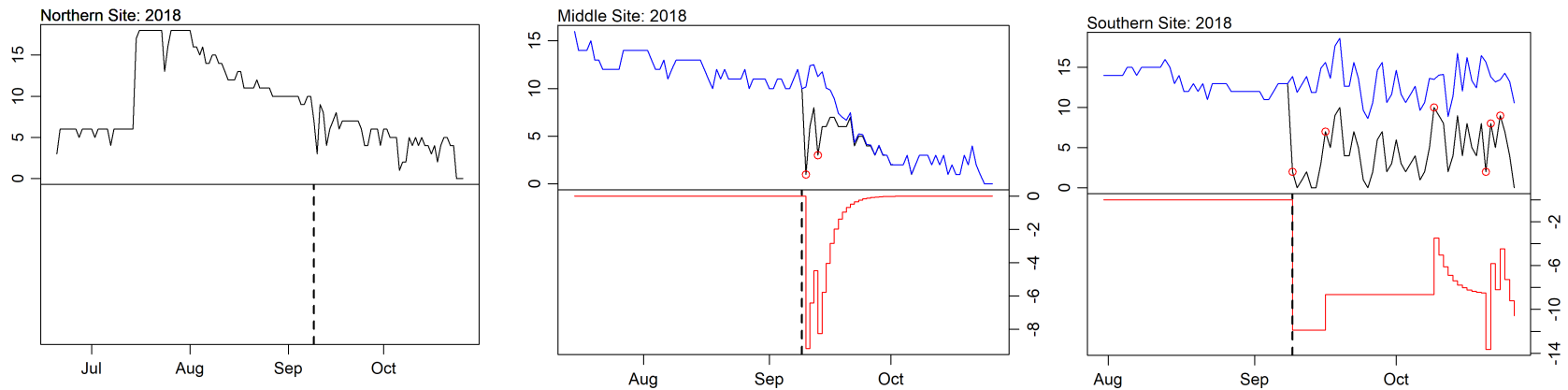


**Figure 2.13.** ARIMA intervention analysis output for 2018 study sites. The black and blue lines in the upper panes refer to the observed transmitter loss time series and modeled ARIMA output, respectively. The red line in the lower panes refers to the model’s identified interventions, where step-wise declines indicate permanent level shifts and sharp curvatures that dip and recover indicate temporary shifts. Note that the model failed to converge and achieve stationarity at the Middle site and failed to identify ARIMA model components in the time series for the Northern site. Thus, no identifiable interventions were detected at those reefs, and no model fit or intervention visualizations were provided for the Northern site. The vertical dashed black lines refer to the date of maximum wind speed associated with the unnamed wind event in early September.

## Chapter 3. The effect of swim bladder presence and morphology on sound sensitivity for marine and freshwater fishes.

### *Introduction*

Anthropogenic sound and its impacts on fish communities is of urgent concern to scientists and managers alike (Popper and Hastings 2009; Slabbekoorn et al. 2010; Hawkins and Popper 2017; Weilgart 2018). Anthropogenic sound in the world's oceans has increased steadily over the past several decades, related to increases in commercial shipping and recreational vessel traffic in coastal areas (National Research Council 2003; McDonald et al. 2006; Frisk et al. 2007) as well as seismic exploration (McCauley et al. 2002; Nowacek et al. 2015; Carroll et al. 2017). Sound related to offshore energy development, primarily pile-driving sound—which can reach peak sound pressure levels at 200 dB re: 1  $\mu$ Pa with the highest energy levels concentrated at low frequencies ( $>1000$  Hz) (Bailey et al. 2010; Casper et al. 2013)—has been identified as a significant source of acoustic disturbance to fish communities, one that will likely increase exponentially in shelf waters during the next several decades (BOEM 2018). Percussive noise related to pile-driving has a wide frequency spectrum, but lower frequencies ( $<1000$  Hz) within the hearing ranges of fishes tend to carry the highest energies during hammer impact (Bailey et al. 2010). Resulting effects can range from behavioral changes to auditory threshold shifts to tissue damage and death (Hildebrand 2009; Halvorsen et al. 2012; Casper et al. 2013). The use of seismic airguns in geophysical surveys—another impulse sound similar to pile-driving, ranging from 160-1000 Hz and peaking at approximately 200 dB re: 1  $\mu$ Pa (McCauley et al. 2000)—is also a significant source of acoustic

disturbance to fish communities, affecting movement behaviors as well as hearing threshold shifts in individuals (Skalski et al. 1992; Wardle et al. 2001; McCauley et al. 2002; Popper et al. 2005).

Current levels and future projected increases of anthropogenic sound disturbance fuel an increased interest in understanding their impacts on fish populations. More specifically, there is a need to better characterize where fish operate in the surrounding soundscape—which sound frequencies and sensitivities are detected, and which evoke biological responses (Popper and Hawkins 2019). As hearing capabilities have been explored for only approximately 100 (Ladich and Fay 2013), of the c. 33,000 identified fish species (Froese and Pauly, 2000) there is a priority to efficiently and effectively estimate hearing abilities in diverse fishes, prompted by ever-increasing anthropogenic sound disturbances in marine and freshwater ecosystems.

Hearing structures and sensitivity in fishes are exceptionally diverse in morphology and frequency bandwidths among vertebrates, substantially altering expected responses to anthropogenic sound (Dijkgraaf 1960; Popper and Fay 1993; Popper and Hawkins 2019). Initial empirical evidence relied on behavioral studies to infer audition from a curtailed set of model species (Kenyon et al. 1998; Popper and Fay 2011; Ladich and Fay 2013). Hearing function investigation of a greater number of species was enabled by auditory brainstem response (ABR) techniques developed to measure auditory evoked potential (AEP) (Bullock and Corwin 1979; Kenyon et al. 1998). The ABR technique has allowed more rapid auditory testing, greater replication, and less reliance on the same set of model species with well-characterized

behavioral responses (Kenyon et al. 1998; Ladich and Fay 2013; Ladich and Yan 1998). Conversely, however, the results of this method remain somewhat unreliable, particularly across laboratory settings and when compared to measurements of sensitivity obtained from behavioral methods (Sisneros et al. 2016). Nonetheless, the AEP approach has been applied to a large number and diversity of marine and freshwater species (Ladich and Fay 2013; Popper and Fay 2011; Table 3.1). Still, a call for revision of how we measure sensitivity suggests systematic inaccuracies may have pervaded the literature regardless of testing method (Popper and Fay 2011). Despite a rich physiological literature indicating the otolithic organ directly responds to particle motion rather than pressure waves (Popper and Hawkins 2018), the majority of fish auditory studies have measured received sound as pressure levels (i.e., in units of dB re: 1  $\mu$ Pa) (Table 3.1).

The literature base on fish auditory studies is limited and rather static (Figures 3.1, 3.2) likely owing to the costly equipment and intensive methodology to conduct rigorous studies, yet there is an ever-increasing need for information on fish hearing sensitivity for management purposes. This mismatch has led to past classification schemes that separated hearing specialists and hearing generalists. More recently, a gradient of hearing functions has been proposed in order to better facilitate and guide further exploration of fish hearing (Popper et al. 2014), which uses four categories: (1) fishes without a swim bladder; (2) fishes where the swim bladder does not aid with hearing; (3) fishes where the swim bladder aids with hearing; and (4) fish eggs and larvae. Multiple studies have shown that specialized modifications to the swim bladder confer sensitivity to a wider spectrum of sound frequencies (Poggendorf

1952; Coombs and Popper 1979; Tavolga and Wodinsky 1963; Ladich and Fay 2013). For instance, species with swim bladder extensions towards the inner ear show expanded audible frequency ranges compared to those without (Ramcharitar and Popper 2004; Ramacharitar et al. 2006; Mann et al. 2007; Dale 2014). Furthermore, additional studies argue that evolution of more complex swim bladder morphologies correspond to selective forcing in differing acoustic environments (Ladich and Popper 2004; Ladich 2000). More specifically, the evolution of the swim bladder has been proposed to specifically permit detection of and sensitivity to a broader range of higher sound frequencies via the detection of sound pressure waves in addition to particle motion, as opposed to particle motion alone (Ladich and Popper 2004; Ladich 2000). This expanded range of sound detection conferred by morphology may thus alter how individuals respond to predator-prey interactions, communicate with conspecifics, and navigate marine habitats (Ladich and Popper 2004; Ladich 2000). Despite the influence of the swim bladder in potentially defining a fishes' acoustic scene, no systematic literature review exists to support the hearing classification based upon swim bladder presence and its modification, such as that introduced by Popper et al. (2014).

Here, I evaluate swim bladder specialization, methodology, and measured sound form through a quantitative literature review on hearing threshold and sensitivity data across studied adult marine and freshwater species. I hypothesize, in accordance with Popper et al. (2014), that increases in the structural complexity of the swim bladder will correspond to increased thresholds of detected frequencies. More specifically, I hypothesize that fish species categorized by swim bladder morphology

will detect a broader frequency range and higher optimum frequencies with increasing swim bladder complexity, and that this signal may be captured and described across experimental approaches. Based on previously identified ranges of potential hearing acuity related to swim bladder structure, I broadly categorized comparable hearing types into Type 1 (individuals without swim bladders), Type 2 (individuals with basic swim bladders, without additional structures), Type 3 (individuals with swim bladders that have structural modifications but lack Weberian ossicles—vertebrae connecting skull to swim bladder—or bullae—twin gas bladders directly connected to the ear and skull), and Type 4 (true otophysans [having Weberian ossicles] and mormyrids [having bullae]) (von Frisch 1938; Popper et al. 2014; Hawkins and Popper 2015). I incorporated additional metrics to account for individual studies' experimental conditions and any related confounding variance (Popper et al. 2014; Ladich and Fay 2013; Hawkins et al. 2015). These metrics included methodology used to evaluate response (AEP or behavior); measured sound form (particle motion or sound pressure); experimental rigor (indexed as the number of replicates); and the taxonomic order of each species tested. The relationship between hearing frequency benchmarks (minimum, maximum, and optimal sound frequencies detected) and predictor variables was evaluated using parametric models, ultimately isolating the effect of hearing type on each frequency benchmark while incorporating variance related to experiment-specific parameters.

### *Materials and methods*

#### *Literature Review*

I conducted a literature review of 63 papers that measured sound frequency detection in individual fish species. Studies were identified using online databases of peer-reviewed publications. Databases included the University of Maryland library, *The Journal of the Acoustical Society of America*, JSTOR, Wiley Online Library, Springer, and ProQuest. Search terms included “audiogram,” “hearing ability,” “fish,” “swim bladder,” “audition,” and combinations of said terms. From those papers, I identified 173 unique experiments measuring the audition of individual species under specific laboratory conditions, with many papers providing audiogram data for multiple species. From the experiments identified, I obtained tabulated data reported by the authors from audiograms examining the hearing abilities of 130 species. For each audiogram, I selected the highest and lowest frequencies detected, as well as the frequency detected at the lowest sound level (Figure 3.3); the latter representing the frequency of optimal hearing sensitivity. For audiograms that indicated this nadir occurred for a range of frequencies, the optimum frequency was estimated as the mean of the values within this range. Of the 173 unique experiments, 159 optimal frequencies were single nadir points and 14 were mean estimates. Analysis was limited to detected frequency range, barring hearing sensitivity amplitudes at identified frequency ranges, assuming that the presence of frequency detection alone would be sufficient in determining coarse discriminations of hearing ability bandwidth driven by swim bladder morphology.

Hearing morphologies were classified by increasing complexity of the swim bladder and were categorized as Type 1 (T1; no swim bladder), Type 2 (T2; unmodified swim bladder), and Type 3 (T3; swim bladder structural modifications

barring Weberian ossicles or bullae); otophysan and mormyrid species were classified as Type 4 (T4). The method classes included audio-evoked potential (AEP) methods, where the neurological response to sound was measured directly using electrophysiological techniques, and behavioral (BEH) methods, where changes in behavior or physiology were observed in response to sound (usually following a period of training). Sound-form classes included particle motion (PAL) and sound pressure level (SPL). I also evaluated the influence of taxonomic order and the number of replicate individuals evaluated per experimentally-derived audiogram. Replication was used as an index of experimental rigor. Eleven audiogram experiments of the original 173 experiments evaluated did not contain information on the number of replicates and were excluded from analysis, yielding a final sample size of 162 unique study combinations of species, experimental method, sound form, number of replicates, and taxonomic order (Table 3.2).

#### *Data analysis*

Models were developed and compared for maximum and optimal frequency benchmarks across hearing types. Minimum frequency benchmarks could not be assessed owing to the strongly truncated distribution of minimum detected frequencies in the pooled audiogram data (see Results, Figure 3.4), suggesting a pervasive experimental artifact across studies. The relationship between maximum and optimal frequency benchmark values and hearing type were separately evaluated using linear mixed effect (LME) and generalized least square (GLS) models, incorporating and comparing variance structures to account for the effects of experimental method, taxonomic order, and number of replicates. Models for both



benchmarks examined log<sub>10</sub>-transformed sound frequency as a primary response of hearing type under the following structures, listed in order of increasing complexity: (1) as a linear response to hearing type alone; (2) with hearing frequency fixed with respect to the number of replicates; (3) with the interaction between hearing type and experimental method incorporated as a constant variance structure; (4) with the aforementioned hearing type-experimental method interaction [3] fixed with variance related to the number of replicates; and (5) with the former variance structure [4] and including taxonomic order incorporated as a random effect. Models were selected based on lowest Akaike Information Criterion (AIC) numbers. All models were developed using the *nlme* package in R (Pinheiro et al. 2018).

Sound form was not included in model comparisons based on the substantial dominance in the number of studies testing sound pressure (N=133) versus particle motion (N=29); the latter subsample was further curtailed when divided across the additional metrics of hearing type, experimental method, number of replicates, and taxonomic order. Post hoc analyses included calculations of least square mean contrasts across hearing types using the selected model and a Bonferroni adjustment of p-values. Post hoc calculations were conducted using the *lsmeans* (Russel 2016) and *multcompView* (Graves et al. 2015) packages in R.

The influence of experimental method and sound form on detected hearing frequencies were examined within each hearing type. As the data violated assumptions of normality and heterogeneity of variance, a non-parametric Kruskal-Wallis test was conducted for each hearing type, testing for significant differences in maximum and optimal frequencies between BEH and AEP methods. Similarly,

Kruskal-Wallis tests were applied to evaluate differences in hearing metrics between SPL and PAL sound forms. Although the effects of experimental method and sound form are likely confounded—both with each other as well as with hearing type—this analysis was undertaken to provide a broader-scale assessment of the distributions of frequencies detected under each method and each sound form.

Lastly, the relationship between detected frequency benchmarks across hearing types and sound form was separately assessed. Spearman correlation coefficients ( $r$ ) were calculated and compared to evaluate correlations between maximum and optimum frequency benchmarks for both hearing types and taxonomic groups. For expedient and effective analysis across the latter category, taxonomic orders ( $n=23$ ) were assigned to broader phylogenetic classifications based on common morphological characteristics inherent to individual orders (Table 3.3).

### Results

Distributions of detected frequency benchmarks among species increased with swim bladder complexity (Figure 3.4). Still, these distributions were confounded by differences in experimental method, sound form, taxonomy, and number of replicates, which were then explicitly considered in statistical model fitting. Selected models that incorporated these factors confirmed a statistically significant and positive association between detected frequencies and swim bladder morphology. The model for maximum hearing threshold with the lowest AIC was an LME model including all predictor variables (Table 3.4). This model contained the interaction between hearing type and method incorporated as a constant variance structure, then adjusted by the variance related to the number of replicates, with taxonomic order included as a

random effect. The optimal hearing frequency model with the lowest AIC was a GLS model that included the hearing type-method interaction as a constant variance structure alone. Unlike the maximum frequency model, neither adjusting the variance associated with the number of replicates nor incorporating the effects of taxonomic order improved the AIC (Table 3.4).

Post hoc comparisons of least square mean contrasts across hearing types for each of the selected final models indicated significant differences across maximum and optimal hearing thresholds based on swim bladder presence and its specialization. Contrasts among maximum frequency benchmarks across hearing types based on the selected model (Model 5 in Table 3.4) were significantly different across all groups ( $\alpha=0.05$ ), with least square means increasing with increasing swim bladder complexity and the presence of Weberian ossicles or bullae (Figure 3.5). Contrasts among optimal frequency benchmarks across hearing types based on the selected model (Model 3 in Table 3.4) were significantly different across combined hearing types T1-T3 and T4 ( $\alpha=0.05$ ) (Figure 3.6).

Kruskal-Wallis tests identified significant influences of experimental method and sound form on both maximum and optimal frequency benchmarks when applied within hearing types. While maximum frequency benchmarks across hearing types were generally lower for studies using BEH methods than those using AEP methods, significant differences in maximum frequency benchmarks between methods were identified only for Type 3 ( $p<0.05$ ; Figure 3.7). Note that the AEP maximum hearing metrics were increasingly ordered by hearing type, while BEH metrics were not. Optimal frequency metrics also showed this differing pattern across hearing types

according to AEP (consistent increasing trend) and BEH (interrupted trend) methods. Within hearing Type 2 (unmodified swim bladder), BEH methods yielded significantly higher optimal frequencies than AEP methods for Type 2 experiments alone ( $p < 0.05$ ; Figure 3.8). Kruskal-Wallis tests comparing frequency benchmarks across sound forms within groups demonstrated an influence of sound form tested on the estimation of both maximum and optimal frequencies detected. Distributions of maximum frequency benchmarks across hearing types were consistently lower for PAL-derived frequencies as opposed to SPL-derived frequencies, with PAL-frequencies significantly lower only within hearing type T2 ( $p < 0.05$ ; Figure 3.9). Broad distributions of optimal frequency benchmarks followed a similar pattern, with benchmarks for types T1 and T2 were significantly lower for PAL sound forms than SPL sound forms ( $p < 0.05$ ; Figure 3.10). For the literature pool reviewed, no PAL experiments were identified for Type 4 species.

Evaluation of Spearman's correlation coefficients ( $r$ ) revealed high variance in the associations between optimum and maximum frequencies (Figures 3.11, 3.12). All associations across hearing types and phylogenetic groups were positive, though they varied in strength depending on type and group (Table 3.5). Type 1 (T1) hearing morphologies demonstrated the strongest correlation ( $r = 0.63$ ), while Type 4 (T4) morphologies demonstrated the weakest correlation ( $r = 0.15$ ). Similarly, optimum and maximum frequency benchmarks were most strongly correlated for Elasmobranchs ( $r = 0.63$ ) and most weakly correlated for neoteleosts ( $r = 0.11$ ). A correlation coefficient could not be calculated for the Chondrostei/Holostei group due to limited sample size ( $n = 4$ ) and a lack of variance among this sample's data points.

Distributions of frequency benchmarks across hearing type (Figure 3.11) or phylogenetic groups (Figure 3.12) suggested an increase in frequency detection range with increased swim bladder complexity, with experiments measuring response to particle motion detecting a more limited range of lower frequencies than those studies measuring response to pressure waves. Phylogenetic groups with less complex swim bladder morphologies demonstrate a narrower range of frequency detection, concentrated at lower frequencies and in response to particle motion (Figure 3.12).

### Discussion

The literature on fish hearing sensitivity is surprisingly limited (63 identified studies) given the diversity of species and species habitats that are impacted by anthropogenic sound. This in part has led to past classification schemes that can model likely hearing sensitivity across broad hearing types. My literature analysis of diverse fish taxa supported the view that the generalist vs. specialist dichotomy is over simplistic (Popper et al. 2011) and that sensitivity threshold classifications based on swim bladder elaboration would be an improvement. Across taxa, experimental types, and sound forms, the literature analysis supported a more resolved, statistically significant and reliable classification of hearing performance corresponding to the presence and specialization of the swim bladder as an accessory hearing structure. Hearing type classification showed significant differences in audition between two hearing benchmarks (maximum and optimum frequencies): associations that were robust to possible confounding effects of study method, rigor (replication), and taxa. Evaluation of the relationship between optimum and maximum benchmarks supported the hypothesis that more complex swim bladder morphologies permit a

broader range of detection frequency, related to the ability of the swim bladder to facilitate detection of pressure waves.

The literature's skew towards sound pressure over particle motion in particular directs caution in drawing inferences from a review of past literature. Still, the limited particle motion literature base supported the overall inference of increased acuity with swim bladder presence and specialization. This finding corresponds with increasing recognition by the bioacoustics community of the potential for swim bladder specializations to widen frequency bandwidths in fishes, likely associated with convergent radiations into acoustic niche space (i.e., predator avoidance, conspecific communication, prey detection, etc.)—though direct drivers of its evolution remain unknown (Popper and Coombs 1982; Ladich and Popper 2004; Braun and Grande 2008).

Analyses of published audiograms are subject to sources of error associated with (1) the quality of the audiogram data used, and (2) an overall skew in the existing literature towards sound forms measured as pressure waves rather than particle motion. The veracity of individual audiogram studies—both AEP and behavioral in acquisition—in providing an accurate estimate of fish hearing acuity is contingent upon appropriate measurement and incorporation of the experimental sound field and received noise level; these levels can be quite heterogenous within tank systems and can result in substantial error in nominal (treatment) frequency and amplitude levels, should the acoustic conditions of the tank and background noise levels not be measured appropriately (Rogers et al. 2016; Sisneros et al. 2016). The use of AEP-derived audiograms has evoked caution from the scientific community,

given that AEP techniques measures microphonic potentials of auditory hair cells—a physical stimulus, rather than proof of auditory processing and response achieved with behavioral studies (Sisneros et al. 2016). The value of such experimental results may be further confounded when attempting to relate audiometrically-derived hearing thresholds to thresholds detected in the natural environment, during which issues of auditory masking in experimental settings and mismatching of impedance levels between environments (ratios of sound pressure to particle motion levels) may occur and distort results (Ladich and Fay 2013; Hawkins et al. 2015; Popper et al. 2014). Furthermore, the accurate comparison of data obtained from multiple audiograms demands similar, mathematically accurate measurements of the experimental sound field among studies, the absence of which would allow for increased variance across study-specific audiograms (Popper and Fay 2011; Hawkins 2015; Sisneros et al. 2016).

Experimental variables that affect hearing performance—method of detection, replication, and taxonomic order—were all included in best fitted models of hearing acuity. Of these variables, method of detection was associated with the greatest drop in AIC (affording the model with the highest explanatory power) for both maximum and optimum frequency benchmarks. The AEP-derived measurements exhibited poorer sensitivities and broader frequency thresholds than measurements derived from behavioral methods (Figures 3.7, 3.8; Popper and Fay 2011; Hawkins et al. 2015). Taxonomic effects were most apparent for the maximum frequency benchmark, which is not surprising as the T1 and T4 hearing type species originate from small sets of orders respectively; the former consists mainly of elasmobranchs

and a small subset of teleosts, while the latter is confined to a small set of orders comprising the otophysans and mormyrids. Replication had a significant, but more limited influence on hearing acuity wherein its inclusion in both benchmark models increased AIC (reducing model explanatory power) unless either experimental method, sound form, or both were incorporated as well. This response suggests that the inclusion of replication was successful in capturing a degree of experimental variance, but likely not a significant driver of acuity differences, alone.

An important source of uncertainty, particularly related to the absolute values of hearing benchmarks stems from the discord identified in the literature across experiments evaluating fish response to sound pressure level as opposed to particle motion. Of the 173 experiments reviewed, 143 monitored response to sound pressure waves and only 30 monitored response to particle motion. Recent advances provide strong evidence that the prevalent mode of hearing in fish is in response to particle motion (Popper and Fay 2011; Popper and Hawkins 2018). It is therefore likely that the sensitivities recorded in audiograms derived from pressure wave stimulus are inaccurate measurements, providing a wider bandwidth of threshold response to pressure waves in the given setting. The amplitudes of the corresponding sensitivities are most likely underestimated at dominant particle motion-sensitive frequencies, which are probably misrepresented by their sound pressure wave measurements (Popper et al. 2014). Still, I posit that the relative differences between the four hearing types are likely robust across particle motion and pressure wave sound forms (Figures 3.9, 3.10).



These findings contribute to the current dialogue of how to characterize fish audition in a more effective and efficient manner. I utilized a fairly coarse taxonomy of hearing types in an effort to start delving through existing—albeit imperfect—resources in the literature pool in an effort to more rigorously identify and quantify categories of fish hearing abilities. As a jumping off point to gauge possible impacts of anthropogenic and environmental noise to the hearing ecology of fishes, swim bladder presence and specialization merits attention. Hearing type classes could inform expectations on likely fish responses in impact studies of anthropogenic noise. Doing so might support more efficient field and laboratory study designs associated with hearing types to begin informing hearing abilities across a wide spectrum of fish species.

As common to literature reviews, certain themes within fish hearing function emerged associated with methodology, taxonomic bias, and rigor. One of the broader themes surrounding this dialogue has been the need for greater experimentation in the field and expanded datasets focusing on the detection of particle motion in a standardized sound field, an undertaking that will require greater priority and retooled methodology within fish audition studies.

## References

- Amoser, S., & Ladich, F. (2005). Are hearing sensitivities of freshwater fish adapted to the ambient noise in their habitats? *The Journal of Experimental Biology*, 208, 3533-3542. <https://doi.org/10.1242/jeb.01809>
- Amoser, S., Wysocki, L. E., & Ladich, F. (2004). Noise emission during the first powerboat race in an Alpine lake and potential impact on fish communities. *The Journal of the Acoustical Society of America*, 116(6), 3789-3797. <https://doi.org/10.1121/1.1808219>
- Bailey, H., Senior, B., Simmons, D., Rusin, J., Picken, G., & Thompson, P. M. (2010). Assessing underwater noise levels during pile-driving at an offshore windfarm and its potential effects on marine mammals. *Marine Pollution Bulletin*, 60, 888-897.
- Belanger, A. J., Bobeica, I., & Higgs, D. M. (2010). The effect of stimulus type and background noise on hearing abilities of the round goby *Negobius melanostomus*. *Journal of Fish Biology*, 77, 1488-1504. <https://doi.org/10.1111/j.1095-8649.2010.02773.x>
- Bureau of Ocean Energy Management. (2018, August). *Outer continental shelf renewable energy leases map book*.
- Braun, C. B., & Grande, T. (2008). Evolution of peripheral mechanisms for the enhancement of sound reception. *Fish Bioacoustics*, 32, 99-144.
- Bullock, T. H., & Corwin, J. T. (1979). Acoustic evoked activity in the brain in sharks. *Journal of Comparative Physiology*, 129, 223-234.
- Carroll, A. G., Przeslawski, R., Duncan, A., Gunning, M., & Bruce, B. (2017). A critical review of the potential impacts of marine seismic surveys on fish and invertebrates. *Marine Pollution Bulletin*, 114, 9-24. <https://doi.org/10.1016/j.marpolbul.2016.11.038>
- Casper, B. M., Smith, M. E., Halvorsen, M. B., Sun, H., Carlson, T. J., & Popper, A. N. (2013). Effects of exposure to pile driving sounds on fish inner ear tissues. *Comparative Biochemistry and Physiology, Part A*, 166. <https://doi.org/10.1016/j.cbpa.2013.07.008>
- Casper, B. M., & Mann, D. A. (2009). Field hearing measurements of the Atlantic sharpnose shark *Rhizoprionodon terraenovae*. *Journal of Fish Biology*, 75, 2768-2776. <https://doi.org/10.1111/j.1095-8649.2009.02477.x>
- Casper, B. M., & Mann, D. A. (2006). Evoked potential audiograms of the nurse shark (*Ginglymostoma cirratum*) and the yellow stingray (*Urobatis*

*jamaicensis*). *Environmental Biology of Fishes*.  
<https://doi.org/10.1007/s10641-006-9012-9>

- Casper, B. M., & Mann, D. A. (2007). Dipole hearing measurements in elasmobranch fishes. *Journal of Experimental Biology*, *210*, 75-81.  
<https://doi.org/10.1242/jeb.02617>
- Casper, B. M., Lobel, P. S., & Yan, H. Y. (2003). The hearing sensitivity of the little skate, *Raja erinacea*: A comparison of two methods. *Environmental Biology of Fishes*, *68*, 371-379.
- Chapman, C. J. (1973). Field studies of hearing in teleost fish. *Helgoländer wissenschaftliche Meeresuntersuchungen*, *24*, 371-390.
- Chapman, C. J., & Hawkins, A. D. (1973). A field study of hearing in the cod, *Gadus morhua* L. *Journal of Comparative Physiology*, *85*, 147-167.
- Codarin, A., Wysocki, L. E., Ladich, F., & Picciulin, M. (2009). Effects of ambient and boat noise on hearing and communication in three fish species living in a marine protected area (Miramare, Italy). *Marine Pollution Bulletin*, *58*, 1880-1887.
- Coombs, S., & Popper, A. N. (1979). Hearing differences among Hawaiian squirrelfish (family Holocentridae) related to differences in the peripheral auditory system. *Journal of Comparative Physiology A*, *132*, 203-207.
- Coombs, S., & Popper, A. N. (1982). Structure and function of the auditory system in the clown knifefish, *Notopterus chitala*. *Journal of Experimental Biology*, *97*, 225-239.
- Dale, J. J., Gray, M. D., Popper, A. N., Rogers, P. H., & Block, B. A. (2015). Hearing thresholds of swimming Pacific bluefin tuna *Thunnus orientalis*. *Journal of Comparative Physiology A*, *201*, 441-454. <https://doi.org/10.1007/s00359-015-0991-x>
- Dijkgraaf, S. (1960). Hearing in bony fishes. *Proceedings of the Royal Society of London, Series B, Biological Sciences*, *152*(946), 51-54.
- Egner, S. A., & Mann, D. A. (2005). Auditory sensitivity of sergeant major damselfish *Abudefduf saxatilis* from post-settlement juvenile to adult. *Marine Ecology Progress Series*, *285*, 213-222.
- Evans, H. M. (1925). A contribution to the anatomy and physiology of the air-bladder and Weberian ossicles in Cyprinidae. *Proceedings of the Royal Society of London Series B*, *97*(686), 545-576.

- Fish, J. F., & Offutt, G. C. (1972). Hearing thresholds from toadfish, *Opsanus tau*, measured in the laboratory and field. *The Journal of the Acoustical Society of America*, 51(4), 1318-1321. <https://doi.org/10.1121/1.1912977>
- von Frisch, K. (1938). The sense of hearing in fish. *Nature*, 141, 8-11.
- Frisk, G. V. (2007). Noiseconomics: The relationship between ambient noise levels in the sea and global economic trends. *Scientific Reports*, 437(2). <https://doi.org/10.1038/srep00437>
- Froese, R. and D. Pauly, Editors. 2000. FishBase 2000: concepts, design and data sources. ICLARM, Los Baños, Laguna, Philippines. 344 p.
- Graves, S., Piepho, H.P., and Selzer, L. (2015). multcompView: Visualizations of Paired Comparisons. R package version 0.1-7. <https://CRAN.R-project.org/package=multcompView>
- Halvorsen, M. B., Casper, B. M., Woodley, C. M., Carlson, T. J., & Popper, A. N. (2012). Threshold for onset of injury in Chinook salmon from exposure to impulsive pile driving sounds. *PLoS One*, 7(6).
- Hawkins, A. D., & Johnstone, D. F. (1978). The hearing of the Atlantic Salmon, *Salmo salar*. *Journal of Fish Biology*, 13, 655-673.
- Hawkins, A. D., Pembroke, A. E., & Popper, A. N. (2015). Information gaps in understanding the effects of noise on fishes and invertebrates. *Reviews in Fish Biology and Fisheries*, 25, 39-64. <https://doi.org/10.1007/s11160-014-9369-3>
- Hawkins, A. D., & Popper, A. N. (2017). A sound approach to assessing the impact of underwater noise on marine fishes and invertebrates. *ICES Journal of Marine Science*, 74(3), 635-651. <https://doi.org/10.1093/icesjms/fsw205>
- Higgs, D. M., Souza, M. J., Wilkins, H. R., Presson, J. C., & Popper, A. N. (2001). Age- and size-related changes in the inner ear and hearing ability of the adult zebrafish (*Danio rerio*). *Journal of the Association for Research in Otolaryngology*, 3, 174-184. <https://doi.org/10.1007/s101620020035>
- Hildebrand, J. A. (2009). Anthropogenic and natural sources of ambient noise in the ocean. *Marine Ecology Progress Series*, 395, 5-20. <https://doi.org/10.3354/meps08353>
- Holt, D. E., & Johnston, C. E. (2011). Hearing sensitivity in two black bass species using the auditory brainstem response approach. *Environmental Biology of Fishes*, 91, 121-126. <https://doi.org/10.1007/s10641-010-9756-0>

- Horodysky, A. Z., Brill, R. W., Fine, M. L., Musick, J. A., & Latour, R. J. (2008). Acoustic pressure and particle motion thresholds in six sciaenid fishes. *Journal of Experimental Biology*, 211, 1504-1511. <https://doi.org/10.1242/jeb.016196>
- Kastelein, R. A., van der Heul, S., Verboom, W. C., Jennings, N., van der Veen, J., & de Haan, D. (2008). Startle response of captive North Sea fish species to underwater tones between 0.1 and 64 kHz. *Marine Environmental Research*, 65, 369-377. <https://doi.org/10.1016/j.marenvres.2008.01.001>
- Kelly, J. C., & Nelson, D. R. (1975). Hearing thresholds of the horn shark, *Heterodontus francisci*. *The Journal of the Acoustical Society of America*, 58(4), 905-909. <https://doi.org/10.1121/1.380742>
- Kenyon, T. N., Ladich, F., & Yan, H. Y. (1998). A comparative study of hearing ability in fishes: The auditory brainstem response approach. *Journal of Comparative Physiology A*, 182, 307-318.
- Kojima, T., Ito, H., Komada, T., Taniuchi, T., & Akamatsu, T. (2005). Measurement of auditory sensitivity in common carp *Cyprinus carpio* by the auditory brainstem response technique and cardiac conditioning method. *Fisheries Science*, 71, 95-100.
- Kojima, T., Suga, T., Kusano, A., Shimizu, S., Matsumoto, H., Aoki, S., . . . Taniuchi, T. (2010). Acoustic pressure sensitivities and effects of particle motion in red sea bream *Pagrus major*. *Fisheries Science*, 76, 13-20. <https://doi.org/10.1007/s12562-009-0194-x>
- Kritzler, H., & Wood, L. (1961). Provisional audiogram for the shark, *Carcharhinus leucas*. *Science*, 133(3463), 1480-1482.
- Kunc, H. P., McLaughlin, K. E., & Schmidt, R. (2016). Aquatic noise pollution: Implications for individuals, populations, and ecosystems. *Proceedings of the Royal Society B*, 283. <https://doi.org/10.1098/rspb.2016.0839>
- Ladich, F. (1999). Did auditory sensitivity and vocalization evolve independently in otophysan fishes. *Brain, Behavior, and Evolution*, 53, 288-304.
- Ladich, F., & Popper, A. N. (2004). Parallel evolution in fish hearing organs. *Evolution of the Vertebrate Auditory System*, 22, 95-127.
- Ladich, F., & Yan, H. Y. (1998). Correlation between auditory sensitivity and vocalization in anabantoid fishes. *Journal of Comparative Physiology A*, 182, 737-746.

- Lechner, W., & Ladich, F. (2008). Size matters: Diversity in swimbladders and Weberian ossicles affects hearing in catfishes. *Journal of Experimental Biology*, *211*, 1681-1689. <https://doi.org/10.1242/jeb.016436>
- Lovell, J. M., Findlay, M. M., Moate, R. M., Nedwell, J. R., & Pegg, M. A. (2005). The inner ear morphology and hearing abilities of the Paddlefish (*Polydon spathula*) and the Lake Sturgeon (*Acipenser fulvenscens*). *Comparative Biochemistry and Physiology*, *142*, 286-296.
- Lovell, J. M., Findlay, M. M., Nedwell, J. R., & Pegg, M. A. (2006). The hearing abilities of the silver carp (*Hypophthalmichthys molitrix*) and bighead carp (*Aristichthys nobilis*). *Comparative Biochemistry and Physiology*, *143*, 286-291. <https://doi.org/10.1016/j.cbpa.2005.11.015>
- Lugli, M., Yan, H. Y., & Fine, M. L. (2003). Acoustic communication in two freshwater gobies: The relationship between ambient noise, hearing thresholds and sound spectrum. *Journal of Comparative Physiology A*, *189*, 309-320. <https://doi.org/10.1007/s00359-003-0404-4>
- Mann, D. A., Hastings, M. C., & Popper, A. N. (1998). Detection of ultrasonic tones and simulated dolphin echolocation clicks by a teleost fish, the American shad (*Alosa sapidissima*). *The Journal of the Acoustical Society of America*, *104*(1), 562-568. <https://doi.org/10.1121/1.423255>
- Mann, D., Higgs, D., Tavalga, W., & Souza, M. J. (2001). Ultrasound detection by clupeiform fishes. *The Journal of the Acoustical Society of America*, *109*(6), 3048-3054.
- Mann, D. A., Cott, P. A., Hanna, B. W., & Popper, A. N. (2007). Hearing in eight species of northern Canadian freshwater fishes. *Journal of Fish Biology*, *70*, 109-120. <https://doi.org/10.1111/j.1095-8649.2006.01279.x>
- Maruska, K. P., Boyle, K. S., Dewan, L. R., & Tricas, T. C. (2007). Sound production and spectral hearing sensitivity in the Hawaiian sergeant damselfish, *Abudefduf abdominalis*. *Journal of Experimental Biology*, *210*, 3990-4004. <https://doi.org/10.1242/jeb.004390>
- McCormick, C. A., & Popper, A. N. (1984). Auditory sensitivity and psychophysical tuning curves in the elephant nose fish, *Gnathonemus petersii*. *Journal of Comparative Physiology A*, *155*, 753-761.
- McCauley, R. D., Fewtrell, J., Duncan, A. J., Jenner, C., Jenner, M.-N., Penrose, J. D., & 4 others. (2000). Marine seismic surveys: A study of environmental implications. *APPEA Journal*, 692-708.

- McCauley, R. D., Fewtrell, J., & Popper, A. N. (2003). High intensity anthropogenic sound damages fish ears. *The Journal of the Acoustical Society of America*, *113*(1), 1-5. <https://doi.org/10.1121/1.1527962>
- McDonald, M. A., Hildebrand, J. A., & Wiggins, S. M. (2006). Increases in deep ocean ambient noise in the Northeast Pacific west of San Nicolas Island, California. *The Journal of the Acoustical Society of America*, *120*(2), 711-718. <https://doi.org/10.1121/1.2216565>
- Myrberg, A. A., & Spires, J. Y. (1980). Hearing in damselfishes: An analysis of signal detection among closely related species. *Journal of Comparative Physiology A*, *140*, 135-144.
- National Research Council. (2003). *Ocean noise and marine mammals*. Washington D.C., USA: The National Academies Press. <https://doi.org/10.17226/10564>.
- Nedwell, J. R., Edwards, B., Turnpenney, A. W. H., & Gorden, J. (2004, September). *Fish and marine mammal audiograms: A summary of available information* (Subacoustech Report No. 534R0214).
- Nelson, D. R. (1967). Hearing thresholds, frequency discrimination, and acoustic orientation in the lemon shark, *Negaprion brevirostris* (poey). *Bulletin of Marine Science*, *17*(3), 741-768.
- Nowacek, D. P., Clark, C. W., Mann, D., Miller, P. J. O., Rosenbaum, H. C., Golden, J. S., . . . Southall, B. L. (2015). Marine seismic surveys and ocean noise: Time for coordinated and prudent planning. *Frontiers in Ecology and the Environment*, *13*(7), 378-386. <https://doi.org/10.1890/130286>
- Offut, G. C. (1974). Structures for the detection of acoustic stimuli in the Atlantic codfish, *Gadus morhua*. *The Journal of the Acoustical Society of America*, *56*(2), 665-671.
- Oxman, D. S., Barnett-Johnson, R., Smith, M. E., Coffin, A., Miller, D. L., Josephson, R., & Popper, A. N. (2007). The effect of vaterite deposition on sound reception, otolith morphology, and inner ear sensory epithelia in hatchery-reared Chinook salmon (*Oncorhynchus tshawytscha*). *Canadian Journal of Fisheries and Aquatic Science*, *64*, 1469-1478. <https://doi.org/10.1139/F07-106>
- Parmentier, E., Colleye, O., & Mann, D. (2009). Hearing ability in three clownfish species. *Journal of Experimental Biology*, *212*, 2023-2026. <https://doi.org/10.1242/jeb.030270>

- Parmentier, E., Mann, K., & Mann, D. (2011). Hearing and morphological specializations of the mojarra (*Eucinostomus argenteus*). *Journal of Experimental Biology*, 214, 2697-2701. <https://doi.org/10.1242/jeb.058750>
- Pinheiro J, Bates D, DebRoy S, Sarkar D, R Core Team (2018). *nlme: Linear and Nonlinear Mixed Effects Models*. R package version 3.1-137, <URL: <https://CRAN.R-project.org/package=nlme>>.
- Poggendorf, D. (1952). Die absoluten hörschwellen des zwerglwelses (*Amiurus nebulosus*) und beiträge zur physik des Weberschen apparatus der Ostariophysen. *Zeitschrift für vergleichende Physiologie*, 34, 222-257.
- Popper, A. N. (1970). Auditory capacities of the Mexican blind cave fish (*Astyanax jordani*) and its eyed ancestor (*Astyanax mexicanus*). *Animal Behavior*, 18, 552-562.
- Popper, A. N., & Coombs, S. (1982). The morphology and evolution of the ear in Actinopterygian fishes. *American Zoologist*, 22, 311-328.
- Popper, A. N., & Fay, R. R. (1993). Sound detection and processing by fish: Critical review and major research questions. *Brain, Behavior and Evolution*, 41, 14-38.
- Popper, A. N., Smith, M. E., Cott, P. A., Hanna, B. W., MacGillivray, A. O., Austin, M. E., & Mann, D. A. (2005). Effects of exposure to seismic airgun use on hearing of three fish species. *The Journal of the Acoustical Society of America*, 117(6), 3958-3971. <https://doi.org/10.1121/1.1904386>
- Popper, A. N., & Hastings, M. C. (2009). The effects of human-generated sound on fish. *Integrative Zoology*, 4, 43-52. <https://doi.org/10.1111/j.1749-4877.2008.00134.x>
- Popper, A. N., & Fay, R. R. (2011). Rethinking sound detection by fishes. *Hearing Research*, 273, 25-36. <https://doi.org/10.1016/j.heares.2009.12.023>
- Popper, A. N., Hawkins, A. D., Fay, R. R., Mann, D. A., Bartol, S., Carlson, T. J., . . . Tavalga, W. N. (2014). *Sound exposure guidelines for fishes and sea turtles: A technical report prepared by ANSI-Accredited Standards Committee S3/SC1 and registered with ANSI* (Technical Report No. 2196-1212). Acoustical Society of America.
- Popper, A. N., & Hawkins, A. D. (2018). The importance of particle motion to fishes and invertebrates. *The Journal of the Acoustical Society of America*, 143(1), 470-488. <https://doi.org/10.1121/1.5021594>



- Popper, A. N., & Hawkins, A. D. (2019). An overview of fish bioacoustics and the impacts of anthropogenic sounds on fishes. *Journal of Fish Biology*, *94*, 692-713. <https://doi.org/10.1111/jfb.13948>
- Ramcharitar, J., & Popper, A. N. (2004). Masked auditory thresholds in sciaenid fishes: A comparative study. *The Journal of the Acoustical Society of America*, *116*(3), 1687-1691. <https://doi.org/10.1121/1.1771614>
- Ramcharitar, J. U., Higgs, D. M., & Popper, A. N. (2006). Audition in sciaenid fishes with different swim bladder-inner ear configurations. *The Journal of the Acoustical Society of America*, *119*(1), 439-443. <https://doi.org/10.1121/1.2139068>
- Rosen, D. E., & Greenwood, P. H. (1970). Origin of the Weberian apparatus and the relationship of the Ostariophysan and Gonorynchiform fishes. *American Museum Novitates*, (2428).
- Russell V. L. (2016). Least-Squares Means: The R Package lsmeans. *Journal of Statistical Software*, *69*(1), 1-33. doi:10.18637/jss.v069.i01
- Scholz, K., & Ladich, F. (2006). Sound production, hearing and possible interception under ambient noise conditions in the topmouth minnow *Pseudorasbora parva*. *Journal of Fish Biology*, *69*, 892-906. <https://doi.org/10.1111/j.1095-8649.2006.01168.x>
- Schulz-Mirbach, T., Metscher, B., & Ladich, F. (2012). Relationship between swim bladder morphology and hearing abilities- A case study on Asian and African cichlids. *PLOS One*, *7*(8). <https://doi.org/10.1371/journal.pone.0042292>
- Sisneros, J. S., Popper, A. N., Hawkins, A. D., & Fay, R. (2015). Audio evoked potential audiograms compared with behavioral audiograms in aquatic animals. *Advances in Experimental Medicine and Biology*, *875*, 1049-1056.
- Skalski, J. R., Pearson, W. H., & Malm, C. I. (1992). Effects of sounds from a geophysical survey device on catch-per-unit-effort in a hook-and-line fishery for rockfish (*Sebastes spp.*). *Canadian Journal of Fisheries and Aquatic Sciences*, *49*, 1357-1365.
- Slabbekoorn, H., Bouton, N., van Opzeeland, I., Coers, A., ten Cate, C., & Popper, A. N. (2010). A noisy spring: The impact of globally rising underwater sound levels on fish. *Trends in Ecology and Evolution*, *25*(7), 419-427. <https://doi.org/10.1016/j.tree.2010.04.005>

- Tavolga, W. N., & Wodinsky, J. (1963). Auditory capacities in fishes: Pure tone thresholds in nine species of marine teleosts. *Bulletin of the American Museum of Natural History*, *126*, 172-240.
- Vasconcelos, R. O., Amorim, M. C. P., & Ladich, F. (2007). Effects of ship noise on the detectability of communication signals in the Lusitanian toadfish. *Journal of Experimental Biology*, *210*, 2104-2112. <https://doi.org/10.1242/jeb.004317>
- Wardle, C. S., Carter, T. J., Urquhart, G. G., Johnstone, A. D. F., Ziolkowski, A. M., Hampson, G., & Mackie, D. (2001). Effects of seismic airguns on marine fish. *Continental Shelf Research*, *21*, 1005-1027.
- Weilgart, L. (2018, May). *The impact of ocean noise pollution on fish and invertebrates*. OceanCare.
- Wright, K. J., Higgs, D. M., Cato, D. H., & Leis, J. M. (2010). Auditory sensitivity in settlement-stage larvae of coral reef fishes. *Coral Reefs*, *29*, 235-243. <https://doi.org/10.1007/s00338-009-0572-y>
- Wysocki, L. E., & Ladich, F. (2005). Hearing in fishes under noise conditions. *Journal of the Association for Research in Otolaryngology*, *6*, 28-36. <https://doi.org/10.1007/s10162-004-4043-4>
- Wysocki, L. E., Codarin, A., Ladich, F., & Picciulin, M. (2009). Sound pressure and particle acceleration audiograms in three marine fish species from the Adriatic Sea. *The Journal of the Acoustical Society of America*, *126*(4), 2100-2107. <https://doi.org/10.1121/1.3203562>
- Yan, H. Y., & Curtsinger, W. S. (2000). The otic gasbladder as an ancillary auditory structure in a mormyrid fish. *Journal of Comparative Physiology A*, *186*, 595-602. <https://doi.org/10.1007/s003590000114>
- Yan, H. Y., Fine, M. L., Horn, N. S., & Colón, W. E. (2000). Variability in the role of the gasbladder in fish audition. *Journal of Comparative Physiology A*, *186*, 435-445. <https://doi.org/10.1007/s003590050443>

Tables

**Table 3.1.** Detected frequency benchmarks, associated metadata, and sourced study for each species-, method-, and sound form-specific audiogram experiment identified. Experiments are listed in alphabetical order of the source studies.

Common name	Genus species	Order	Hearing type	Experimental method	Sound form	No. replicates	Maximum frequency (Hz)	Optimal frequency (Hz)	Minimum frequency (Hz)	Source
Common carp	<i>Cyprinus carpio</i>	Cypriniformes	T4	AEP	SPL	6	4000	800	100	Amoser and Ladich 2005
European perch	<i>Perca fluviatilis</i>	Perciformes	T2	AEP	SPL	6	1000	200	100	Amoser and Ladich 2005
Roach	<i>Rutilus rutilus</i>	Cypriniformes	T4	AEP	SPL	2	4000	800	100	Amoser et al. 2004
European whitefish	<i>Coregonus lavaretus</i>	Salmoniformes	T2	AEP	SPL	6	800	250	100	Amoser et al. 2004
Round goby	<i>Neogobius melanostomus</i>	Perciformes	T1	AEP	SPL	37	600	400	100	Belanger et al. 2010
Round goby	<i>Neogobius melanostomus</i>	Perciformes	T1	AEP	PAL	37	600	100	100	Belanger et al. 2010
Atlantic sharpnose shark	<i>Rhizoprionodon terraenovae</i>	Carcharhiniformes	T1	AEP	PAL	3	1000	20	20	Casper and Mann 2009
Nurse shark	<i>Ginglymostoma cirratum</i>	Orectolobiformes	T1	AEP	PAL	5	1000	600	100	Casper and Mann 2006
Yellow stingray	<i>Urobatis jamicensis</i>	Myliobatiformes	T1	AEP	PAL	5	1000	800	100	Casper and Mann 2006
Nurse shark	<i>Ginglymostoma cirratum</i>	Orectolobiformes	T1	AEP	SPL	5	1000	600	100	Casper and Mann 2006
Brownband bamboo shark	<i>Chiloscyllium punctatum</i>	Orectolobiformes	T1	AEP	PAL	2	200	100	20	Casper and Mann 2007
Whitespotted bamboo shark	<i>Chiloscyllium plagiosum</i>	Orectolobiformes	T1	AEP	PAL	4	200	100	20	Casper and Mann 2007

Common name	Genus species	Order	Hearing type	Experimental method	Sound form	No. replicates	Maximum frequency (Hz)	Optimal frequency (Hz)	Minimum frequency (Hz)	Source
Horn shark	<i>Heterodontus francisci</i>	Heterodontiformes	T1	AEP	PAL	3	300	20	20	Casper and Mann 2007
Whitespotted bamboo shark	<i>Chiloscyllium plagiosum</i>	Orectolobiformes	T1	AEP	PAL	5	200	20	20	Casper and Mann 2007
Little skate	<i>Leucoraja erinacea</i>	Rajiformes	T1	AEP	SPL	3	800	150	100	Casper et al. 2003
Little skate	<i>Leucoraja erinacea</i>	Rajiformes	T1	BEH	SPL	4	800	250	200	Casper et al. 2003
Pollack	<i>Pollachius pollachius</i>	Gadiformes	T3	BEH	SPL	2	470	250	40	Chapman 1973
Haddock	<i>Melanogrammus aeglefinus</i>	Gadiformes	T3	BEH	SPL	9	470	200	30	Chapman 1973
Ling	<i>Molva molva</i>	Gadiformes	T3	BEH	SPL	1	550	200	40	Chapman 1973
Atlantic cod	<i>Gadus morhua</i>	Gadiformes	T3	BEH	SPL	43	470	160	30	Chapman and Hawkins 1973
Brown meagre	<i>Sciaena umbra</i>	Perciformes	T2	AEP	SPL	6	3000	300	100	Codarin 2009
Mediterranean damselfish	<i>Chromis chromis</i>	Perciformes	T2	AEP	SPL	6	600	200	100	Codarin 2009
Red-mouthed goby	<i>Gobius cruentatus</i>	Perciformes	T2	AEP	SPL	6	700	200	100	Codarin 2009
Squirrelfish	<i>Sargocentron xantherythrum</i>	Beryciformes	T2	BEH	SPL	3	800	500	100	Coombs and Popper 1979
Squirrelfish	<i>Mypristis kuntee</i>	Beryciformes	T3	BEH	SPL	2	3000	1000	100	Coombs and Popper 1979
Clown knifefish	<i>Chitala ornata</i>	Osteoglossiformes	T2	BEH	SPL	3	1000	500	100	Coombs and Popper 1982

Common name	Genus species	Order	Hearing type	Experimental method	Sound form	No. replicates	Maximum frequency (Hz)	Optimal frequency (Hz)	Minimum frequency (Hz)	Source
Pacific bluefin tuna	<i>Thunnus orientalis</i>	Perciformes	T2	BEH	SPL	6	800	450	325	Dale 2014
Pacific bluefin tuna	<i>Thunnus orientalis</i>	Perciformes	T2	BEH	PAL	6	800	450	325	Dale 2014
Sergeant major damselfish	<i>Abudefduf saxatilis</i>	Perciformes	T2	AEP	SPL	32	1600	100	100	Egner and Mann 2005
Oyster toadfish	<i>Opsanus tau</i>	Batrachoidiformes	T3	BEH	SPL	3	700	75	37.5	Fish and Offut 1972 Hawkins and Johnstone 1978
Atlantic salmon	<i>Salmo salar</i>	Salmoniformes	T3	BEH	SPL	5	380	160	32	Hawkins and Johnstone 1978
Atlantic salmon	<i>Salmo salar</i>	Salmoniformes	T3	BEH	PAL	5	380	160	32	Hawkins and Johnstone 1978
Zebrafish	<i>Danio rerio</i>	Cypriniformes	T4	AEP	SPL	10	4000	800	100	Higgs et al. 2001
Redeye bass	<i>Micropterus coosae</i>	Perciformes	T2	AEP	SPL	5	2000	100	100	Holt and Johnston 2011
Alabama bass	<i>Micropterus henshalli</i>	Perciformes	T2	AEP	SPL	5	600	100	100	Holt and Johnston 2011
Redeye bass	<i>Micropterus coosae</i>	Perciformes	T2	AEP	PAL	5	2000	100	100	Holt and Johnston 2011
Alabama bass	<i>Micropterus henshalli</i>	Perciformes	T2	AEP	PAL	5	600	100	100	Holt and Johnston 2011
Spotted seatrout	<i>Cynoscion nebulosus</i>	Perciformes	T3	AEP	SPL	6	1000	500	100	Horodysky et al. 2008

Common name	Genus species	Order	Hearing type	Experimental method	Sound form	No. replicates	Maximum frequency (Hz)	Optimal frequency (Hz)	Minimum frequency (Hz)	Source
Red drum	<i>Sciaenops ocellatus</i>	Perciformes	T2	AEP	SPL	6	1000	300	100	Horodysky et al. 2008
Northern kingfish	<i>Menticirrhus saxatilis</i>	Perciformes	T2	AEP	SPL	6	1000	800	100	Horodysky et al. 2008
Weakfish	<i>Cynoscion regalis</i>	Perciformes	T3	AEP	SPL	6	1000	600	100	Horodysky et al. 2008
Spot	<i>Leiostomus xanthurus</i>	Perciformes	T2	AEP	SPL	6	1000	200	100	Horodysky et al. 2008
Atlantic croaker	<i>Micropogonias undulatus</i>	Perciformes	T3	AEP	SPL	6	1000	300	100	Horodysky et al. 2008
Spotted seatrout	<i>Cynoscion nebulosus</i>	Perciformes	T3	AEP	PAL	6	1000	400	100	Horodysky et al. 2008
Red drum	<i>Sciaenops ocellatus</i>	Perciformes	T2	AEP	PAL	6	1000	100	100	Horodysky et al. 2008
Northern kingfish	<i>Menticirrhus saxatilis</i>	Perciformes	T2	AEP	PAL	6	1000	100	100	Horodysky et al. 2008
Weakfish	<i>Cynoscion regalis</i>	Perciformes	T3	AEP	PAL	6	1000	100	100	Horodysky et al. 2008
Spot	<i>Leiostomus xanthurus</i>	Perciformes	T2	AEP	PAL	6	1000	100	100	Horodysky et al. 2008
Atlantic croaker	<i>Micropogonias undulatus</i>	Perciformes	T3	AEP	PAL	6	1000	100	100	Horodysky et al. 2008
Yellowfin tuna	<i>Thunnus albacares</i>	Perciformes	T2	BEH	SPL	NA	800	500	325	Iverson 1969 audiogram, published in Dale 2014
Kawakawa	<i>Euthynnus affinis</i>	Perciformes	T1	BEH	SPL	NA	800	500	325	Iverson 1969 audiogram, published in Dale 2014
European seabass	<i>Dichentrarchus labrax</i>	Perciformes	T2	BEH	SPL	17	700	150	100	Kastelein et al. 2008
Thicklip grey mullet	<i>Chelon labrosus</i>	Mugiliformes	T2	BEH	SPL	11	700	450	400	Kastelein et al. 2008

Common name	Genus species	Order	Hearing type	Experimental method	Sound form	No. replicates	Maximum frequency (Hz)	Optimal frequency (Hz)	Minimum frequency (Hz)	Source
Pout Atlantic horse mackerel	<i>Trisopterus luscus</i>	Gadiformes	T3	BEH	SPL	9	250	100	100	Kastelein et al. 2008
Horn shark	<i>Trachurus trachurus</i>	Perciformes	T2	BEH	SPL	13	2000	100	100	Kastelein et al. 2008
Horn shark	<i>Heterodontus francisci</i>	Heterodontiformes	T1	BEH	PAL	4	160	80	20	Kelly and Nelson 1975
Goldfish	<i>Heterodontus francisci</i>	Heterodontiformes	T1	BEH	SPL	4	160	40	20	Kelly and Nelson 1975
Oscar	<i>Carassius auratus</i>	Cypriniformes	T4	AEP	SPL	8	5000	700	100	Kenyon et al. 1998
Oscar	<i>Astronotus ocellatus</i>	Perciformes	T3	AEP	SPL	8	2000	100	100	Kenyon et al. 1998
Oscar	<i>Astronotus ocellatus</i>	Perciformes	T3	BEH	SPL	NA	800	200	200	Kenyon et al. 1998, audiogram published in Yan and Popper 1992
Common carp	<i>Cyprinus carpio</i>	Cypriniformes	T4	BEH	SPL	5	2000	1000	100	Kojima et al. 2005
Common carp	<i>Cyprinus carpio</i>	Cypriniformes	T4	AEP	SPL	8	3010	505	100	Kojima et al. 2005
Red seabream	<i>Pagrus major</i>	Perciformes	T2	BEH	SPL	35	1100	300	110	Kojima et al. 2010
Red seabream	<i>Pagrus major</i>	Perciformes	T2	AEP	SPL	18	1100	300	110	Kojima et al. 2010
Red seabream	<i>Pagrus major</i>	Perciformes	T2	AEP	PAL	10	200	200	50	Kojima et al. 2010
Bull shark	<i>Carcharhinus leucas</i>	Charcharhiniformes	T1	BEH	SPL	2	1500	500	100	Kritzler and Wood 1961
Blue botia	<i>Yasuhikotakia modesta</i>	Cypriniformes	T4	AEP	SPL	7	5000	600	100	Ladich 1999
Red-bellied piranha	<i>Pygocentrus nattereri</i>	Characiformes	T4	AEP	SPL	6	5000	900	100	Ladich 1999

Common name	Genus species	Order	Hearing type	Experimental method	Sound form	No. replicates	Maximum frequency (Hz)	Optimal frequency (Hz)	Minimum frequency (Hz)	Source
Spotted talking catfish	<i>Agamyxis pectinifrons</i>	Siluriformes	T4	AEP	SPL	12	5000	800	100	Ladich 1999
Pictus catfish	<i>Pimelodus pictus</i>	Siluriformes	T4	AEP	SPL	11	5000	550	100	Ladich 1999
Blue leopard corydoras	<i>Corydoras paleatus</i>	Siluriformes	T4	AEP	SPL	10	4000	600	100	Ladich 1999
Glass knifefish	<i>Eigenmannia virescens</i>	Gymnotiformes	T4	AEP	SPL	6	5000	500	100	Ladich 1999
Dusky pimelodid	<i>Pimelodus blochii</i>	Siluriformes	T4	AEP	SPL	11	5000	500	100	Ladich 1999
Croaking gourami	<i>Trichopsis vittata</i>	Perciformes	T3	AEP	SPL	11	5000	1500	100	Ladich and Yan 1998
Pygmy gourami	<i>Trichopsis pumila</i>	Perciformes	T3	AEP	SPL	9	5000	250	100	Ladich and Yan 1998
Blue gourami	<i>Trichopodus trichopterus</i>	Perciformes	T3	AEP	SPL	9	5000	800	100	Ladich and Yan 1998
Dwarf gourami	<i>Trichogaster lalia</i>	Perciformes	T3	AEP	SPL	9	5000	1000	100	Ladich and Yan 1998
Paradise fish	<i>Macropodus opercularis</i>	Perciformes	T3	AEP	SPL	9	5000	150	100	Ladich and Yan 1998
Tete sea catfish	<i>Ariopsis seemanni</i>	Siluriformes	T4	AEP	SPL	6	5000	3000	50	Lechner and Ladich 2008
Bumblebee jelly catfish	<i>Batrochoglanis raninus</i>	Siluriformes	T4	AEP	SPL	6	5000	2000	50	Lechner and Ladich 2008
Electric catfish	<i>Malapterurus beninensis</i>	Siluriformes	T4	AEP	SPL	6	5000	2000	50	Lechner and Ladich 2008
Onespot squeaker	<i>Synodontis schoutedeni</i>	Siluriformes	T4	AEP	SPL	7	5000	800	50	Lechner and Ladich 2008
Striped woodcat	<i>Trachelyopteric thys taeniatus</i>	Siluriformes	T4	AEP	SPL	6	5000	2000	50	Lechner and Ladich 2008



Common name	Genus species	Order	Hearing type	Experimental method	Sound form	No. replicates	Maximum frequency (Hz)	Optimal frequency (Hz)	Minimum frequency (Hz)	Source
Medusa pleco False network catfish	<i>Ancistrus ranunculus</i>	Siluriformes	T4	AEP	SPL	8	5000	1000	50	Lechner and Ladich 2008
Flagtail catfish	<i>Corydoras sodalis</i>	Siluriformes	T4	AEP	SPL	6	5000	500	50	Lechner and Ladich 2008
Pinocchio whiptail catfish	<i>Dianema urostriatum</i>	Siluriformes	T4	AEP	SPL	8	5000	500	50	Lechner and Ladich 2008
Big-eyed armored catfish	<i>Hemiodontichthys acipenserinus</i>	Siluriformes	T4	AEP	SPL	7	5000	500	50	Lechner and Ladich 2008
American paddlefish	<i>Hypoptopoma thoracatum</i>	Siluriformes	T4	AEP	SPL	7	5000	800	50	Lechner and Ladich 2008
Lake sturgeon	<i>Polyodon spathula</i>	Acipenseriformes	T2	AEP	SPL	12	500	250	100	Lovell et al. 2005
American paddlefish	<i>Acipenser fulvescens</i>	Acipenseriformes	T2	AEP	SPL	12	500	200	100	Lovell et al. 2005
Lake sturgeon	<i>Polyodon spathula</i>	Acipenseriformes	T2	AEP	PAL	12	500	250	100	Lovell et al. 2005
Silver carp	<i>Acipenser fulvescens</i>	Acipenseriformes	T2	AEP	PAL	12	500	200	100	Lovell et al. 2005
Bighead carp	<i>Hypophthalmichthys molitrix</i>	Cypriniformes	T4	AEP	SPL	12	3000	750	100	Lovell et al. 2006
Padanian goby	<i>Aristichthys nobilis</i>	Cypriniformes	T4	AEP	SPL	12	3000	1500	100	Lovell et al. 2006
Arno goby	<i>Padogobius bonelli</i>	Perciformes	T2	AEP	SPL	5	800	100	75	Lugli et al. 2003
American shad	<i>Padogobius nigricans</i>	Perciformes	T2	AEP	SPL	4	800	100	75	Lugli et al. 2003
	<i>Alosa sapidissima</i>	Clupeiformes	T3	AEP	SPL	8	4000	800	100	Mann et al. 1998

Common name	Genus species	Order	Hearing type	Experimental method	Sound form	No. replicates	Maximum frequency (Hz)	Optimal frequency (Hz)	Minimum frequency (Hz)	Source
Gulf menhaden	<i>Brevoortia patronus</i>	Clupeiformes	T3	AEP	SPL	10	1500	300	300	Mann et al. 2001
Bay anchovy	<i>Anchoa mitchilli</i>	Clupeiformes	T3	AEP	SPL	15	2000	100	100	Mann et al. 2001
Scaled sardine	<i>Harengula jaguana</i>	Clupeiformes	T3	AEP	SPL	16	1500	800	100	Mann et al. 2001
Spanish sardine	<i>Sardinella aurita</i>	Clupeiformes	T3	AEP	SPL	2	1500	100	100	Mann et al. 2001
Lake chub	<i>Couesius plumbeus</i>	Cypriniformes	T4	AEP	SPL	5	1600	500	100	Mann et al. 2007
Longnose sucker	<i>Catostomus catostomus</i>	Cypriniformes	T4	AEP	SPL	4	1600	600	100	Mann et al. 2007
Trout-perch	<i>Percopsis omiscomaycus</i>	Percopsiformes	T2	AEP	SPL	4	1600	100	100	Mann et al. 2007
Ninespine stickleback	<i>Pungitius pungitius</i>	Gasterosteiformes	T2	AEP	SPL	4	1600	200	100	Mann et al. 2007
Northern pike	<i>Esox lucius</i>	Esociformes	T2	AEP	SPL	5	1600	200	100	Mann et al. 2007
Spoonhead sculpin	<i>Cottus ricei</i>	Scorpaeniformes	T1	AEP	SPL	4	1600	200	100	Mann et al. 2007
Burbot	<i>Lota lota</i>	Gadiformes	T3	AEP	SPL	1	1600	200	100	Mann et al. 2007
Broad whitefish	<i>Coregonus nasus</i>	Salmoniformes	T2	AEP	SPL	5	1600	200	100	Mann et al. 2007
Hawaiian sergeant damselfish	<i>Abudefduf abdominalis</i>	Perciformes	T2	AEP	SPL	6	1000	125	90	Maruska et al. 2007
Peter's elephant nose fish	<i>Gnathonemus petersii</i>	Osteoglossiformes	T4	BEH	SPL	4	2500	400	100	McCormick and Popper 1984

Common name	Genus species	Order	Hearing type	Experimental method	Sound form	No. replicates	Maximum frequency (Hz)	Optimal frequency (Hz)	Minimum frequency (Hz)	Source
Dusky damselfish	<i>Stegastes adustus</i>	Perciformes	T2	BEH	SPL	4	1200	500	100	Myrberg and Spires 1980
Beaugregory	<i>Stegastes leucosticus</i>	Perciformes	T2	BEH	SPL	4	1200	500	100	Myrberg and Spires 1980
Bicolor damselfish	<i>Stegastes partitus</i>	Perciformes	T2	BEH	SPL	2	1200	500	100	Myrberg and Spires 1980
Coccodamselfish	<i>Stegastes variabilis</i>	Perciformes	T2	BEH	SPL	3	1200	500	100	Myrberg and Spires 1980
Honeygregory	<i>Eupomacentrus mellis</i>	Perciformes	T2	BEH	SPL	2	1200	500	100	Myrberg and Spires 1980
Longfin damselfish	<i>Stegastes diencaeus</i>	Perciformes	T2	BEH	SPL	2	1200	500	100	Myrberg and Spires 1980
Threespot damselfish	<i>Stegastes planifrons</i>	Perciformes	T2	BEH	SPL	4	1200	500	100	Myrberg and Spires 1980
European seabass	<i>Dicentrarchus labrax</i>	Perciformes	T2	AEP	SPL	NA	1600	100	10	Nedwell 2004 Chapman and Sand 1974; audiogram taken from Nedwell 2004
Common dab	<i>Limanda limanda</i>	Pleuronectiformes	T1	BEH	PAL	3	250	60	40	Buerle et al. 1967; audiogram taken from Nedwell et al. 2004
Atlantic cod	<i>Gadus morhua</i>	Gadiformes	T3	BEH	SPL	NA	400	17.6	17.6	Nedwell et al. 2004

Common name	Genus species	Order	Hearing type	Experimental method	Sound form	No. replicates	Maximum frequency (Hz)	Optimal frequency (Hz)	Minimum frequency (Hz)	Source
Lemon shark	<i>Negaprion brevirostris</i>	Carcharhiniformes	T1	BEH	SPL	3	640	320	10	Nelson 1967
Atlantic cod	<i>Gadus morhua</i>	Gadiformes	T3	BEH	SPL	20	600	150	10	Offut 1974
Scalloped hammerhead	<i>Sphyrna lewini</i>	Carcharhiniformes	T1	BEH	SPL	NA	750	310	250	Olla 1962; audiogram taken from Nelson 1967
Chinook salmon	<i>Oncorhynchus tshawytscha</i>	Salmoniformes	T2	AEP	SPL	40	1000	250	75	Oxman et al. 2007
Tomato clownfish	<i>Amphiprion frenatus</i>	Perciformes	T2	AEP	SPL	5	1800	150	75	Parmentier et al. 2009
Clownfish anemone fish	<i>Amphiprion ocellaris</i>	Perciformes	T2	AEP	SPL	7	1800	75	75	Parmentier et al. 2009
Yellowtail clownfish	<i>Amphiprion clarkii</i>	Perciformes	T2	AEP	SPL	5	1800	75	75	Parmentier et al. 2009
Silver mojarra	<i>Eucinostomus argenteus</i>	Perciformes	T3	AEP	SPL	15	1800	300	75	Parmentier et al. 2011
Mexican tetra	<i>Astyanax mexicanus</i>	Characiformes	T4	BEH	SPL	11	7500	200	50	Popper 1970
Cave tetra	<i>Astyanax jordani</i>	Characiformes	T4	BEH	SPL	6	7500	1000	50	Popper 1970
Black drum	<i>Pogonias cromis</i>	Perciformes	T2	AEP	SPL	7	800	300	100	Ramcharitar and Popper 2004
Atlantic croaker	<i>Micropogonias undulatus</i>	Perciformes	T3	AEP	SPL	7	1000	300	100	Ramcharitar and Popper 2004
Silver perch	<i>Bairdiella chrysoura</i>	Perciformes	T3	AEP	SPL	17	4000	600	100	Ramcharitar et al. 2004

Common name	Genus species	Order	Hearing type	Experimental method	Sound form	No. replicates	Maximum frequency (Hz)	Optimal frequency (Hz)	Minimum frequency (Hz)	Source
Weakfish	<i>Cynoscion regalis</i>	Perciformes	T3	AEP	SPL	5	2000	500	100	Ramcharitar et al. 2006
Spot	<i>Leiostomus xanthurus</i>	Perciformes	T2	AEP	SPL	5	700	500	200	Ramcharitar et al. 2006
Topmouth minnow	<i>Pseudorasbora parva</i>	Cypriniformes	T4	AEP	SPL	8	4000	500	100	Scholz and Ladich 2006
Slender lion head cichlid	<i>Steatocranus tinanti</i>	Perciformes	T2	AEP	SPL	8	700	200	100	Schulz-Mirbach et al. 2012
Jewel cichlid	<i>Hemichromis guttatus</i>	Perciformes	T2	AEP	SPL	7	3000	200	100	Schulz-Mirbach et al. 2012
Black diamond cichlid	<i>Paratilapia polleni</i>	Perciformes	T3	AEP	SPL	5	3000	500	100	Schulz-Mirbach et al. 2012
Orange chromide	<i>Etroplus maculatus</i>	Perciformes	T3	AEP	SPL	8	3000	500	100	Schulz-Mirbach et al. 2012
Slender lion head cichlid	<i>Steatocranus tinanti</i>	Perciformes	T2	AEP	PAL	8	700	200	100	Schulz-Mirbach et al. 2012
Jewel cichlid	<i>Hemichromis guttatus</i>	Perciformes	T2	AEP	PAL	7	1000	100	100	Schulz-Mirbach et al. 2012
Black diamond cichlid	<i>Paratilapia polleni</i>	Perciformes	T3	AEP	PAL	5	1000	500	100	Schulz-Mirbach et al. 2012
Orange chromide	<i>Etroplus maculatus</i>	Perciformes	T3	AEP	PAL	8	1000	500	100	Schulz-Mirbach et al. 2012
Cubbyu	<i>Pareques acuminatus</i>	Perciformes	T2	BEH	SPL	3	2000	600	100	Tavolga and Wodinsky 1963
Beau gregory	<i>Stegastes leucosticus</i>	Perciformes	T2	BEH	SPL	4	1200	550	100	Tavolga and Wodinsky 1963

Common name	Genus species	Order	Hearing type	Experimental method	Sound form	No. replicates	Maximum frequency (Hz)	Optimal frequency (Hz)	Minimum frequency (Hz)	Source
Beaugregory Blue striped Schoolmaster Schoolmaster snapper	<i>Stegastes leucosticus</i>	Perciformes	T2	BEH	SPL	4	600	200	100	Tavolga and Wodinsky 1963
Blue striped grunt	<i>Haemulon sciurus</i>	Perciformes	T2	BEH	SPL	4	1100	250	100	Tavolga and Wodinsky 1963
Schoolmaster snapper	<i>Lutjanus apodus</i>	Perciformes	T2	BEH	SPL	3	1000	400	100	Tavolga and Wodinsky 1963
Schoolmaster snapper	<i>Lutjanus apodus</i>	Perciformes	T2	BEH	SPL	3	400	300	100	Tavolga and Wodinsky 1963
Leopard searobin	<i>Prionotus scitulus</i>	Scorpaeniformes	T3	BEH	SPL	3	600	400	100	Tavolga and Wodinsky 1963
Dusky squirrelfish	<i>Holocentrus vexillarius</i>	Beryciformes	T3	BEH	SPL	3	1200	600	100	Tavolga and Wodinsky 1963
Squirrelfish	<i>Holocentrus adscensionis</i>	Beryciformes	T3	BEH	SPL	5	2800	700	100	Tavolga and Wodinsky 1963
Lusitanian toadfish	<i>Halobatrachus didactylus</i>	Batrachoidiformes	T2	AEP	SPL	9	1000	50	50	Vasconcelos et al. 2007
Nagasaki damselfish	<i>Pomacentrus nagasakiensis</i>	Perciformes	T2	AEP	SPL	NA	2000	600	100	Wright et al. 2010
Leopard coral grouper	<i>Plectropomus leopardus</i>	Perciformes	T2	AEP	SPL	NA	2000	600	100	Wright et al. 2010
Spanish flag snapper	<i>Lutjanus carponotatus</i>	Perciformes	T2	AEP	SPL	NA	2000	700	100	Wright et al. 2010
Ambon damsel	<i>Pomacentrus amboinensis</i>	Perciformes	T2	AEP	SPL	NA	2000	600	100	Wright et al. 2010
Rainbow runner	<i>Elagatis bipinnulata</i>	Perciformes	T2	AEP	SPL	NA	800	700	100	Wright et al. 2010

Common name	Genus species	Order	Hearing type	Experimental method	Sound form	No. replicates	Maximum frequency (Hz)	Optimal frequency (Hz)	Minimum frequency (Hz)	Source
Golden trevally	<i>Gnathanodon speciosus</i>	Perciformes	T2	AEP	SPL	NA	2000	700	100	Wright et al. 2010
Goldfish	<i>Carassius auratus</i>	Cypriniformes	T4	AEP	SPL	7	4000	500	200	Wysocki and Ladich 2005
Striped raphael catfish	<i>Platydoras costatus</i>	Siluriformes	T4	AEP	SPL	6	4000	500	200	Wysocki and Ladich 2005
Pumpkin seed sunfish	<i>Lepomis gibbosus</i>	Perciformes	T2	AEP	SPL	7	800	100	100	Wysocki and Ladich 2005
Red-mouthed goby	<i>Gobius cruentatus</i>	Perciformes	T2	AEP	SPL	6	700	200	100	Wysocki et al. 2009
Mediterranean damselfish	<i>Chromis chromis</i>	Perciformes	T2	AEP	SPL	6	600	200	100	Wysocki et al. 2009
Brown meagre	<i>Sciaena umbra</i>	Perciformes	T2	AEP	SPL	6	3000	300	100	Wysocki et al. 2009
Red-mouthed goby	<i>Gobius cruentatus</i>	Perciformes	T2	AEP	PAL	6	700	200	100	Wysocki et al. 2009
Mediterranean damselfish	<i>Chromis chromis</i>	Perciformes	T2	AEP	PAL	6	600	200	100	Wysocki et al. 2009
Brown meagre	<i>Sciaena umbra</i>	Perciformes	T2	AEP	PAL	6	1000	300	100	Wysocki et al. 2009
Black baby whale	<i>Brienomyrus brachyistius</i>	Osteoglossiformes	T4	AEP	SPL	4	4000	500	100	Yan and Curtis 2000
Oyster toadfish	<i>Opsanus tau</i>	Batrachoidiformes	T3	AEP	SPL	5	800	100	100	Yan et al. 2000
Blue gourami	<i>Trichopodus trichopterus</i>	Perciformes	T3	AEP	SPL	7	4000	800	300	Yan et al. 2000

Common name	Genus species	Order	Hearing type	Experimental method	Sound form	No. replicates	Maximum frequency (Hz)	Optimal frequency (Hz)	Minimum frequency (Hz)	Source
Goldfish	<i>Carassius auratus</i>	Cypriniformes	T4	AEP	SPL	6	4000	650	300	Yan et al. 200



**Table 3.2.** Counts of available unique studies, experimental method (BEH, AEP), sound form (SPL, PAL), mean number of replicates per experiment  $\pm$  standard deviation (SD), and number of taxonomic orders across hearing type (types 1-4).

Hearing type	BEH	AEP	SPL	PAL	Mean no. replicates $\pm$ SD	No. taxonomic order	Total (no. experiments)
1	6	12	8	10	7.39 $\pm$ 10.81	8	18
2	21	47	54	14	7.56 $\pm$ 6.89	10	68
3	13	28	36	5	8.29 $\pm$ 7.06	7	41
4	4	31	35	0	7.26 $\pm$ 2.51	5	35
Total	44	118	133	29	7.66 $\pm$ 6.78	23	162

**Table 3.3.** Orders of species included in this literature review categorized by broader phylogenetic subgroups, based on common morphological characteristics.

Order	Phylogenetic subgroup	N
Carcharhiniiformes	Elasmobranchs	15
Heterodontiformes		
Myliobatiformes		
Orectolobiformes		
Rajiformes		
Acipenseriformes	Chondrostei/Holostei	4
Characiformes	Otomorph	42
Clupeiformes		
Cypriniformes		
Gymnotiformes		
Mugiliformes		
Osteoglossiformes		
Siluriformes	Protocanthopterygii	3
Esociformes		
Salmoniformes	Neoteleost	107
Batrachoidiformes		
Beryciformes		
Gadiformes		
Gasterosteiformes		
Perciformes		
Percopsiformes		
Pleuronectiformes		
Scorpaeniformes		

**Table 3.4.** Model structures, predictor variables, degrees of freedom, and absolute AIC values for both maximum and optimal hearing frequency benchmarks. Generalized least squares (GLS) and linear mixed effect (LME) models were constructed and compared.

Response variable	Model (N)	Model structure	Predictor variables	Degrees of freedom	AIC
Maximum frequency detected	1	GLS	Hearing type	5	37.08
	2	GLS	Hearing type, no. replicates	5	74.69
	3	GLS	Hearing type, experimental method	12	3.68
	4	GLS	Hearing type, experimental method, no. replicates	12	21.71
	5	LME	Hearing type, experimental method, no. replicates, taxonomic order	13	0.58
Optimal frequency detected	1	GLS	Hearing type	5	120.18
	2	GLS	Hearing type, no. replicates	5	137.83
	3	GLS	Hearing type, experimental method	12	101.18
	4	GLS	Hearing type, experimental method, no. replicates	12	116.94
	5	LME	Hearing type, experimental method, no. replicates, taxonomic order	13	119.80

**Table 3.5.** Spearman correlation coefficients (r) measuring the correlation between maximum and optimum frequency benchmarks for individual hearing types and phylogenetic groups

Hearing type	r	Phylogenetic group	r
T1	0.63	Elasmobranchs	0.63
T2	0.13	Chondrostei/Holostei	-
T3	0.52	Otomorph	0.36
T4	0.15	Protocanthopterygii	0.35
		Neoteleost	0.11

*Figures*

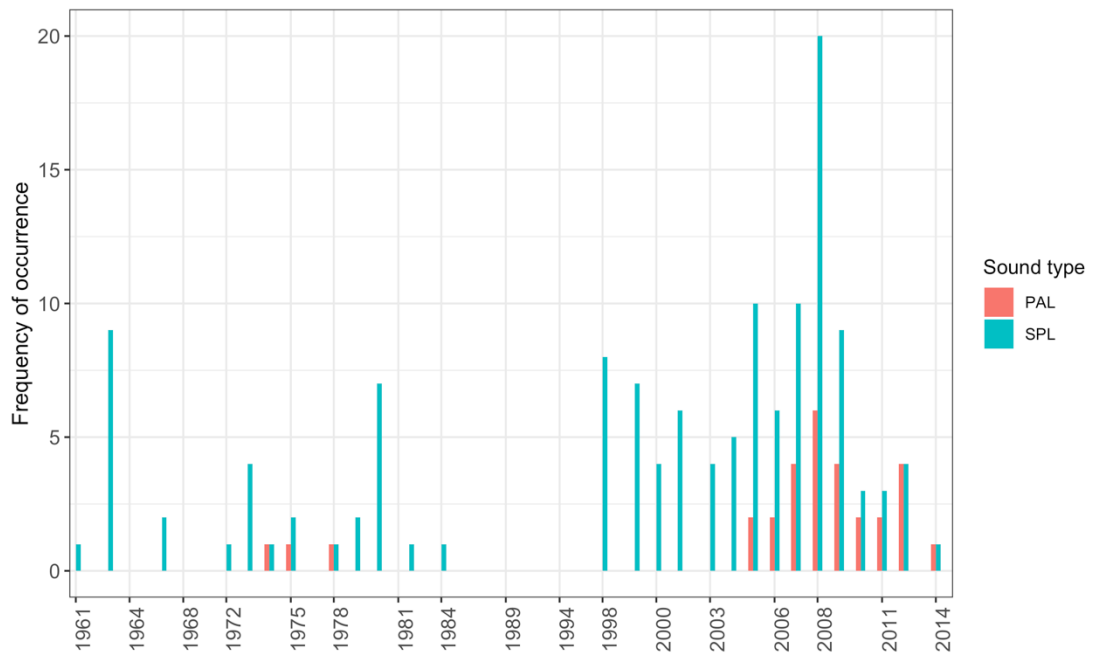


**Figure 3.1.** Distribution of fish hearing sensitivity studies over time, categorized by sound form type used: particle acceleration (PAL) or sound pressure level (SPL).

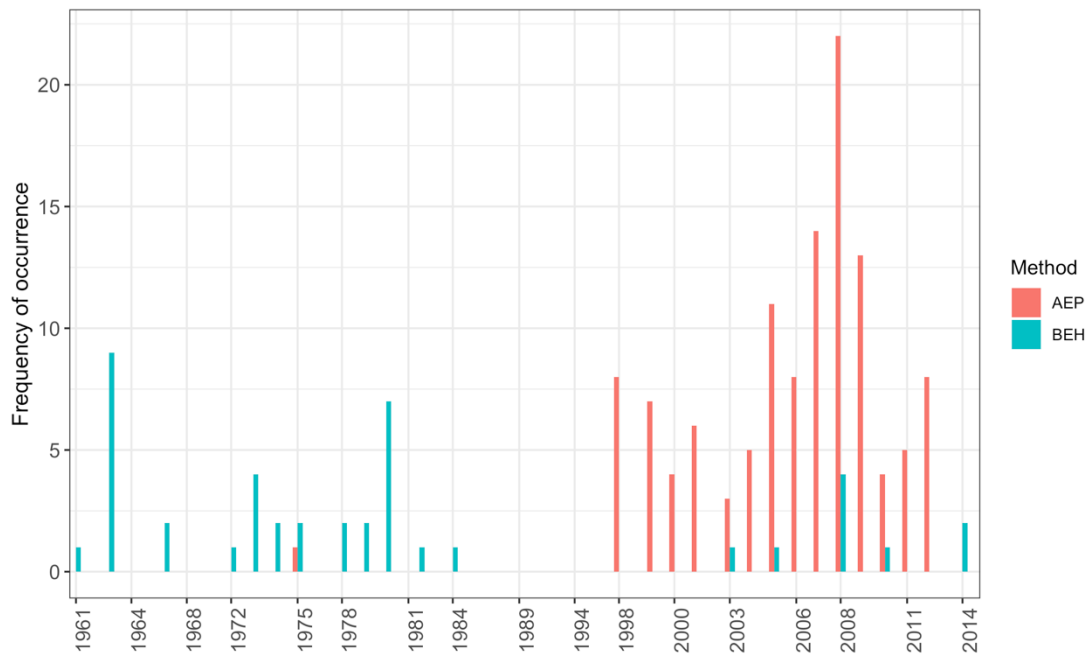


**Figure 3.2.** Distribution of fish hearing sensitivity studies over time, categorized by method of sound detection used: auditory-evoked potential (AEP) or behavioral (BEH).

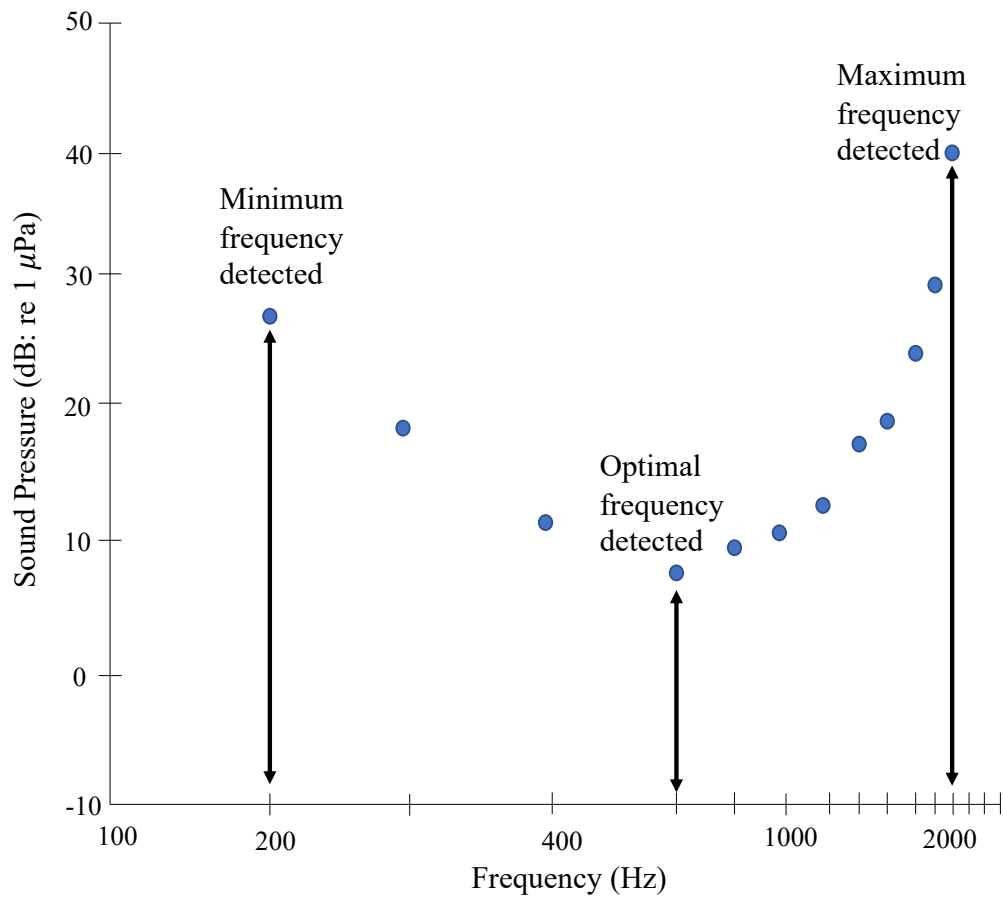


**Figure 3.3.** An example audiogram, showing frequency benchmarks. Maximum and minimum frequency benchmarks refer to the maximum and minimum frequencies detected (the endpoint frequency values of the audiogram). The optimal frequency benchmark refers to the frequency detected with the greatest sensitivity to sound and at the lowest sound level (here, the frequency value corresponding to the sound pressure minimum.)

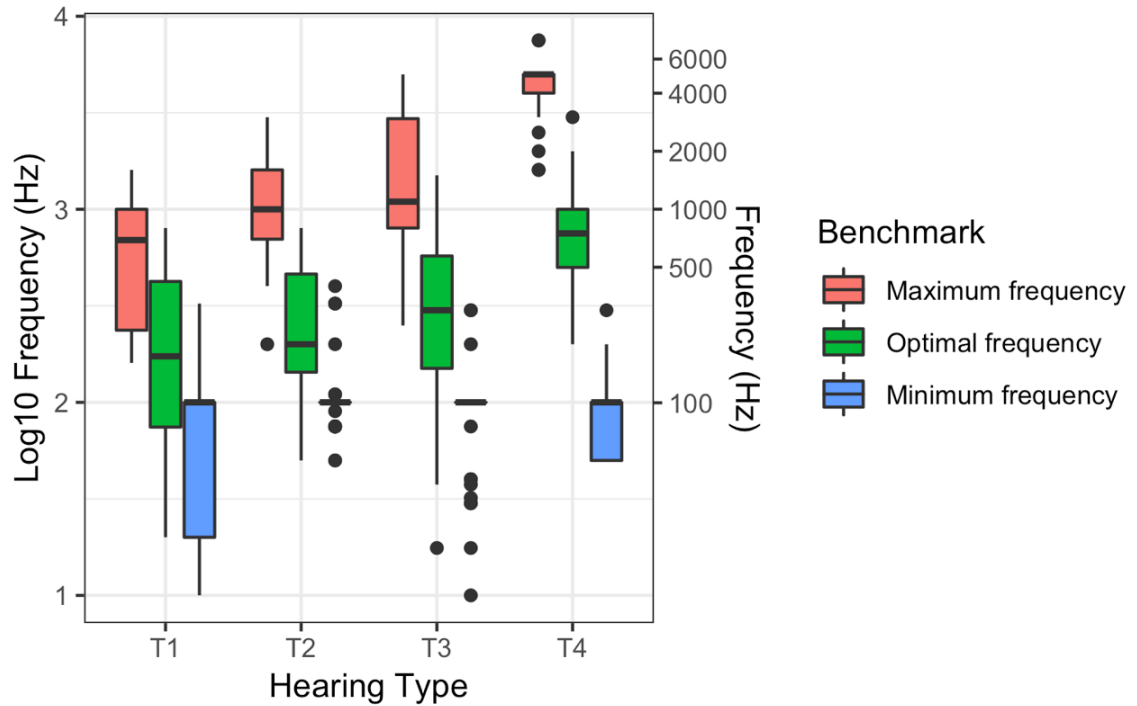


**Figure 3.4.** Distributions of log10-transformed frequency benchmarks detected for each hearing type under all study conditions included in the literature review. Box and whisker plots are shown where the black horizontal line central to each plot defines the median; the horizontal lines above and below the median (completing the box) describe the range of the upper and lower quartile values; the vertical lines extending above and below each box provide upper and lower extremes, respectively; and the black dots provide outliers.



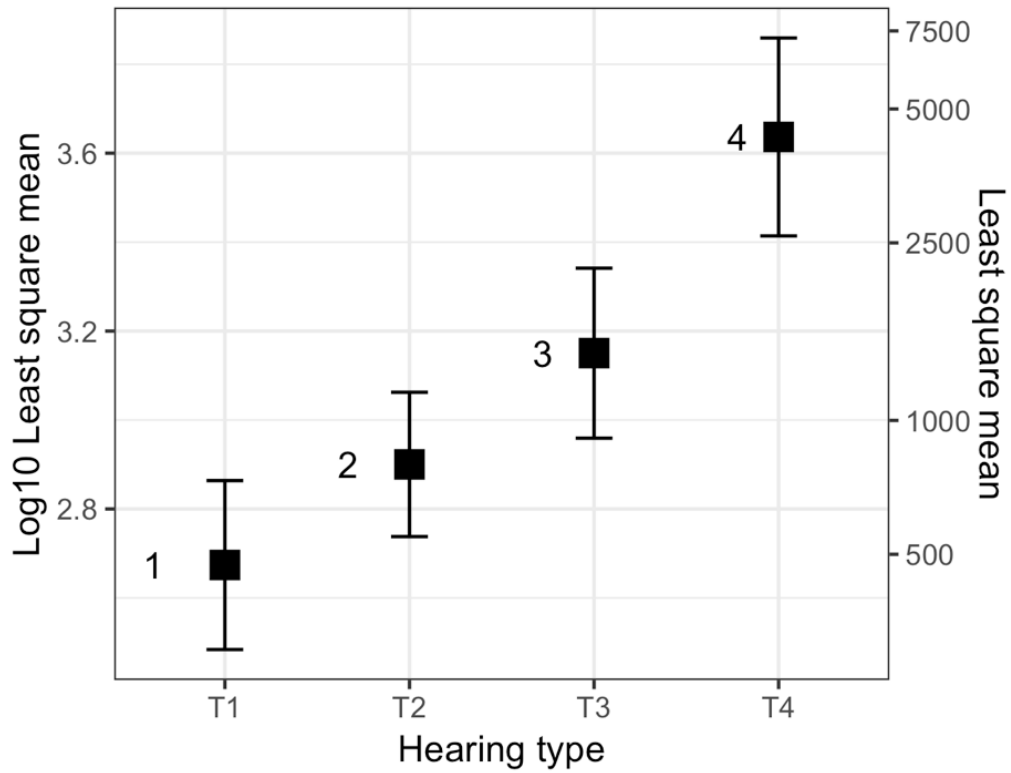


**Figure 3.5.** Log10-transformed least square means and 0.95 confidence intervals across hearing type for maximum detected frequency benchmarks. Hearing types with significantly different numbers next to their means were significantly different at  $p < 0.05$ .

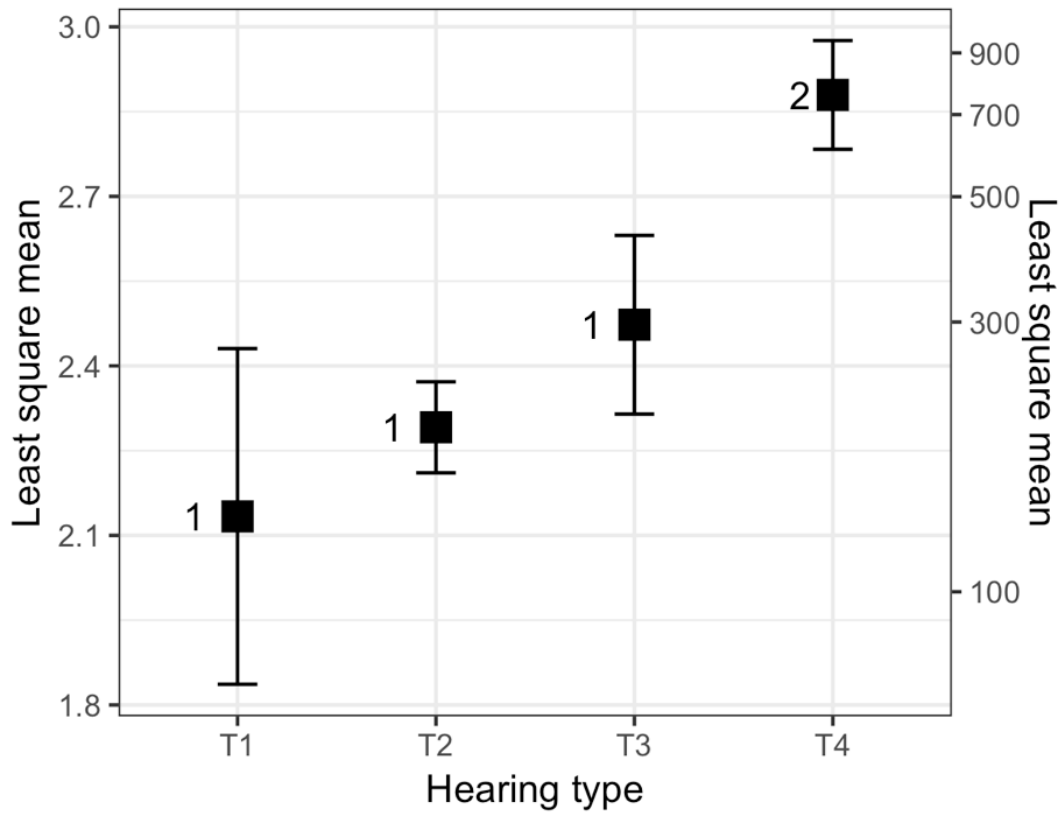


**Figure 3.6.** Log10-transformed least square means and 0.95 confidence intervals across hearing type for optimal detected frequency benchmarks. Hearing types with significantly different numbers next to their means were significantly different at  $p < 0.05$ .

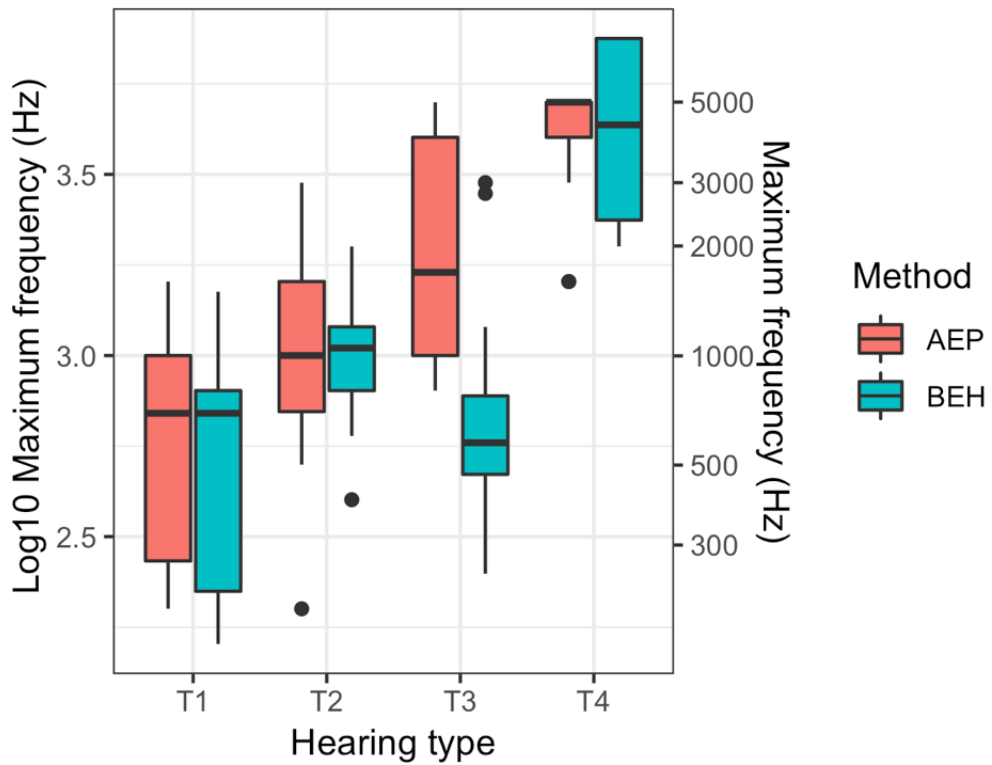


**Figure 3.7.** Log10-transformed values for maximum frequencies detected across hearing types, broken down by the method of identifying sound detection used in the study. Box and whisker plots are shown where the black horizontal line central to each plot defines the median; the horizontal lines above and below the median (completing the box) describe the range of the upper and lower quartile values; the vertical lines extending above and below each box provide upper and lower extremes, respectively; and the black dots provide outliers.

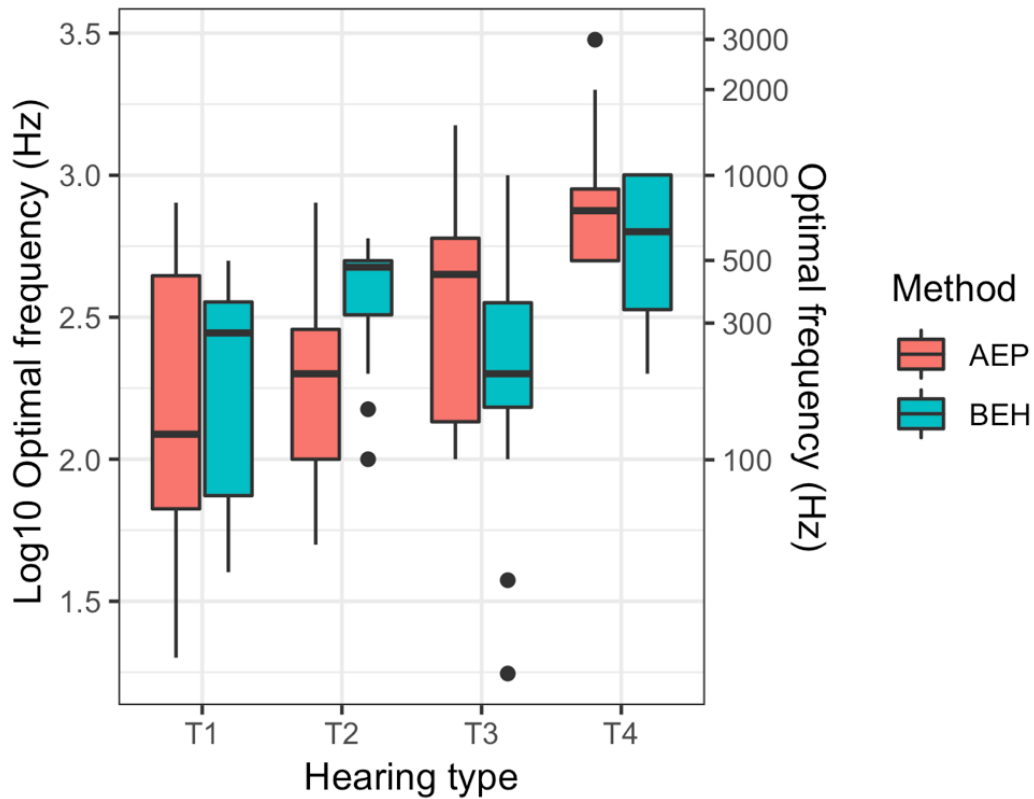


**Figure 3.8.** Log10-transformed values for optimal frequencies detected across hearing types, broken down by the method of identifying sound detection used in the study. Box and whisker plots are shown where the black horizontal line central to each plot defines the median; the horizontal lines above and below the median (completing the box) describe the range of the upper and lower quartile values; the vertical lines extending above and below each box provide upper and lower extremes, respectively; and the black dots provide outliers.

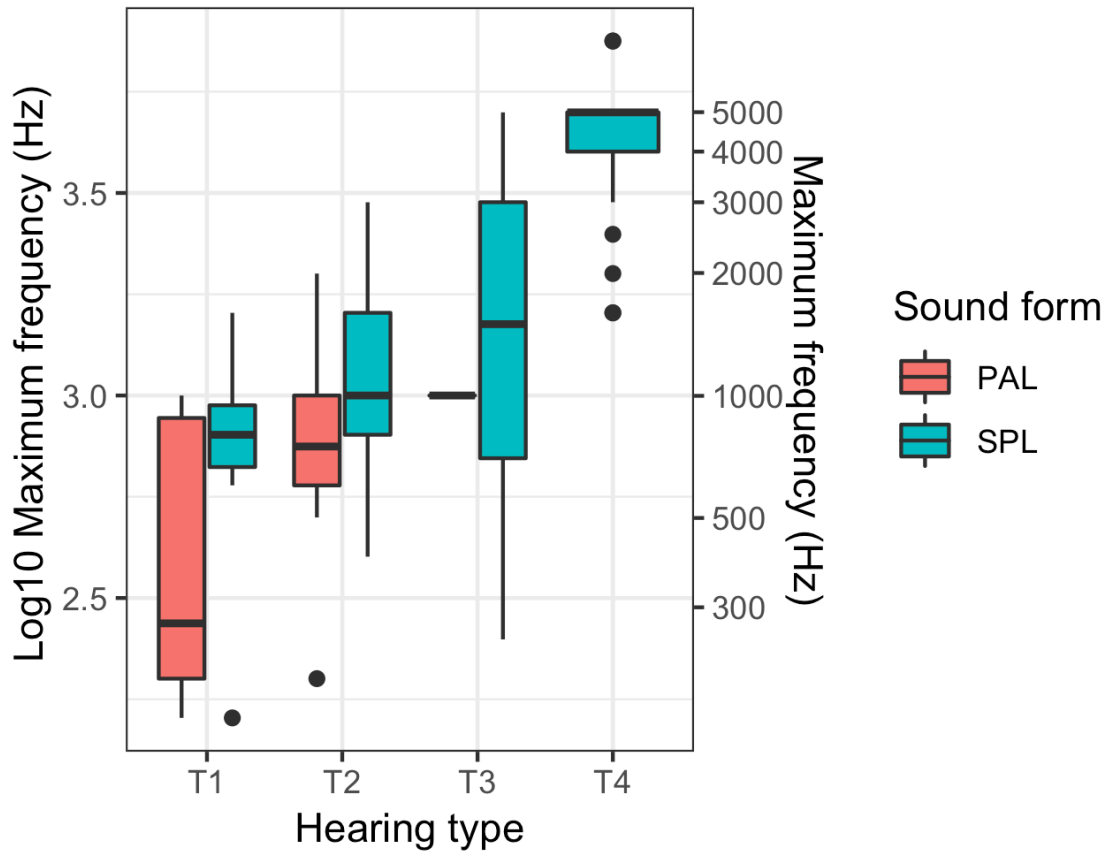


**Figure 3.9.** Log10-transformed values for maximum frequencies detected across hearing types, broken down by the sound form measured in the study. Box and whisker plots are shown where the black horizontal line central to each plot defines the median; the horizontal lines above and below the median (completing the box) describe the range of the upper and lower quartile values; the vertical lines extending above and below each box provide upper and lower extremes, respectively; and the black dots provide outliers.

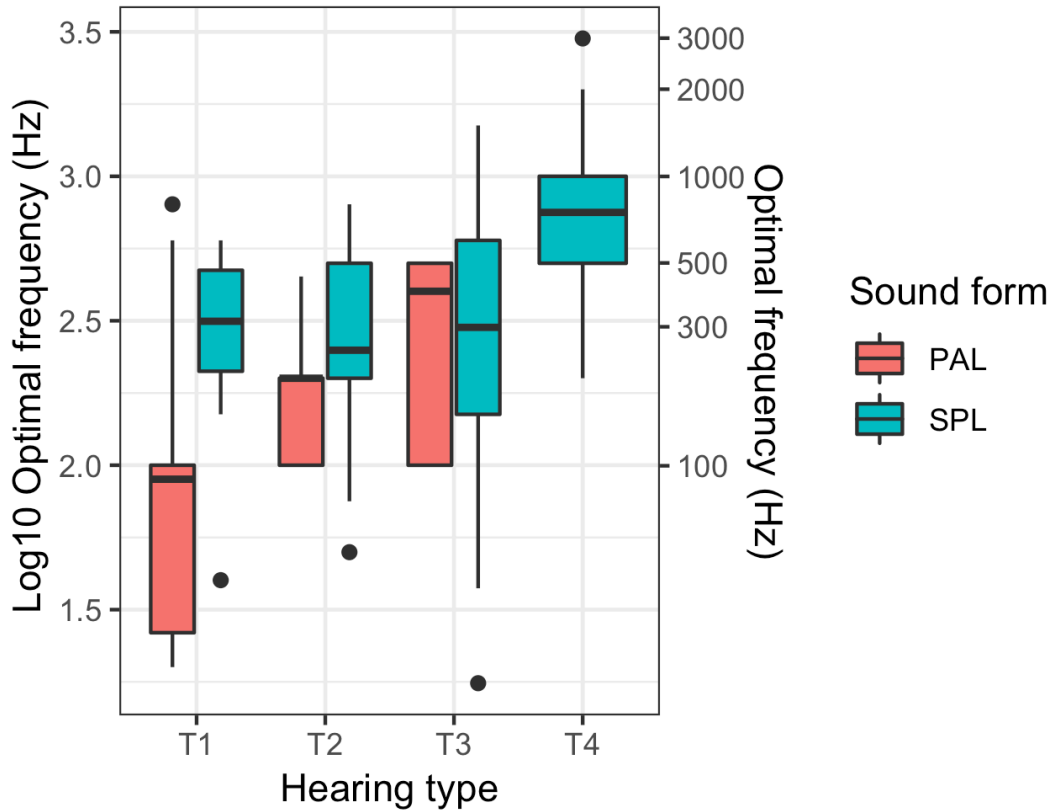


**Figure 3.10.** Log10-transformed values for optimal frequencies detected across hearing types, broken down by the sound form measured in the study. Box and whisker plots are shown where the black horizontal line central to each plot defines the median; the horizontal lines above and below the median (completing the box) describe the range of the upper and lower quartile values; the vertical lines extending above and below each box provide upper and lower extremes, respectively; and the black dots provide outliers.

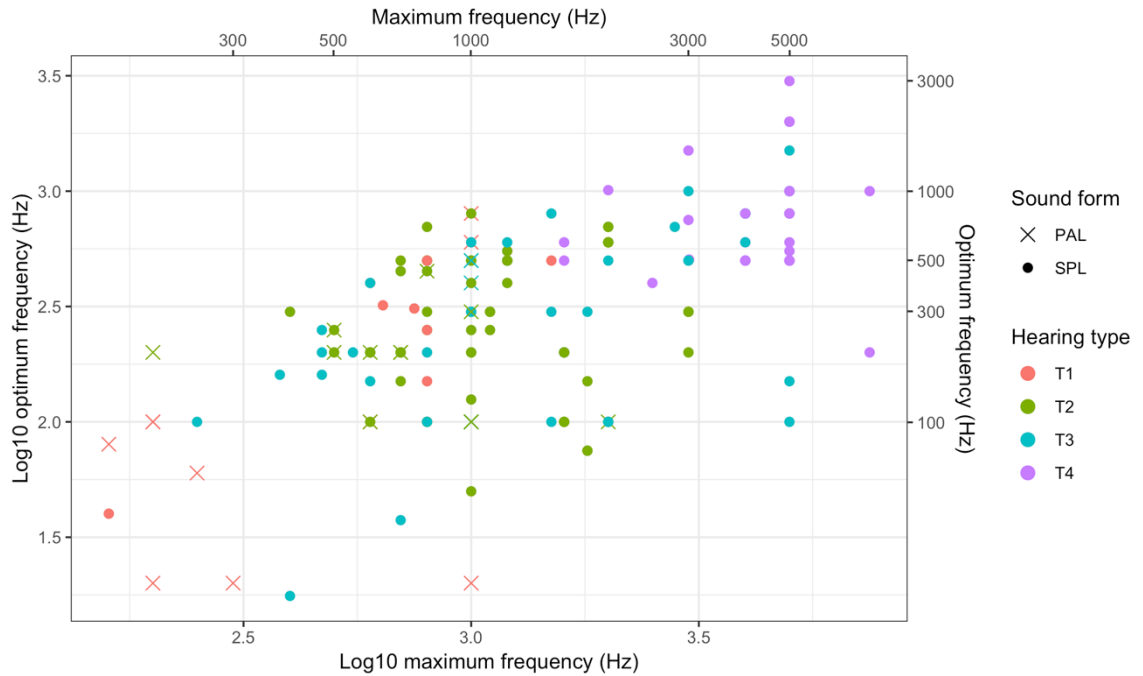


**Figure 3.11.** Log10 optimum frequency benchmarks v. log10 maximum benchmarks from same experiments. Colors refer to hearing types (T1-T4), with shapes referring to sound forms measured: particle acceleration (PAL) and pressure waves (SPL).

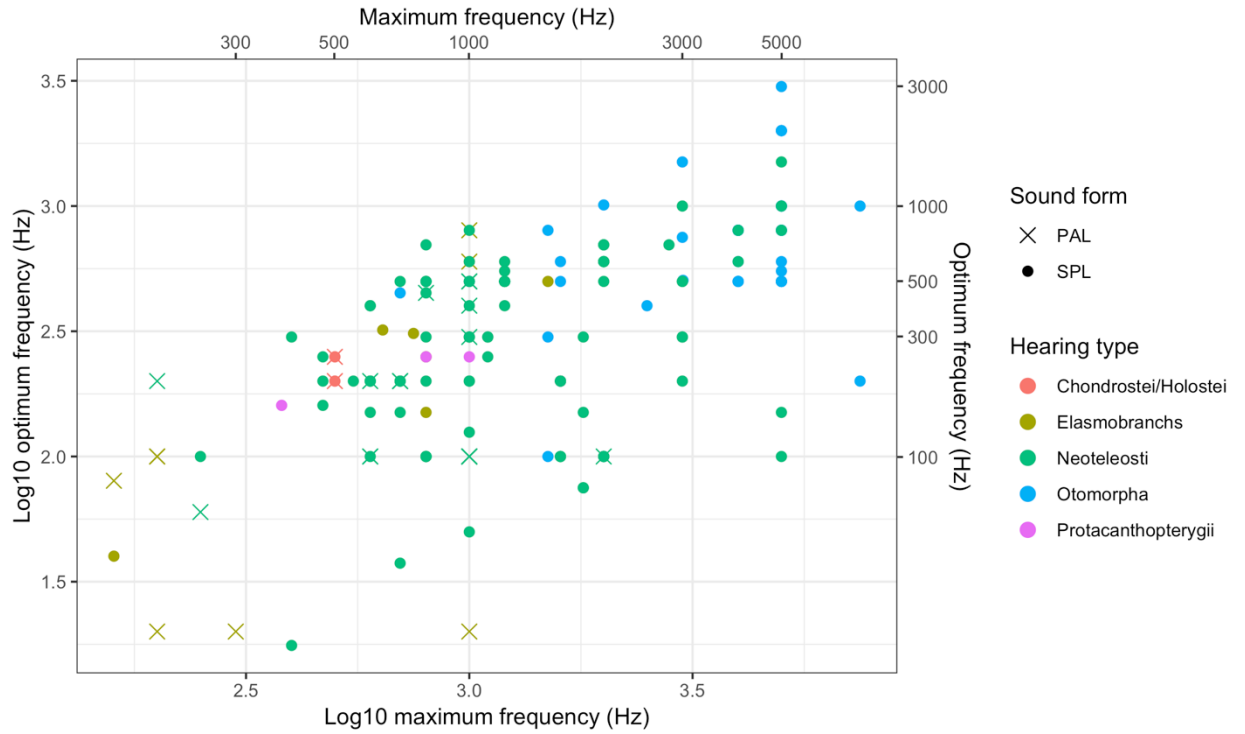


**Figure 3.12.** Log10 optimum frequency benchmarks v. log10 maximum benchmarks from same experiments. Colors refer to groups of similar phylogenetic characteristics, with shapes referring to sound forms measured: particle acceleration (PAL) and pressure waves (SPL).



## Appendix A. Supplemental Figures to Chapter 2: FVCOM performance, spatiotemporal estimates of current velocity and turbulent kinetic energy, and GAMLSS movement model diagnostics.

### Methods

#### *FVCOM model performance*

Prior to running spatial and time series estimates of storm variables, the Finite Volume Community Ocean Model (FVCOM) was assessed for performance. Model outputs for bottom water temperature were compared to observed bottom water temperatures obtained from VR2AR receivers at each site.

#### *FVCOM current velocity and TKE output*

In addition to estimates of bottom water temperature, the FVCOM was also used to estimate cross-sectional of current velocity and both cross-sectional and later estimates of turbulent kinetic energy (TKE), during the summer-fall of 2016-2018. Again, the model was initialized from August 25 to September 29 for 2016, and from January 1 to December 31 for 2017 and 2018, with model configuration, optimization, and execution carried out by the Li Lab (M. Li and F. Zhang; Horn Point Laboratory, Cambridge, MD). Estimated regional measurement extended across the shelf in the DelMarVa portion of the MAB, and estimated cross-sectional measurements were taken along a 39 km transect, bisecting the Middle study site (Chapter 2; Figure 2.1).

#### *Movement model sex-length interaction*

Model estimates of the mu parameter (or the magnitude of the fitted response for a given variable) for sex and length suggested a potentially contradictory effect. The model identified males and unidentified fish as having significantly higher

movement indices compared to females, while length was identified as having a negative impact on movement. However, the model did not identify the direction of impact on length. In order to inform both the direction of the impact of length on movement, between relatively larger and smaller fish, as well as the potential for an interaction between length and sex, I evaluated the distributions of movement index across length and sex of each individual tagged fish.

#### *Movement model diagnostics*

Following the development and implementation of the Generalized Additive Model for Location, Scale, and Shape, model performance was assessed through evaluation of quantile residual values and plots. Assessments include evaluating distributions of quantile residuals over fitted values, quantile residuals against index values, density estimates against quantile residuals and the linear fit of sample vs. theoretical quantiles.

#### *Results*

##### *FVCOM model performance*

Modeled bottom water temperatures estimated by the FVCOM were overall consistent with available observed data. Estimations of hourly bottom water temperature produced by the model mirrored threshold changes during storm events but slightly underestimated observed hourly temperatures at all sites and years (Figure A.1a-c). Importantly, the model consistently tracked destratification and recovery of cold pool temperatures relative to storm presence and elevated wind speed.

##### *FVCOM current velocity and TKE output*

Cross-sectional FVCOM estimates of current velocities during 2016-2018 summer storms revealed short-term patterns in storm-driven currents across single-storm and multi-storm years. During 2016 and 2018, where only one storm event occurred, current velocities were stratified during and immediately after the storm (Figure A.2). On days that TS Hermine (2016) and the unnamed wind event (2018) peaked in wind speeds, inshore current movement increased near the surface while offshore current increased towards the bottom of the water column. This stratification dissipated four days after each storm had passed, where after current velocities were predominantly inshore throughout the entire water column, decreasing in magnitude with increasing depth. During summer-fall 2017, when multiple storms occurred, a similar pattern of stratified current velocity was modeled, with surface currents moving inshore and bottom currents moving offshore during and immediately following the day of peak wind speeds for each storm (Figure A.3). However, unlike the post-storm period for TS Hermine and the unnamed wind-event, in 2016 and 2018 respectively, four days following the first storm of 2017 (the July nor'easter) and four days following the second of 2017 (PTC10), surface current velocities shifted strongly offshore throughout the entire water column, diminishing with depth. For the third storm of 2017 (TS Jose), current velocity stratification was comparatively weaker, and four days after the storm inshore current velocities dominated the entire water column.

Cross-sectional FVCOM peak estimates of TKE were inconsistently timed across storm events from 2016-2018, but were also tightly coupled to either the surface or bottom boundary layer, as well as wind speed. During 2016, where a single

storm event occurred (TS Hermine), cross sectional estimates of TKE increased initially at the surface (during the day prior to storm arrival); once the storm arrived, and later peaked in wind speed, on September 3, 2016, TKE values increased rapidly and tracked estimates of bottom topography. Elevated values of bottom TKE were estimated four days after TS Hermine passed (Figure A.4). Lateral shelf estimates during TS Hermine indicate that elevated bottom levels of TKE increased across all study sites and continued to encompass all study sites up to four days after the storm left the area (Figure A.6). During the 2018 unnamed wind event, cross-sectional estimates bottom TKE values increased slightly during the day before the storm—reflecting estimates of bathymetry—but remained consistently low during the day of maximum wind speed and the days after (Figure A.4). Lateral estimates of bottom turbulent kinetic energy values during the 2018 event suggest a patchy, ephemeral disturbance that unequally impacted reef sites and transited from the area shortly after the storm wind’s peaked and the event moved from the southern MAB (Figure A.6). Model cross-sectional estimates of TKE for adjacent storm events occurring in 2017 reflect a lag to maximum wind speed (with peak storm-specific increases to TKE occurring the day after peak winds occurred), a tight coupling of increased TKE values to surface and bottom boundary layers (with the latter reflecting patterns in bathymetry) as well as the dissipation of elevated TKE shortly after the storm event passed (Figure A.5). Modeled lateral estimates of TKE during 2017 reflect both the lag in TKE with regards to peak storm wind speed, as well as dissipation in TKE values with decreased wind (Figure A.7). For the first three storms to occur in 2017,

TKE peaked the day after storm winds peaked and subsequently declined across shelf after the storms left the region.

*Movement model sex-length interaction*

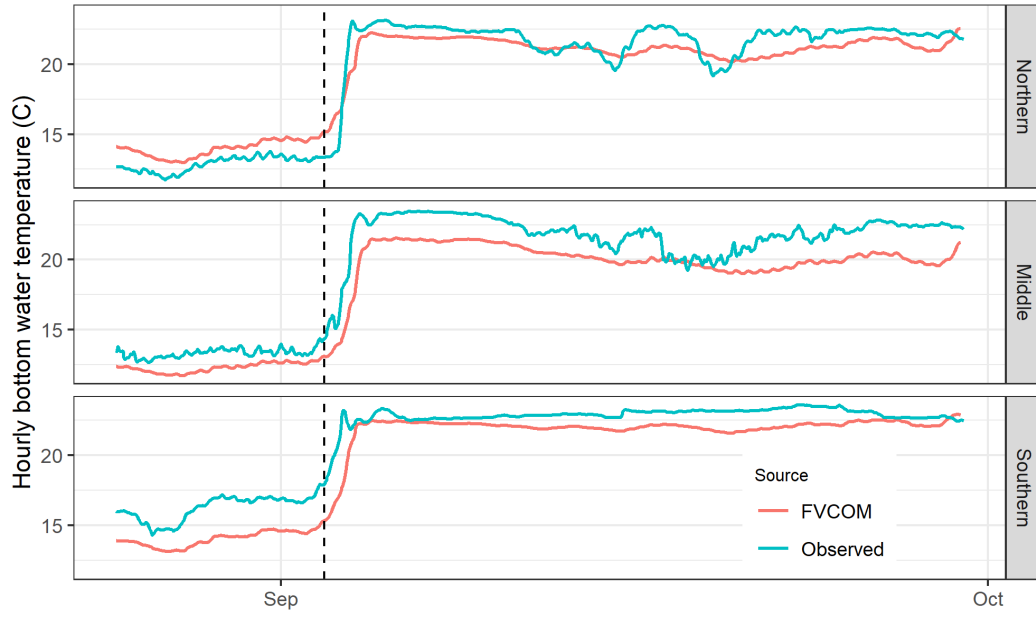
Distributions of movement index across individual tagged fish, coded by length and sex, strongly support the presence of an interaction between the two terms though such an interaction was not directly incorporated into the original GAMLSS model (2017 data only; Figure A.8). Distributions of movement index, ordered by increasing length, indicate the highest movement indices concentrated around smaller individuals (< 240 mm) of unidentified sex. Male fish only occurred at larger sizes (>270 mm), but females also occurred at this large size interval. Within this larger size interval, males showed higher movement rates than females.

*Movement model diagnostics*

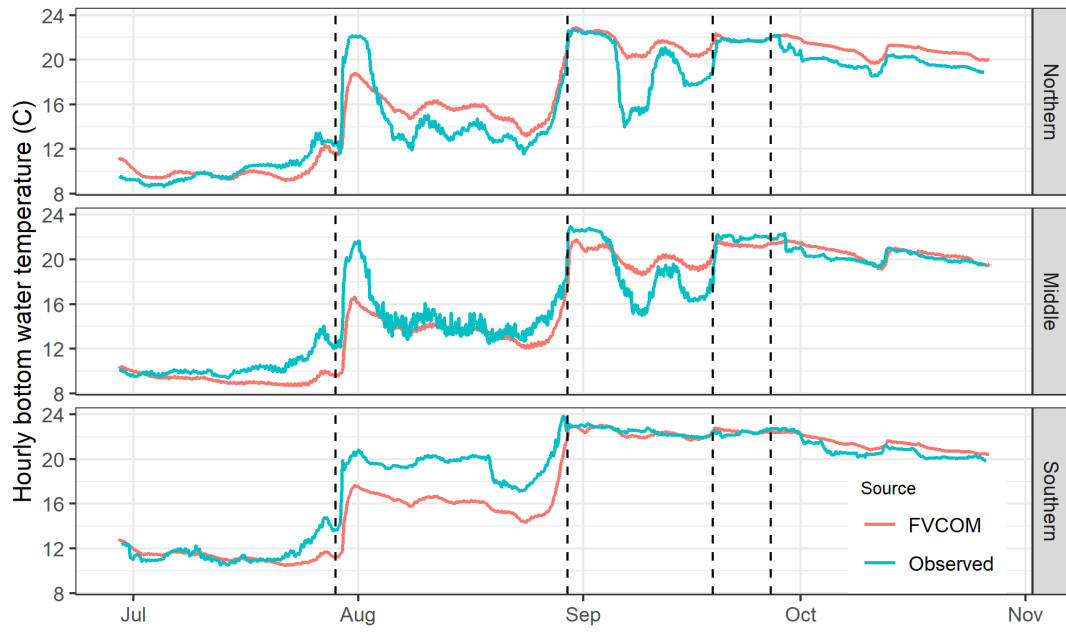
Quantile residual summary plots indicate overall randomness and normality of GAMLSS movement model residuals (Figure A.9). The distribution of quantile residuals against fitted values is random and symmetric at zero, indicating that the model achieved homoscedasticity. However, there is still an artifact structure for lower fitted values (< 2), likely due to the distribution of the response variable (movement index) and the compatibility with the family distribution used in the model. Similarly, the quantile residual vs. index plot is predominantly random in distribution (again suggesting homoscedasticity was achieved). The density distribution of quantile residuals, as well as the sample vs. theoretical quantile distribution also suggest that normality of quantile residuals was achieved. However, the bimodal density distribution of quantile residuals indicates some lingering structure within residuals. This is again likely due to slight structural differences of

the response variable distribution relative to the selected distribution family used in the model.

*Figures*

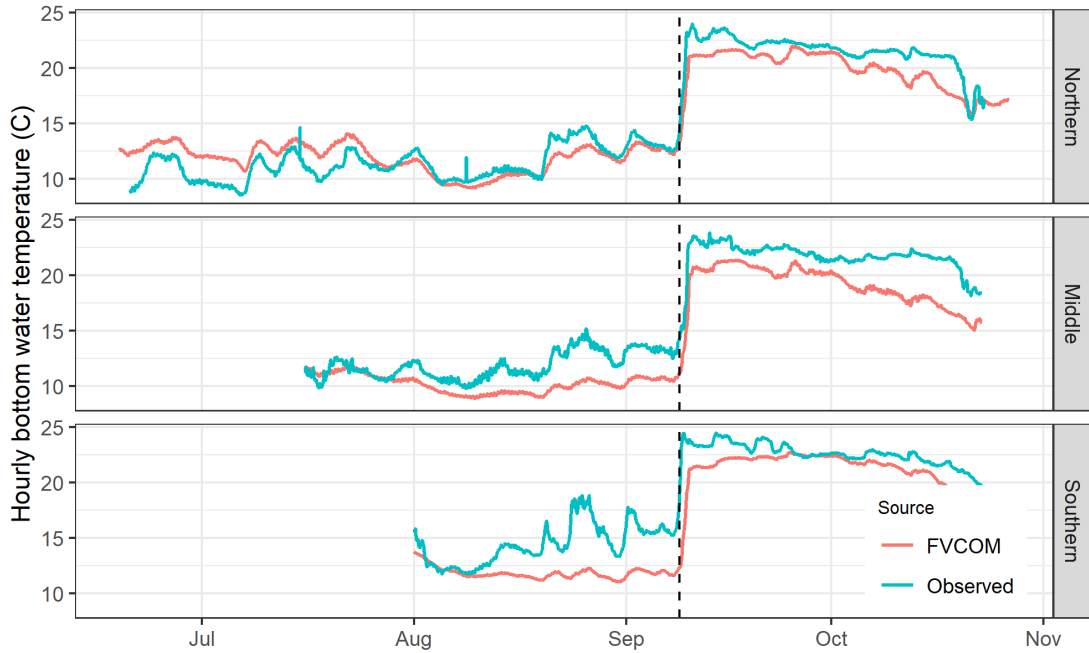


**A.1.a.**



**A.1.b.**





**A.1.c.**

**Figure A.1.a-c.** Modeled and observed hourly bottom water temperature values across sites for 2016-2018. Vertical black dashed lines refer to maximum wind speed dates for identified storm events.

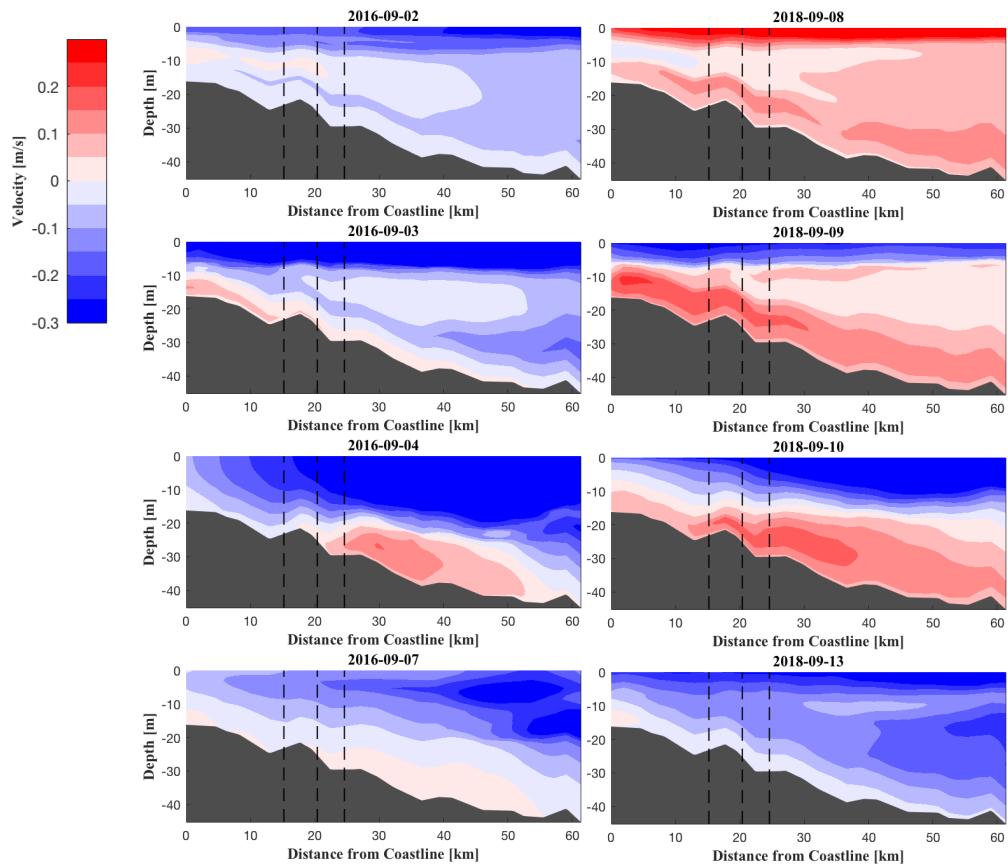


**Figure A.2.** Modeled current velocity cross-sectional profiles predicted by the FVCOM for storm events in 2016 and 2018. The left column predicts current speed and direction related to TS Hermine (2016); the right column predicts current speed and direction related to the unnamed wind event (2018). Red colors refer to offshore current movement, and blue colors refer to inshore current movement. Vertical black dashed lines in each pane refer to the transmitter release locations central to each study site (Southern, Northern, and Middle, for both years in increasing depth and distance from coastline). Cross sections are taken along a transect spanning the Middle site (Figure 2.1), and depict snapshot predictions at 00:00 for each given day.

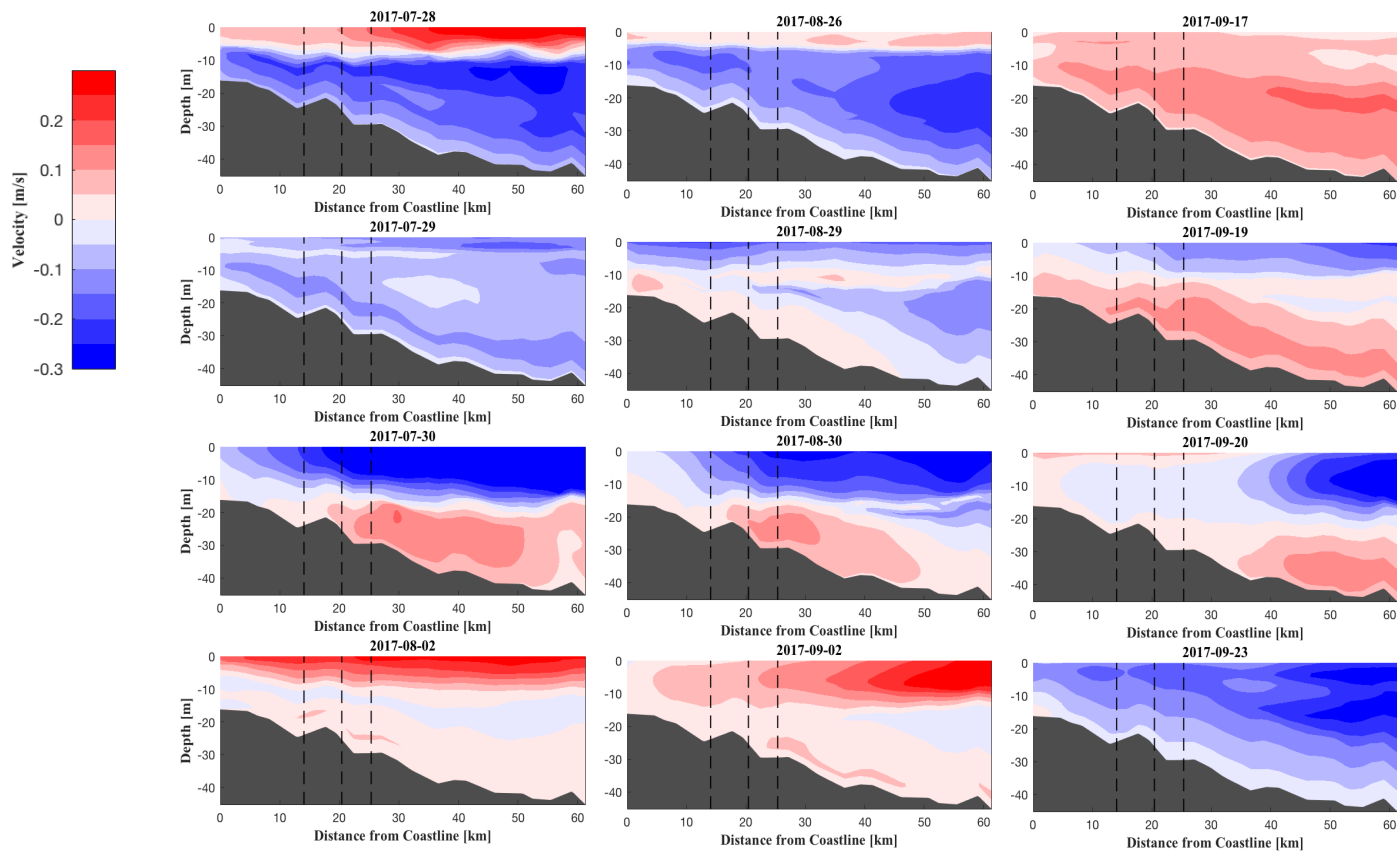


**Figure A.3.** Modeled current velocity cross-sectional profiles predicted by the FVCOM for storm events in 2017. The left column predicts current direction and speed related to the July nor'easter; the middle column predicts current direction and speed related to PTC10; and the right column predicts current and speed related to TS Jose. Red colors refer to offshore current movement, and blue colors refer to inshore current movement. Vertical black dashed lines in each pane refer to the transmitter release locations central to each study site (Southern, Northern, and Middle, increasing depth and distance from coastline). Cross sections are taken along a transect spanning the Middle site (Figure 2.1), and depict snapshot predictions at 00:00 for each given day.

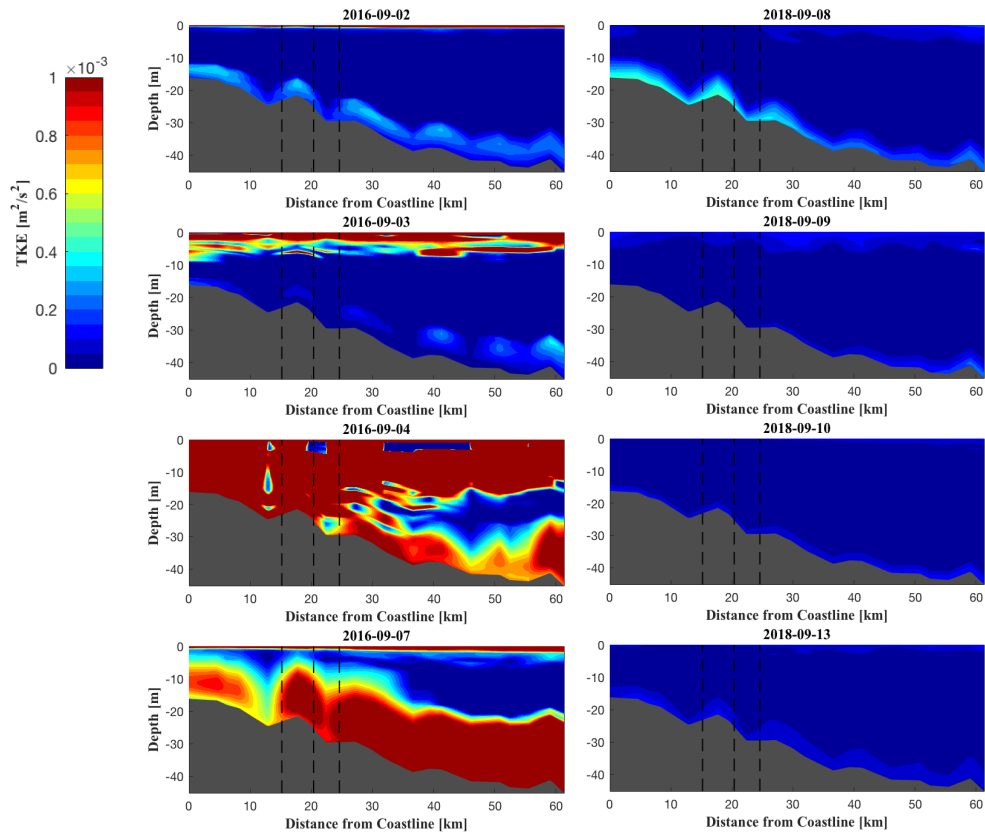


**Figure A.4.** Modeled turbulent kinetic energy (TKE) cross-sectional profiles predicted by the FVCOM for storm events in 2016 and 2018. The left column predicts TKE values related to TS Hermine (2016); the right column predicts TKE values related to the unnamed wind event (2018). Vertical black dashed lines in each pane refer to the transmitter release locations central to each study site (Southern, Northern, Middle, for both years in increasing depth and distance from coastline). Cross sections are taken along a transect spanning the Middle site (Figure 2.1), and depict snapshot predictions at 00:00 for each given day.

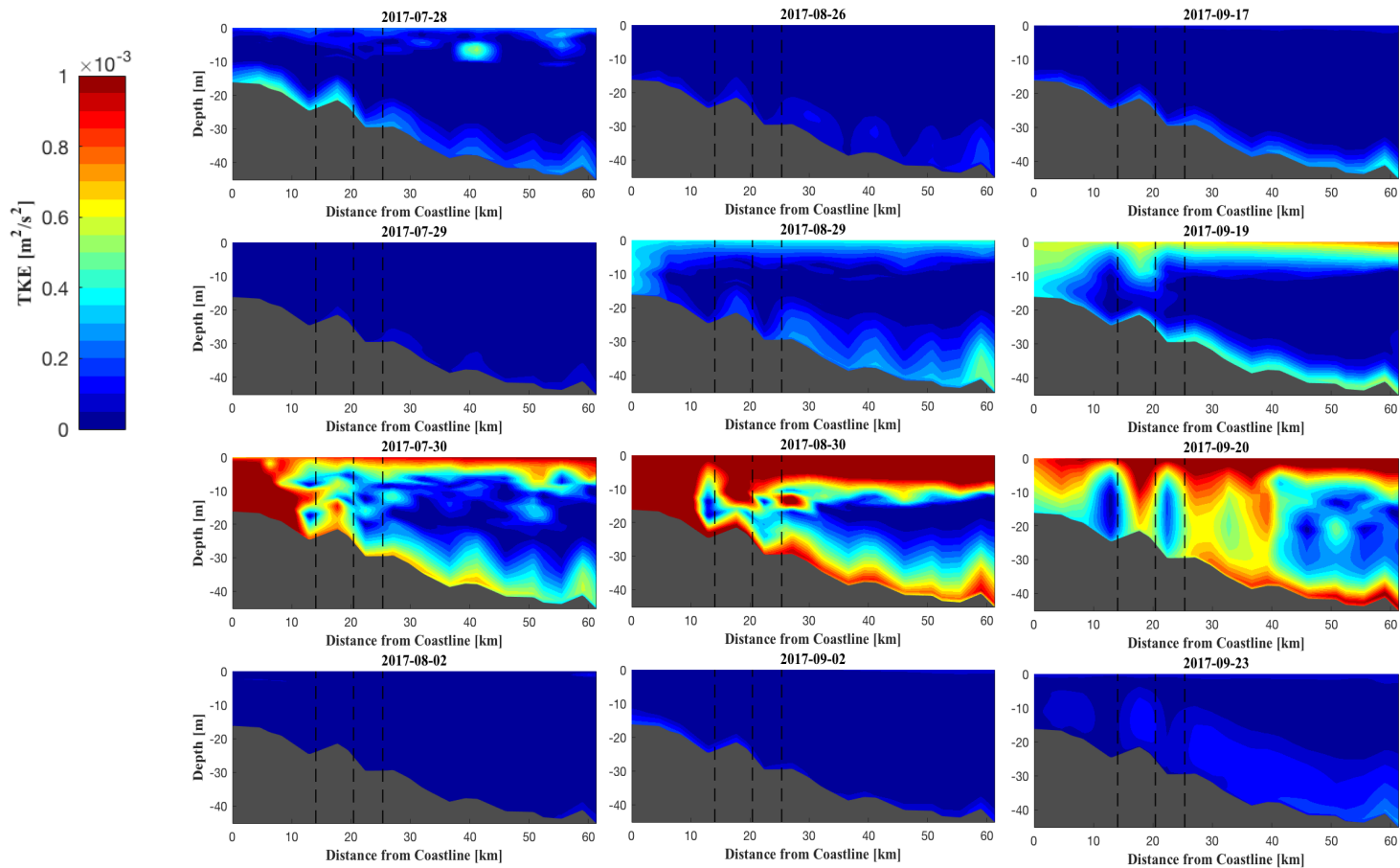


**Figure A.5.** Modeled turbulent kinetic energy (TKE) profiles predicted by the FVCOM for storm events in 2017. The left column predicts TKE values related to the July nor'easter; the middle column predicts TKE values related to PTC10; and the right column predicts temperatures related to TS Jose. Vertical black dashed lines in each pane refer to the transmitter release locations central to each study site (Southern, Northern, and Middle, increasing depth and distance from coastline). Cross sections are taken along a transect spanning the Middle site (Figure 2.1), and depict snapshot predictions at 00:00 for each given day.

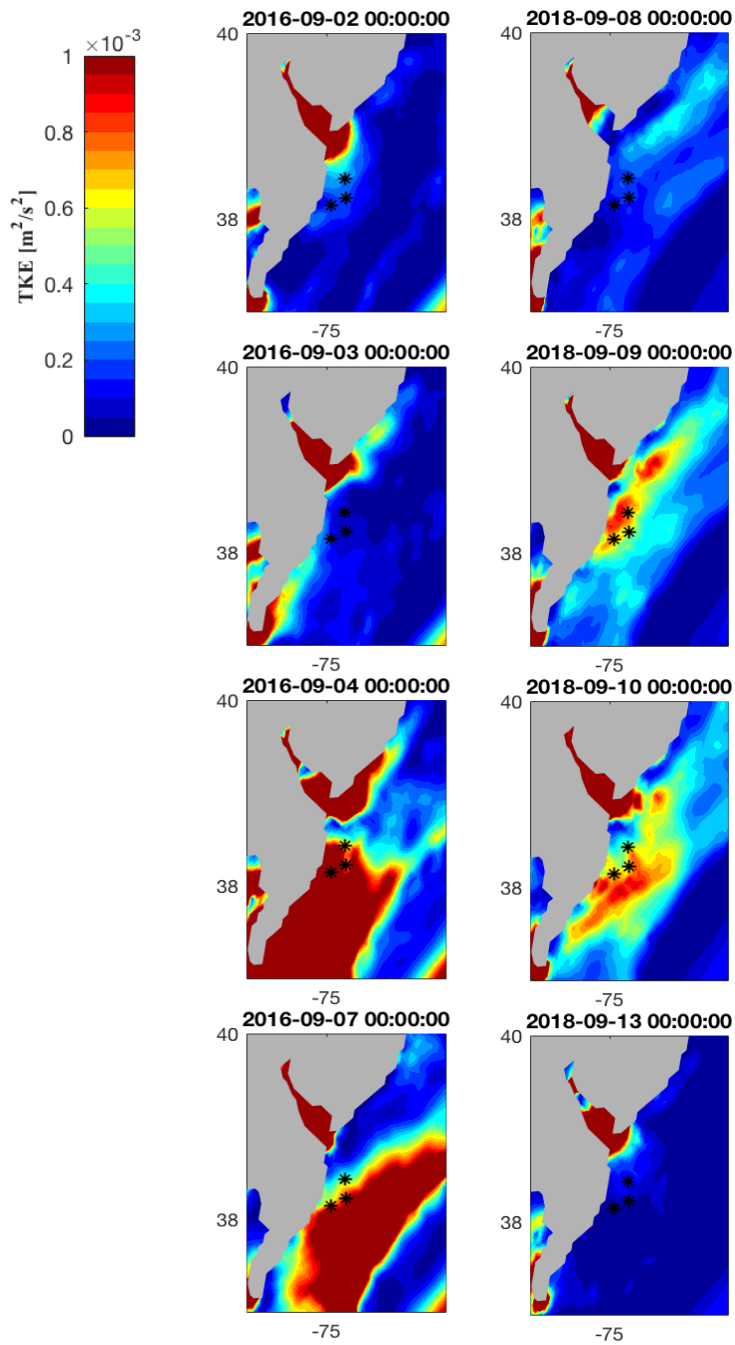


**Figure A.6.** Modeled turbulent kinetic energy (TKE) in the southern MAB predicted by the FVCOM for single storm events occurring in 2016 (left column) and 2018 (right column). Black asterisks refer to the location of transmitter release, central to each study site.

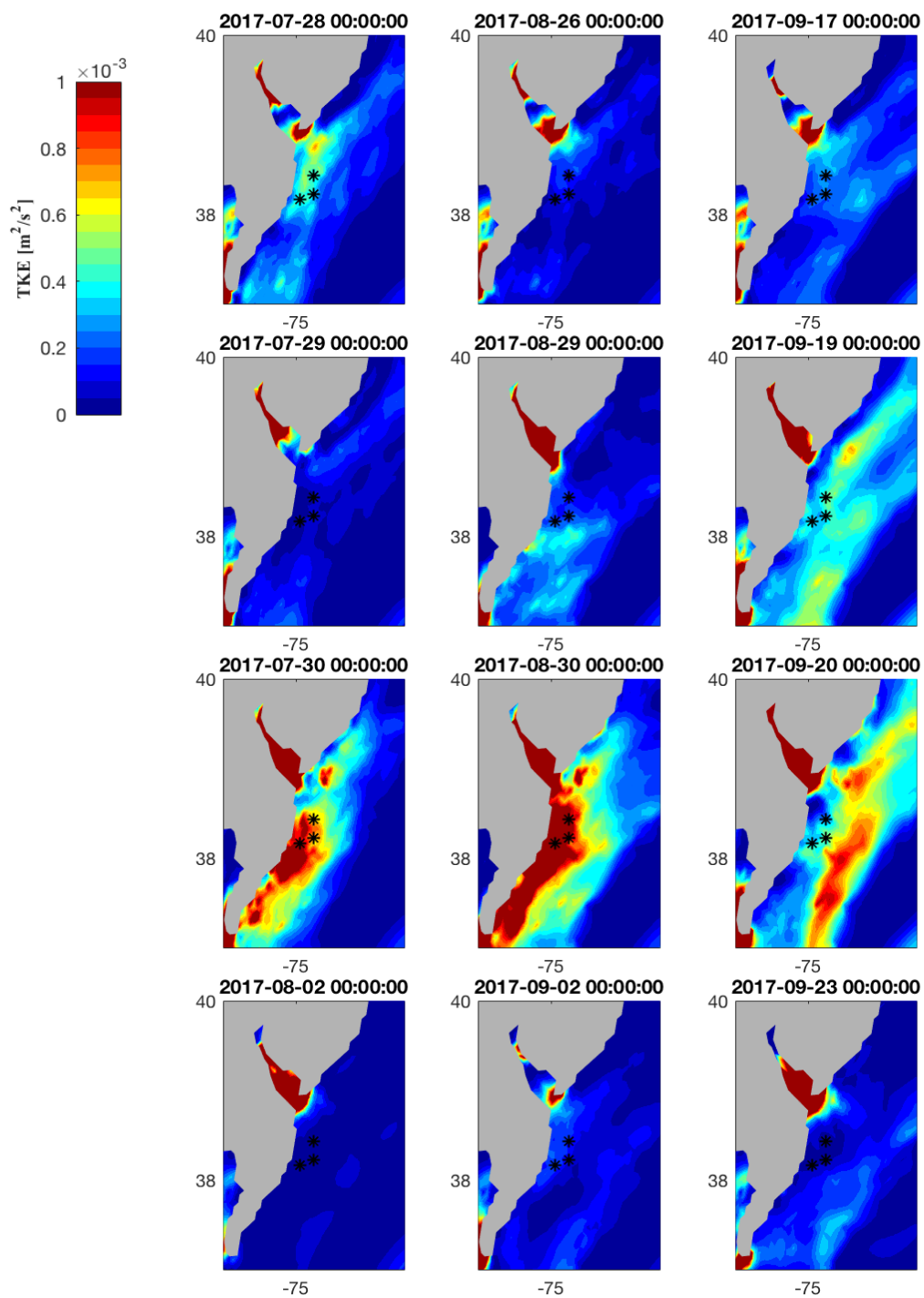


**Figure A.7.** Modeled turbulent kinetic energy (TKE) in the southern MAB predicted by the FVCOM for storm events occurring in 2017. The left column predicts TKE values related to the July nor'easter; the middle column predicts TKE values related to PTC10; and the right column predicts TKE values related to TS Jose. Black asterisks refer to the location of the transmitter release, central to each site.

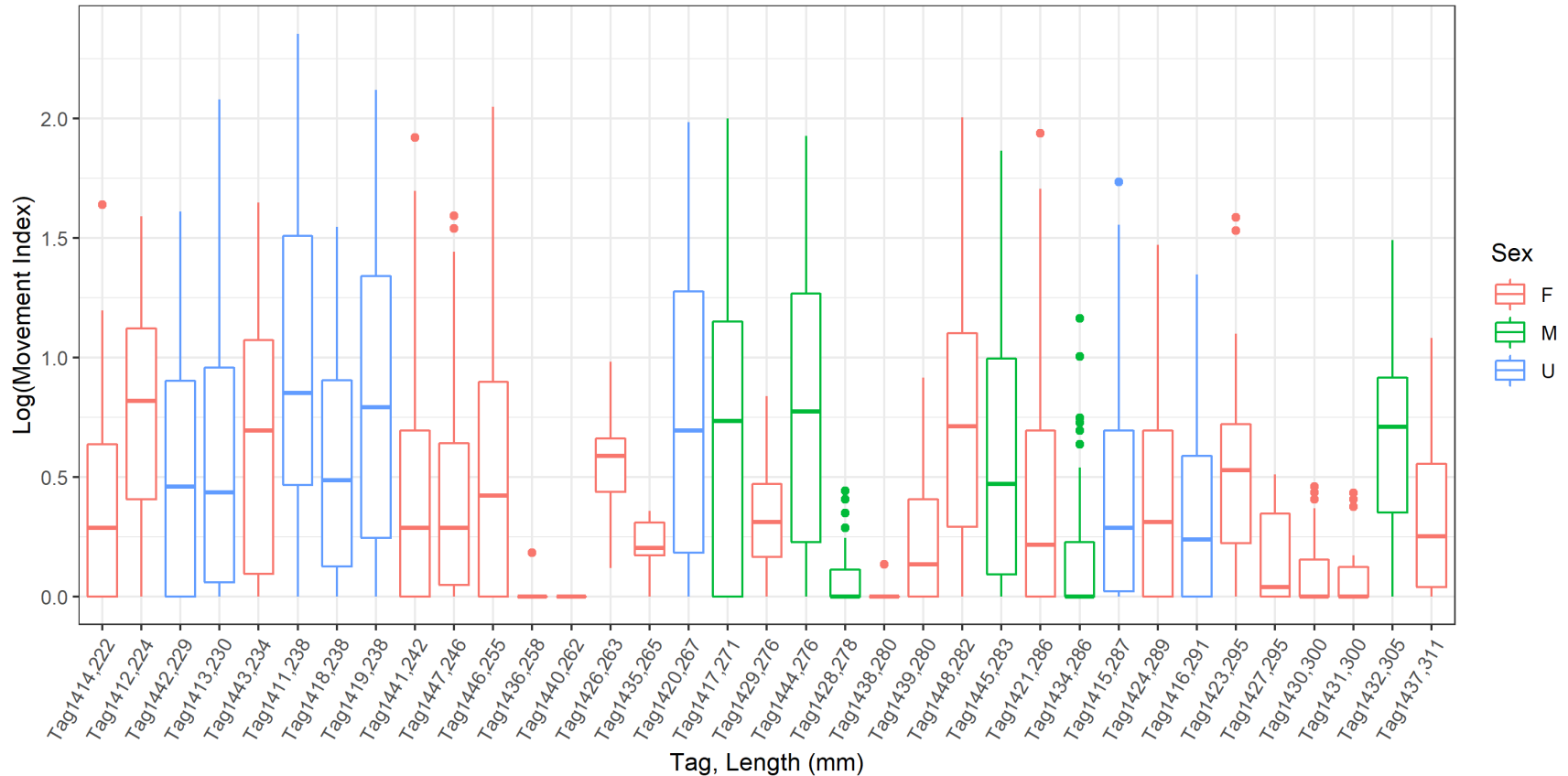


**Figure A.8.** Distributions of log-transformed movement index across individual tagged fish in 2017, ordered by increasing length and color-coded by sex; F, M, and U refer to female, male, and unidentified fish, respectively. X-axis labels refer to the tag number, as well as the length of the individual (mm). Box and whisker plots are shown where the black horizontal line central to each plot defines the median; the horizontal lines above and below the median (completing the box) describe the range of the upper and lower quartile values; the vertical lines extending above and below each box provide upper and lower extremes, respectively; and the black dots provide outliers.



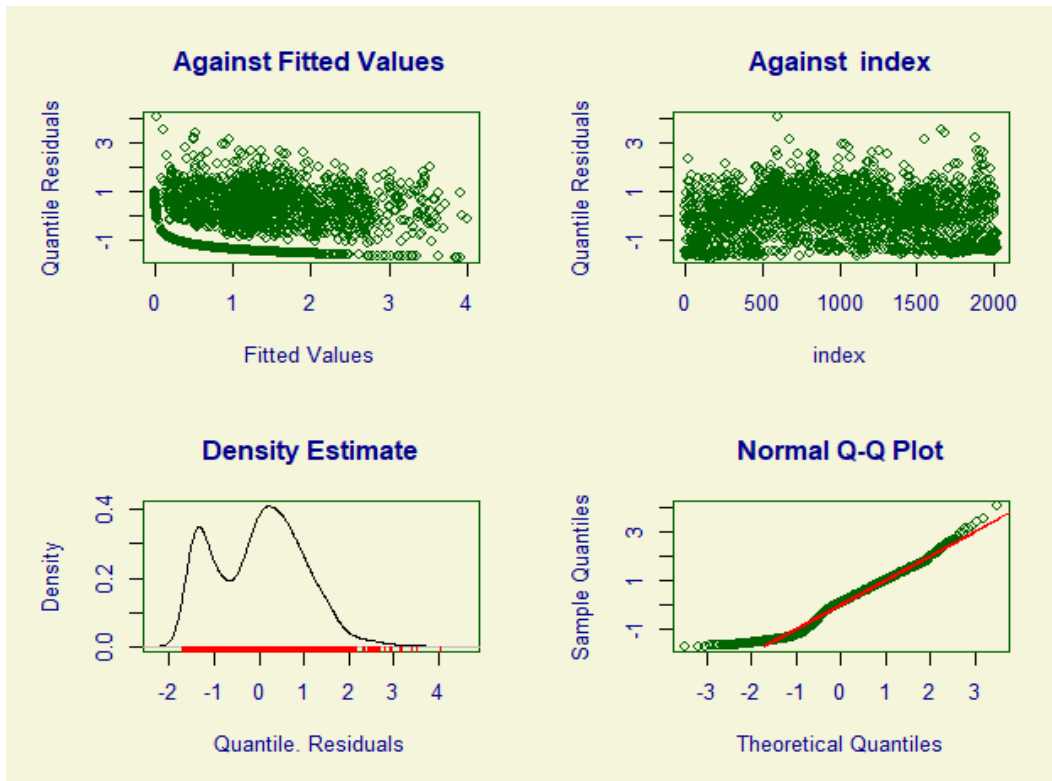


**Figure A.9.** Quantile residual summary plots for the final fitted Generalized Additive Model for Location, Shape, and Scale (GAMLSS) model.

## Appendix B. Temporal and spectral characterization of sound data obtained from a single Mid-Atlantic Bight storm event, 2018.

### Methods

During June 2018, three acoustic recorders—two Snap and one LX1 hydrophones (Loggerhead Instruments)—were deployed 16-46 km east of the coast of Maryland. Each hydrophone was deployed at one mooring within one of three arrays of acoustic receivers, with arrays deployed surrounding previously identified black sea bass reef habitat (Figure B.1; Table B.1). The two Snap recorders were programmed to operate at a 1:9 minute (on:off) duty cycle, while the LX1 was programmed with a 5:5 (on:off) duty cycle. The Snap recorder deployed at the Northern site was retrieved, the data offloaded, and the instrument redeployed during early August 2018. All three recorders were retrieved in late October 2018.

Sound files obtained from retrieved hydrophones were assessed for temporal and spectral signals. Temporal analysis consisted of calculating root mean square (RMS) sound pressure levels (SPL) (dB re: 1  $\mu$ Pa) for the total deployment period, using MATLAB and R. Prior to calculation of RMS SPL values, signals were adjusted for removal of DC offset [signal – mean signal], as well as individual hydrophone sensitivity, gain, (Table B.2), and the transmission of the signal through water [signal/10<sup>((calibration + gain)/20)</sup>]. Spectral analysis consisted of calculating hourly detected frequency sound (dB re: 1  $\mu$ Pa) and power dB re:  $\mu$ Pa<sup>2</sup> Hz<sup>-1</sup> levels during the week of storm activity (September 6 – September 11, 2018). Both band sound level and power spectral density analyses were conducted using MATLAB and PAMGuard respectively. Calculations of band sound level were conducted across third octave levels, with an additional band defining low frequencies (0-100 Hz,

anticipated to be within black sea bass hearing range [Chapter 3]). Power spectral density identified dominant frequencies with the highest power during the week storm activity.

### Results

The temporal signal RMS SPL values at two of the three sites captured the presence of the September 9, 2018 unnamed wind event (Figure B.2). The Middle site stopped recording on August 8, 2018 (21 days into deployment), and missed the event entirely. The Northern site stopped recording on September 10, 2018 (57 days into deployment), and was able to capture the SPL RMS signal for the first half of the storm but stopped recording before the event left the area. This truncation of the anticipated recording at both sites was likely caused by errors within the hydrophones' battery sensors, which may have incorrectly read a false low battery voltage and triggered a premature shutdown of the instruments (David Mann, Loggerhead Instruments, Sarasota, FL; pers. comm.) The Southern site however successfully logged sound measurements for the duration of its deployment period and captured the RMS SPL signal for the entire period of time the wind event was in the study area. SPL values recorded at both the Southern and Northern sites indicate a rapid increase ( $13.74 \pm 2.77$  dB re: 1  $\mu$ Pa) in sound levels occurring on the date of maximum wind speed associated with the storm. Furthermore, RMS SPL values at the Southern site remained elevated following the storm, with the average sound pressure level during the post-storm increasing period by 12.12 dB re: 1  $\mu$ Pa, compared to pre-storm average.

Due to the unanticipated truncation of recordings at the Northern and Middle sites, spectral energy level and power analyses were conducted on sound files obtained at the Southern site alone, for the week of September 6-September 11, 2018. Calculations of sound levels within third octave bands identified a gradual increase in sound levels across all frequency bands as wind speeds approached maximum levels on September 9 (Figure B.3). However, sound levels within the low frequency band (0-100 Hz) were substantially elevated before the storm and increased the most during the storm, compared to the third octave bands. Across all frequency bands, sound levels increase cumulatively and remain increased following the storm event. The PAMGuard software used for this analysis did not account for DC signal offset, however, so while the peaks maintained in sound pressure levels over time are likely accurate, the magnitude of said peaks in dB re: 1  $\mu$ Pa should not be interpreted directly.

Calculations of hourly power spectral density values demonstrated an isolated increase in power within low frequencies (<1000 Hz) corresponding to storm presence in the area and declining after the storm passes (Figure B.4). During the entire week, power levels are concentrated in frequencies below 1000; however, during the wind event, they increase and decline rapidly with storm arrival and departure. On September 6, prior to the storm's arrival, dominant power levels sporadically occur in frequencies below 1000 Hz, but for the greater part of the day fluctuate at approximately 80-90 dB re:  $\mu$ Pa<sup>2</sup> Hz<sup>-1</sup>. When the storm winds peak in the evening on September 9 (Chapter 2), power levels in frequencies below 1000 Hz increase and are consistently sustained between approximately 95-105 dB re:  $\mu$ Pa<sup>2</sup>

Hz<sup>-1</sup>. After the storm departs in the afternoon on September 10, low frequency power levels remain relatively high, and do not return to sustained pre-storm ranges until September 11.

*Tables*

**Table B.1.** Moorings, locations, deployment duration, and recording settings for each hydrophone deployed in the summer of 2018.

Hydrophone	Site, Mooring	Location		Deployment summary			
		Latitude	Longitude	Date Deployed	Date Retrieved	# Days deployed	Duty cycle (on:off, min)
Snap	Northern, SE	38.42878	-74.75977	6/16	10/23	126	1:9
Snap	Middle, SW	38.21886	-74.76277	7/17	10/23	100	1:9
LX1	Southern, N	38.15602	-74.94942	7/31	10/26	87	5:5

**Table B.2.** Moorings, calibration sensitivities, and gain values for each deployed hydrophone.

Hydrophone	Site, Mooring	Calibration (dB)	Gain (dB)
Snap	Northern, NE	-179.7	2.05
Snap	Middle, SW	-180.2	2.05
LX1	Southern, N	-180.2	2.05

Figures

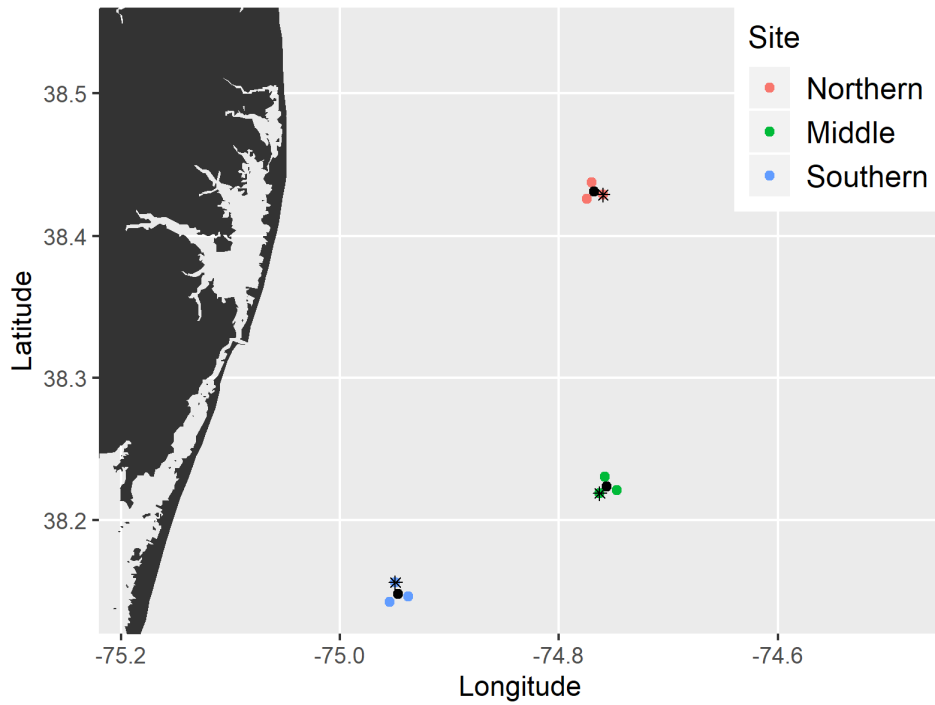


**Figure B.1.** Experimental study sites, including locations of receiver sites, tagging sites, and hydrophone deployments. Colored points refer to receiver deployment locations, while black points refer to approximate tagging locations. Black asterisks refer to hydrophone deployment locations at each receiver site.



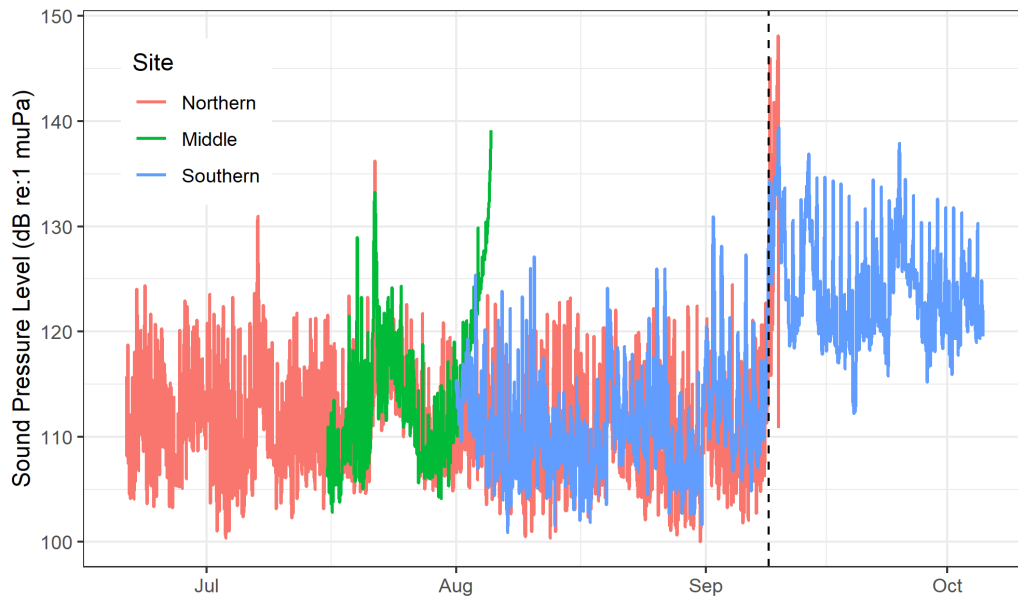


**Figure B.2.** Root mean square (RMS) sound pressure levels (SPL) calculated from sound voltage measurements taken at each site during 2018. The black dotted line refers to the date of maximum wind speed associated with the 2018 unnamed wind event.

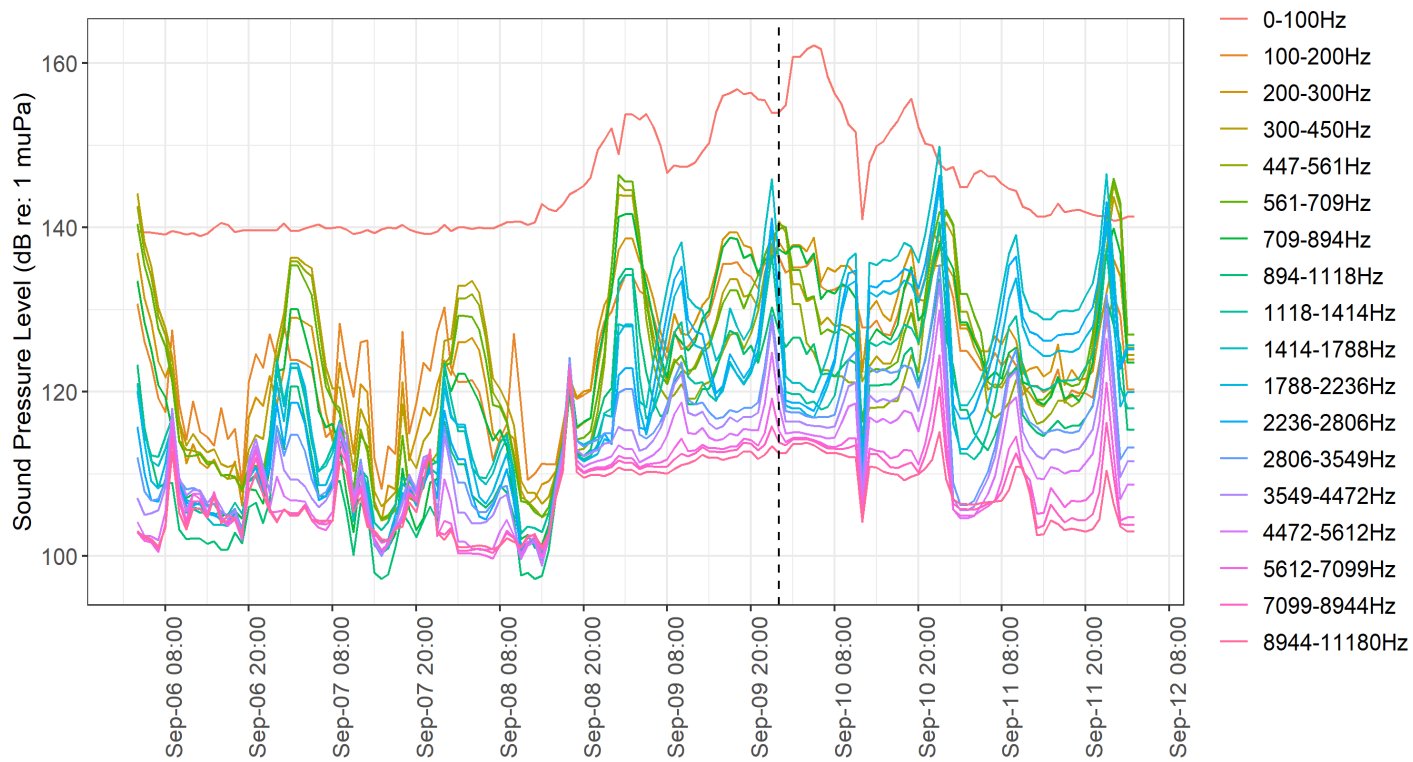


**Figure B.3.** Sound pressure levels calculated during the week of storm activity, September 6 – September 11, 2018, calculated across third octave bands and a predefined low frequency band (0-100 Hz). The black dotted line refers to the date of maximum wind speed associated with the 2018 unnamed wind event.

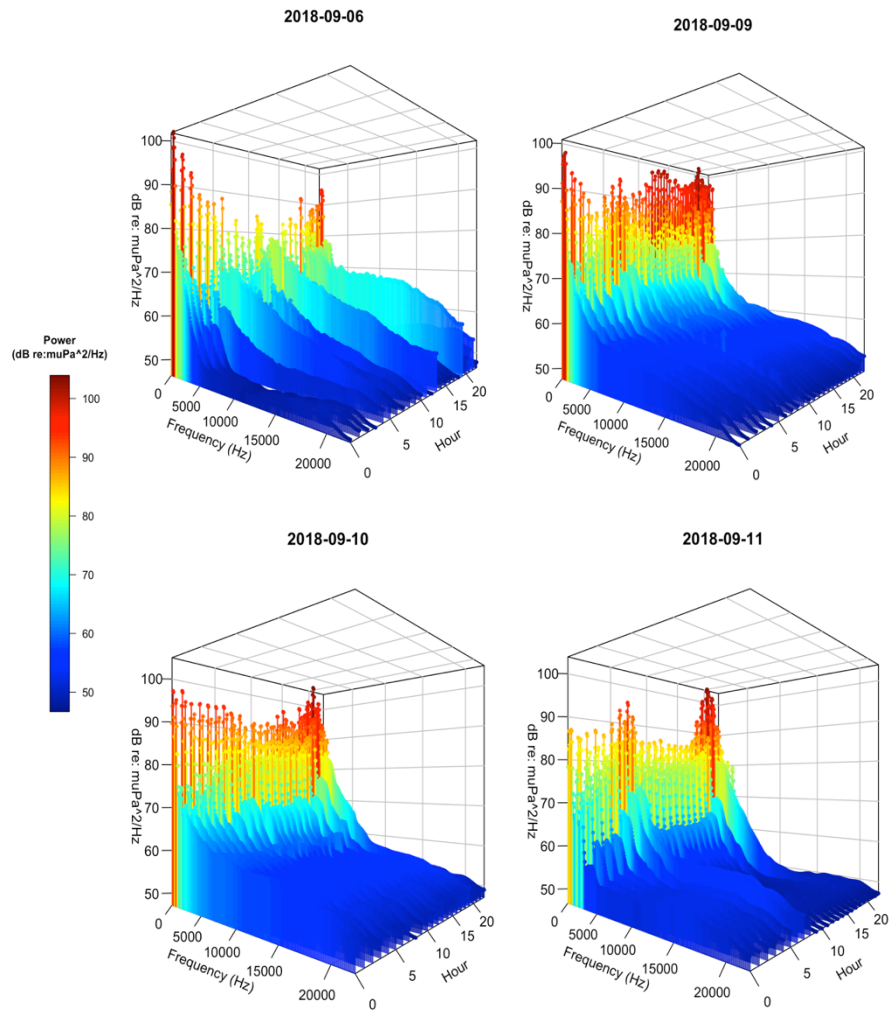


**Figure B.4.** Hourly power spectral density values calculated across detected frequencies for September 6, 9, 10, and 11 of September, 2018. Warmer colors indicate higher power values.

## Appendix C. Body condition and feeding ecology of black sea bass sampled from the Middle-Atlantic Bight 2018.

### Methods

During the summer and fall 2018 deployments and retrievals of acoustic recorders and receivers, a total of 116 black sea bass were collected at the Northern, Middle, and Southern sites for laboratory diet analysis (Table C.1; see Figure 2.1). Individuals were sampled at all sites in the summer (June 19 and July 15, 31) during receiver deployment and at the Northern and Southern sites during the fall retrieval (October 23). No individuals were sampled from the Middle site during the fall season due to increasing sea state and wind speed on site, which interfered with angling. Individuals were frozen in dry ice immediately following capture, then transported to Chesapeake Biological Laboratory, Solomons, MD for freezer storage and processing. Individuals were thawed prior to dissection and disposed immediately post-dissection. Dissection processing included taking measurements of length, body weight, gonad weight, liver weight, total stomach weight, stomach lining weight, and individual prey item weight. All weight measurements were taken as wet weights (g), and prey items were identified and categorized by phyla.

Sampled fish were processed for measurements describing body condition and diet composition. Body condition was evaluated and described using Fulton's condition factor (K):

$$K = 100 * \frac{\text{Total body weight}}{\text{Length}^3} ;$$

gonadosomatic index (GSI) as the percent bodyweight contribution of gonad weight:

$$GSI = 100 * \frac{\text{Gonad weight}}{\text{Total body weight}} ;$$

hepatosomatic index (HSI) as the percent bodyweight contribution of liver weight:

$$HSI = 100 * \frac{Liver\ weight}{Total\ body\ weight} ;$$

and a linear regression of log-transformed body length by log-transformed weight.

This regression model was used to fit predictions of weight based on length. Possible differences in K, GSI, HSI, and length-weight regression across site and sampling season were evaluated using separate ANOVA and Tukey multiple comparison tests for each metric. Diet composition was evaluated through the calculation of percent gut fullness:

$$\% Gut\ fullness = 100 * \frac{(Total\ stomach\ weight - stomach\ lining\ weight)}{Total\ body\ weight} ;$$

and stomach content. Stomach content was assessed by percent number (%N) and percent weight (%W) expressed relative to percent frequency of occurrence (%FO) of prey items identified in non-empty stomachs.

$$\%N = 100 * \frac{Number\ of\ prey\ item\ i}{Total\ number\ of\ prey\ items} ;$$

$$\%W = 100 * \frac{Weight\ of\ prey\ item\ i}{Total\ weight\ of\ prey\ items} ;$$

$$\%FO = 100 * \frac{Number\ of\ stomachs\ with\ prey\ item\ i}{Total\ number\ of\ non-empty\ stomachs} ;$$

All statistical analyses were conducted in R, utilizing the *car* package (Fox and Weisberg 2019).

## Results

Body condition of sampled individuals differed across site and season, for all metrics used. Significant differences in K were identified between seasons (ANOVA,  $p < 0.05$ ); within the summer sampling period, additional significant differences were identified between samples taken from the Northern and Southern sites (Tukey HSD,

$p < 0.01$ ) and samples taken from the Middle and Southern sites (Tukey HSD,  $p < 0.01$ ) (Figure C.1). No significant differences were identified across sites sampled during the fall (ANOVA,  $p = 0.77$ ). Measurements of GSI indicated differential contributions of gonad weight to total body weight across both sites and season (Figure C.2). Fish sampled during the fall had a significantly lower GSI than those fish sampled during the summer (ANOVA,  $p < 0.01$ ), suggesting that spawning activity occurred at some point during the June-October study period at monitored reef sites. Within the subset of fish sampled during the summer, GSI differed significantly across sites (ANOVA,  $p < 0.01$ ), with significant differences occurring between those fish sampled at the Northern versus Middle sites (Tukey HSD,  $p < 0.01$ ) and those sampled at the Northern versus Southern sites (Tukey HSD,  $p < 0.05$ ). Measurements of HSI indicated similar seasonal differences in condition (Figure C.3), as were observed through K and GSI, with HSI values for summer-sampled fish being significantly higher than those values for fall-sampled fish (ANOVA,  $p < 0.01$ ). HSI values differed significantly across sites during the summer sampling period (ANOVA,  $p < 0.05$ )—similar to trends described in GSI values—with differences in percent contributions of liver to total bodyweight observed between the Northern and Middle sites (Tukey HSD,  $p < 0.05$ ) as well as between Northern and Southern sites (Tukey HSD,  $p < 0.05$ ). Unlike those relationships observed in GSI values, HSI values also differed significantly across sites—Northern and Southern—during the fall (ANOVA,  $p < 0.05$ ).

Predictions of the length-weight regression model, predicting weight based on a logarithmic relationship to observed length, were overall consistent with observed

weight (Figure C.4). An ANOVA test for log-transformed weights as a function of the model residuals, nested by site and sampling season, identified a significant effect of site ( $p < 0.01$ ), but not sampling season ( $p = 0.176$ ); post-hoc comparisons further specified a significant difference between fish sampled at the Middle site ( $p < 0.05$ ) and fish sampled at the Southern site during the summer ( $p < 0.05$ ) (Figure C.5).

Of the 116 black sea bass stomachs evaluated for diet composition, 50 contained prey items, 58 were empty, and 8 were inverted (likely due to barotrauma from sampling) and subsequently discarded (Table C.2). Percent gut fullness was consistently low across sites and season, with the exception being substantially higher percentages observed in fish sampled at the Southern site during the summer, where barotrauma was less frequently encountered (Figure C.6). Gut fullness across seasons did not differ significantly (ANOVA,  $p = 0.12$ ), although it did differ significantly, across sites within seasons, between Northern and Southern sites (ANOVA,  $p < 0.05$ ; TukeyHSD,  $p < 0.01$ ) and Middle and Southern sites (Tukey HSD,  $p < 0.05$ ). Identified prey types included arthropods (i.e., multiple crab species), mollusks (i.e., clams, squid), and bony fish (i.e., sand eels), with one stomach containing intact synthetic bait. Comparisons of %N and %W by %FO suggested a unanimous dominance of Arthropoda in the diet of sampled black sea bass (Table C.3; Figure C.7). The presence of Arthropoda in sampled stomachs was not skewed by either quantity or weight of the prey items observed. Presence of Mollusca and Osteichthyes prey, however, was skewed towards fewer, heavier prey items in the former phylum and towards more numerous, albeit lighter, prey items in the latter phylum.

*References*

Fox, J. and Weisberg, S. (2019). An {R} Companion to Applied Regression, Third Edition. Thousand Oaks CA: Sage.

URL: <https://socialsciences.mcmaster.ca/jfox/Books/Companion/>



Tables

**Table C.1.** Distribution of individuals sampled for diet study, across site and season of sampling. Summer refers to the months of June-July, whereas Fall refers to October. No fish were sampled at the Middle site during the Fall season because of inclement weather and sea state conditions on site.

	No. individuals	
	Summer	Fall
Northern	32	20
Middle	20	-
Southern	23	21

**Table C.2.** Counts of sampled stomachs, categorized by stomachs found containing prey, empty, or inverted, across site and season.

	No. sampled stomachs					
	Contained prey		Empty		Inverted	
	Summer	Fall	Summer	Fall	Summer	Fall
Northern	11	8	20	10	1	2
Middle	8	-	8	-	4	-
Southern	18	5	5	15	0	1
Total	50		58		8	

**Table C.3.** Calculations of percent number (%N), percent weight (%W), and percent frequency of occurrence (%FO), alongside respective counts, for each phylum of prey type.

Prey type	%N	%W	%FO	n
Anthropoda	76.03	71.84	70	74
Mollusca	14.83	11.65	24	12
Osteichthys	7.17	10.68	22	5
Synthetic bait	1.17	4.85	10	1
Unknown	0.79	0.97	2	11

Figures

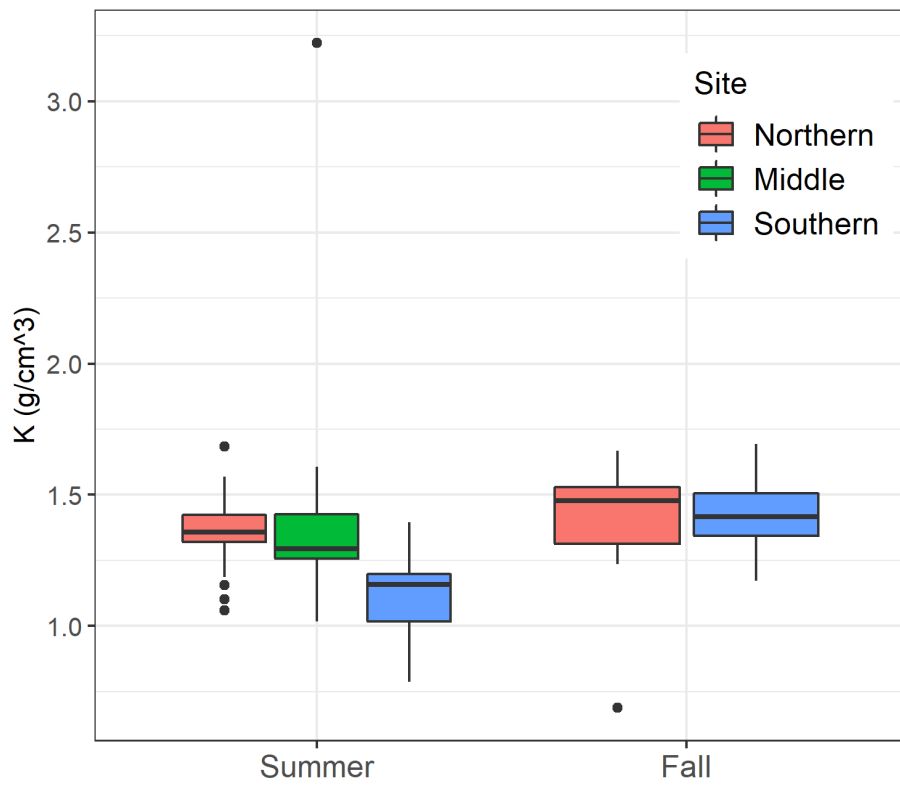


**Figure C.1.** Distributions of Fulton's K (K) for sampled fish, calculated across sampling site and season. K assumes an allometric relationship where weight (g) = length (cm)<sup>3</sup>. Here K was thus determined by dividing observed weight (g) by cubed observed length (cm) and multiplying the quotient by 100.

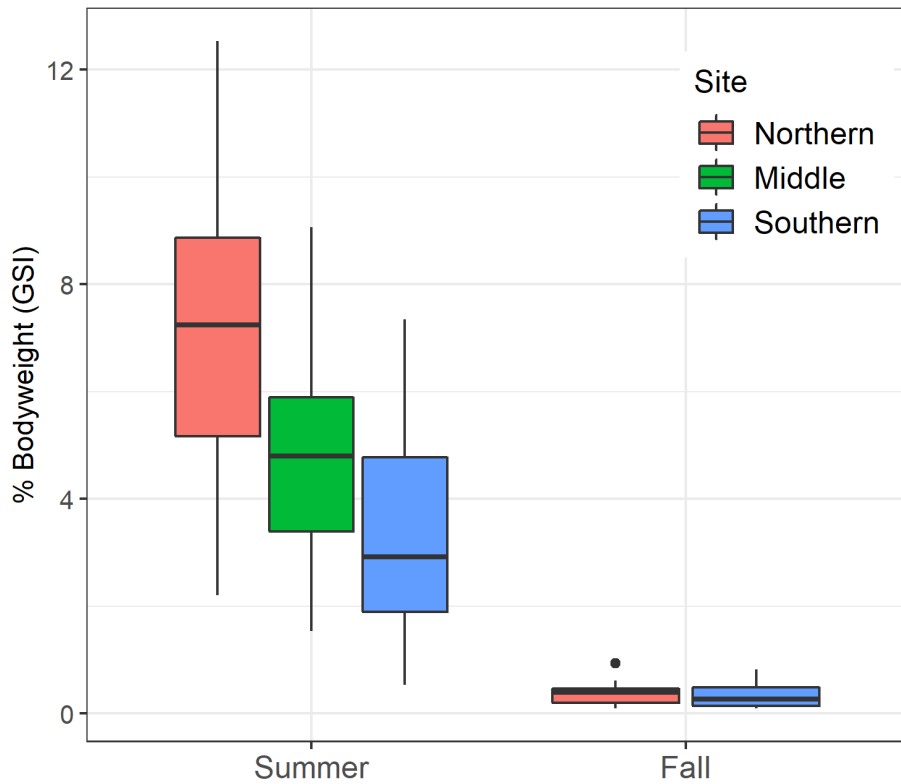


**Figure C.2.** Distribution of GSI calculations for sampled fish, across site and season of sampling. GSI was calculated as the percent contribution of gonad weight (g) relative to total body weight (g) per individual.

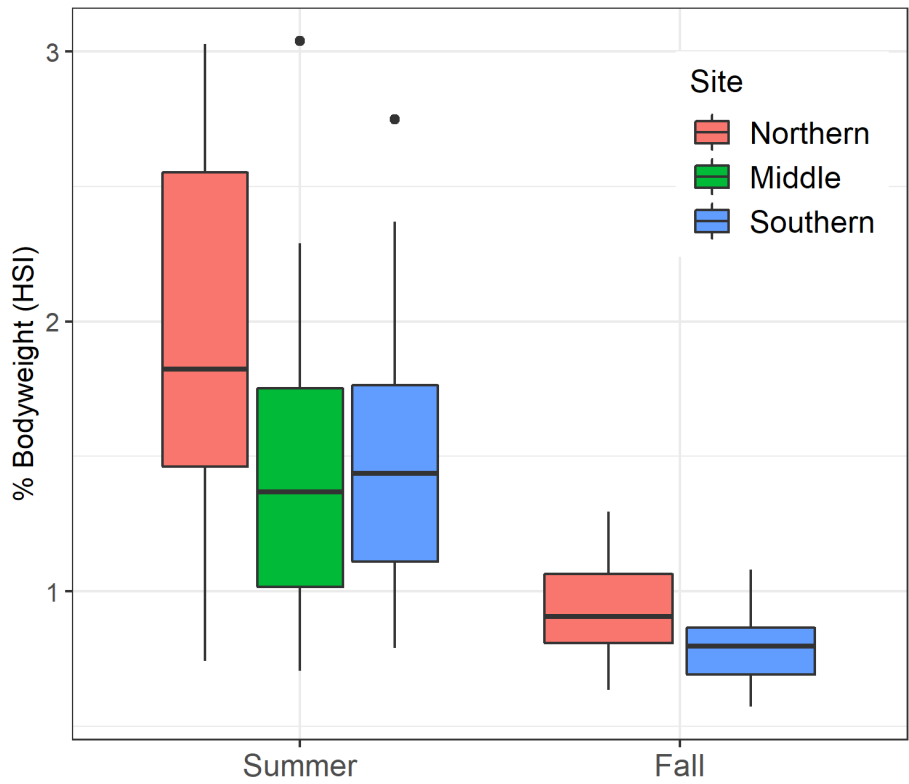


**Figure C.3.** Distribution of HSI calculations for sampled fish, across site and season of sampling. HSI was calculated as the percent contribution of liver weight (g) relative to total body weight (g) per individual.

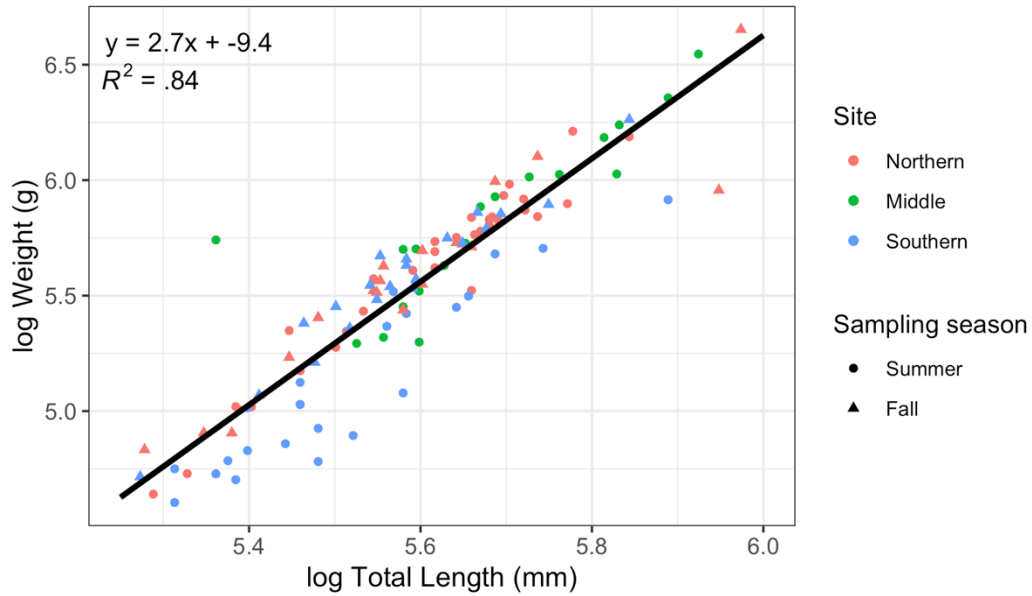


**Figure C.4.** Log-transformed measurements of weight plotted as a function of log-transformed measurements of length for individuals sampled. The black line refers to log length-weight regression model predictions of weight based on input observed length. The color and shape of the plotted points refer to the site of sampling and the sampling season, respectively.

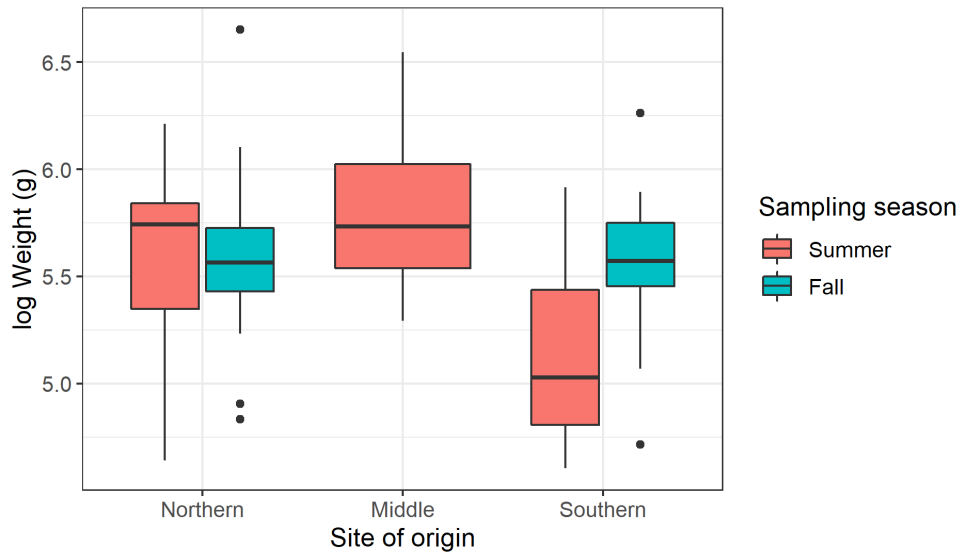


**Figure C.5.** Distribution of weights across sampling site and season. Site had a significant effect (ANOVA,  $p < 0.01$ ) but sampling season did not (ANOVA,  $p = 0.176$ ). Weights taken from the Middle and Southern sites were significantly different from other distributions (Tukey HSD,  $p < 0.05$ ).



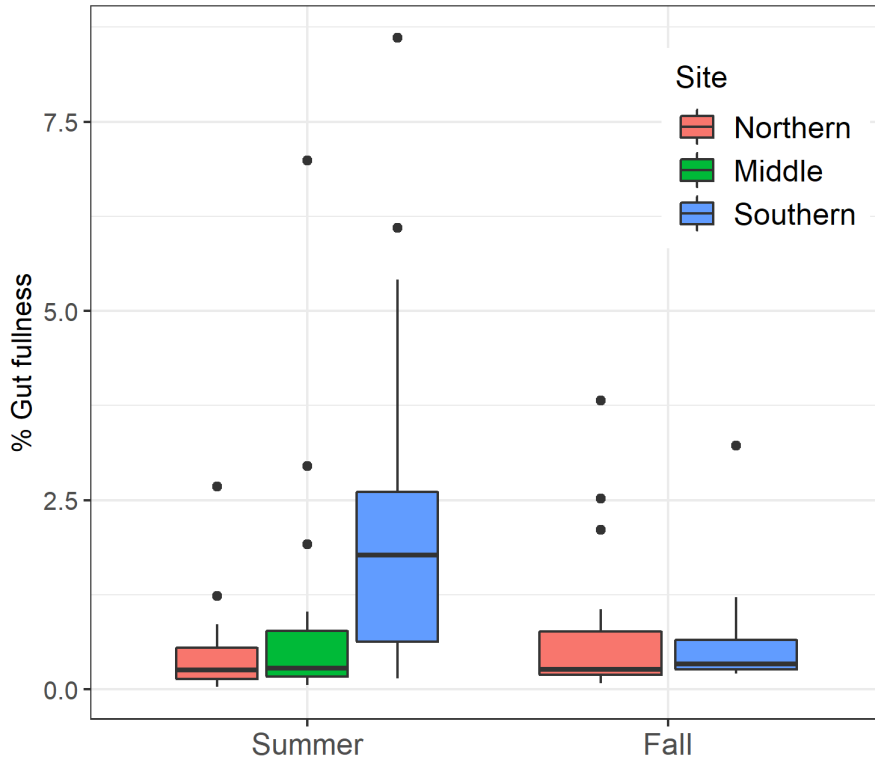


**Figure C.6.** Distributions of percent gut fullness of sampled individuals, across sampling site and season. Gut fullness was calculated as the percent weight of stomach contents (stomach weight minus the weight of stomach lining; (g)) relative to total body weight (g).

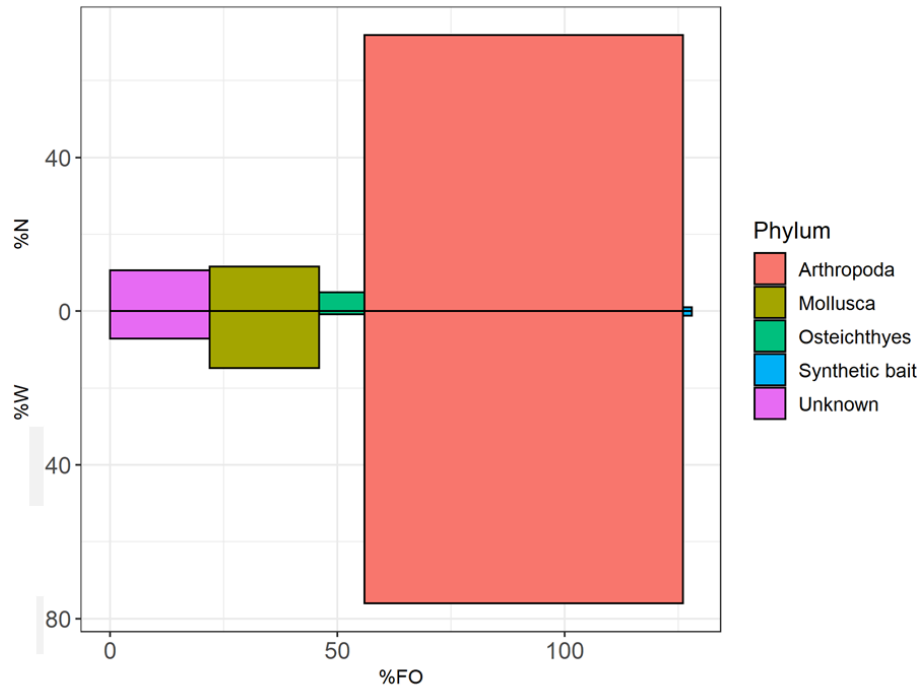


**Figure C.7.** Percent number (%N) and percent weight (%W) of each identified prey phylum, plotted against respective prey percent frequency of occurrence (%FO).

## Bibliography

- Amoser, S., & Ladich, F. (2005). Are hearing sensitivities of freshwater fish adapted to the ambient noise in their habitats? *The Journal of Experimental Biology*, *208*, 3533-3542. <https://doi.org/10.1242/jeb.01809>
- Amoser, S., Wysocki, L. E., & Ladich, F. (2004). Noise emission during the first powerboat race in an Alpine lake and potential impact on fish communities. *The Journal of the Acoustical Society of America*, *116*(6), 3789-3797. <https://doi.org/10.1121/1.1808219>
- Andersson, M. H., & Öhman, M. C. (2010). Fish and sessile assemblages associated with wind-turbine constructions in the Baltic Sea. *Marine and Freshwater Research*, *61*, 642-650.
- Araga, C., & Tanase, H. (1966). Fish stranding caused by a typhoon in the vicinity of Seto. *Publications of the Seto Marine Biological Laboratory*, *14*(2), 155-160.
- Atwood, H. L., Young, S. P., Tomasso, J. R., Jr., & Smith, T. I. J. (2001). Salinity and temperature tolerances of black sea bass juveniles. *North American Journal of Aquaculture*, *63*, 285-288.
- Bacheler, N. M., Shertzer, K. W., Cheshire, R. T., & MacMahan, J. H. (2019). Tropical storms influence the movement behavior of a demersal oceanic fish species. *Scientific Reports*, *9*(1481), 1-13. <https://doi.org/10.1038/s41598-018-37527-1>
- Bailey, H., Senior, B., Simmons, D., Rusin, J., Picken, G., & Thompson, P. M. (2010). Assessing underwater noise levels during pile-driving at an offshore windfarm and its potential effects on marine mammals. *Marine Pollution Bulletin*, *60*, 888-897.
- Bailey, H., & Secor, D. H. (2016). Coastal evacuations by fish during extreme weather events. *Scientific Reports*, 1-9. <https://doi.org/10.1038/srep30280>
- Bates, D., Maechler, M., Bolker, B., Walker, S. (2015). Fitting Linear Mixed-Effects Models Using lme4. *Journal of Statistical Software*, *67*(1), 1-48. <[doi:10.18637/jss.v067.i01](https://doi.org/10.18637/jss.v067.i01)>.
- Baranowski, D. B., Flatau, P. J., Chen, S., & Black, P. G. (2014). Upper ocean response to the passage of two sequential typhoons. *Ocean Science*, *10*, 559-570. <https://doi.org/10.5194/os-10-559-2014>
- Beardsley, R. C., Chapman, D. C., Brink, K. H., Ramp, S. R., & Schlitz, R. (1985). The Nantucket Shoals Flux Experiment (NSFE79). Part I: A basic

description of the current and temperature variability. *Journal of Physical Oceanography*, 15, 713-748.

- Belanger, A. J., Bobeica, I., & Higgs, D. M. (2010). The effect of stimulus type and background noise on hearing abilities of the round goby *Negobius melanostomus*. *Journal of Fish Biology*, 77, 1488-1504.  
<https://doi.org/10.1111/j.1095-8649.2010.02773.x>
- Beven, J., & Cobb, H. (2004, July). *Tropical cyclone report: Hurricane Isabel*. National Hurricane Center.
- Bergström, L., Sundqvist, F., & Bergström, U. (2013). Effect of an offshore wind farm on temporal and spatial patterns in the demersal fish community. *Marine Ecology Progress Series*, 485, 199-210.  
<https://doi.org/10.3354/meps10344>
- Bigelow, H. B. (1933). Studies of the waters on the continental shelf, Cape Cod to Chesapeake Bay, I, The cycle of temperature. *Papers in Physical Oceanography and Meteorology*, 11(4), 1-134.
- Biggs, C. R., Lowerre-Barbieri, S. K., & Erisman, B. (2018). Reproductive resilience of an estuarine fish in the eye of a hurricane. *Biology Letters*, 14, 1-5.  
<https://doi.org/10.1098/rsbl.2018.0579>
- Bin, O., Dumas, C., Poulter, B., & Whitehead, J. (2007, March). *Measuring the impacts of climate change on North Carolina coastal resources*. Washington DC, USA: National Commission on Energy Policy.
- Bouchon, C., Bouchon-Navaro, Y., & Louis, M. (1994). Changes in the coastal fish communities following Hurricane Hugo in Guadeloupe Island (French West Indies). *Atoll Research Bulletin*, (422), 1-19.
- Bureau of Ocean Energy Management, Office of Renewable Energy Programs. (2012, January). *Commercial wind lease issuance and site assessment activities on the Atlantic outer continental shelf offshore New Jersey, Delaware, Maryland, and Virginia* (OCS EIS/EA BOEM No. 2012-003). U.S. Department of the Interior,
- Bureau of Ocean Energy Management. (2018, August). *Outer continental shelf renewable energy leases map book*.
- Braun, C. B., & Grande, T. (2008). Evolution of peripheral mechanisms for the enhancement of sound reception. *Fish Bioacoustics*, 32, 99-144.
- Bullock, T. H., & Corwin, J. T. (1979). Acoustic evoked activity in the brain in sharks. *Journal of Comparative Physiology*, 129, 223-234.

- Byrnes, J. E., Reed, D. C., Cardinale, B. J., Cavanaugh, K. C., Holbrook, S. J., & Schmitt, R. J. (2011). Climate-driven increases in storm frequency simplify kelp forest food webs. *Global Change Biology*, *17*, 2513-2524.  
<https://doi.org/10.1111/j.1365-2486.2011.02409.x>
- Bythell, J. C., Hillis-Starr, Z. M., & Rogers, C. S. (2000). Local variability but landscape stability in coral reef communities following repeated hurricane impacts. *Marine Ecological Progress Series*, *204*, 93-100.
- Carroll, A. G., Przeslawski, R., Duncan, A., Gunning, M., & Bruce, B. (2017). A critical review of the potential impacts of marine seismic surveys on fish and invertebrates. *Marine Pollution Bulletin*, *114*, 9-24.  
<https://doi.org/10.1016/j.marpolbul.2016.11.038>
- Casper, B. M., Lobel, P. S., & Yan, H. Y. (2003). The hearing sensitivity of the little skate, *Raja erinacea*: A comparison of two methods. *Environmental Biology of Fishes*, *68*, 371-379.
- Casper, B. M., & Mann, D. A. (2006). Evoked potential audiograms of the nurse shark (*Ginglymostoma cirratum*) and the yellow stingray (*Urobatis jamaicensis*). *Environmental Biology of Fishes*.  
<https://doi.org/10.1007/s10641-006-9012-9>
- Casper, B. M., & Mann, D. A. (2007). Dipole hearing measurements in elasmobranch fishes. *Journal of Experimental Biology*, *210*, 75-81.  
<https://doi.org/10.1242/jeb.02617>
- Casper, B. M., & Mann, D. A. (2009). Field hearing measurements of the Atlantic sharpnose shark *Rhizoprionodon terraenovae*. *Journal of Fish Biology*, *75*, 2768-2776. <https://doi.org/10.1111/j.1095-8649.2009.02477.x>
- Casper, B. M., Smith, M. E., Halvorsen, M. B., Sun, H., Carlson, T. J., & Popper, A. N. (2013). Effects of exposure to pile driving sounds on fish inner ear tissues. *Comparative Biochemistry and Physiology, Part A*, *166*.  
<https://doi.org/10.1016/j.cbpa.2013.07.008>
- Chapman, C. J. (1973). Field studies of hearing in teleost fish. *Helgoländer wissenschaftliche Meeresuntersuchungen*, *24*, 371-390.
- Chapman, C. J., & Hawkins, A. D. (1973). A field study of hearing in the cod, *Gadus morhua* L. *Journal of Comparative Physiology*, *85*, 147-167.
- Chen, C., & Liu, H. (2003). An unstructured grid, finite-volume, three-dimensional, primitive equations ocean model: Application to coastal ocean and estuaries. *Journal of Atmospheric and Oceanic Technology*, *20*, 159-186.

- Chen, Z., Curchitser, E., Chant, R., & Kang, D. (2018). Seasonal variability of the cold pool over the Mid-Atlantic Bight continental shelf. *Journal of Geophysical Research: Oceans*, *123*, 8203-8226. <https://doi.org/10.1029/2018JC014148>
- Coastal Fisherman. (2012, September 19). Straight from the Maryland DNR fisheries service. Retrieved November 15, 2019, from Coastal Fisherman website: <https://coastalfisherman.net/issues.cfm?issue=8A13C17C-5056-9F21-090A10DE6EFB925B&story=B2C7507E-5056-9F21-0933D8A161BE1084>
- Codarin, A., Wysocki, L. E., Ladich, F., & Picciulin, M. (2009). Effects of ambient and boat noise on hearing and communication in three fish species living in a marine protected area (Miramare, Italy). *Marine Pollution Bulletin*, *58*, 1880-1887.
- Collins, S. L., & Barber, S. C. (1986). Effects of disturbance on diversity in a mixed-grass prairie. *Plant Ecology*, *64*, 87-94. <https://doi.org/10.1007/BF00044784>
- Colvocoresses, J. A., & Musick, J. A. (1984). Species associations and community composition of Middle Atlantic Bight continental shelf demersal fishes. *Fishery Bulletin*, *82*(2), 295-313.
- Coombs, S., & Popper, A. N. (1979). Hearing differences among Hawaiian squirrelfish (family Holocentridae) related to differences in the peripheral auditory system. *Journal of Comparative Physiology A*, *132*, 203-207.
- Coombs, S., & Popper, A. N. (1982). Structure and function of the auditory system in the clown knifefish, *Notopterus chitala*. *Journal of Experimental Biology*, *97*, 225-239.
- Cullen, D. W., & Stevens, B. G. (2017). Use of an underwater video system to record observations of black sea bass (*Centropristis striata*) in waters off the coast of Maryland. *Fishery Bulletin*, *115*(3), 408-418. <https://doi.org/10.7755/FB.115.3.10>
- Dale, J. J., Gray, M. D., Popper, A. N., Rogers, P. H., & Block, B. A. (2015). Hearing thresholds of swimming Pacific bluefin tuna *Thunnus orientalis*. *Journal of Comparative Physiology A*, *201*, 441-454. <https://doi.org/10.1007/s00359-015-0991-x>
- Dayton, P. K., Currie, V., Gerrodette, T., Keller, B. D., Rosenthal, R., & Ven Tresca, D. (1984). Patch dynamics and stability of some California kelp communities. *Ecological Monographs*, *54*(3), 253-289.

- Dernie, K. M., Kaiser, M. J., & Warwick, R. M. (2003). Recovery rates of benthic communities following physical disturbance. *Journal of Animal Ecology*, 72, 1043-1056.
- Dijkgraaf, S. (1960). Hearing in bony fishes. *Proceedings of the Royal Society of London, Series B, Biological Sciences*, 152(946), 51-54.
- Dollar, S. J., & Tribble, G. W. (1993). Recurrent storm disturbance and recovery: A long-term study of coral communities in Hawaii. *Coral Reefs*, 12, 223-233.
- Ebeling, A. W., Laur, D. R., & Rowley, R. J. (1985). Sever storm disturbances and reversal of community structure in a southern California kelp forest. *Marine Biology*, 84, 287-294.
- Egner, S. A., & Mann, D. A. (2005). Auditory sensitivity of sergeant major damselfish *Abudefduf saxatilis* from post-settlement juvenile to adult. *Marine Ecology Progress Series*, 285, 213-222.
- ESS Group Inc. (2016). *Site assessment plan, Maryland offshore wind project* (ESS Project No. U167).
- Evans, H. M. (1925). A contribution to the anatomy and physiology of the air-bladder and Weberian ossicles in Cyprinidae. *Proceedings of the Royal Society of London Series B*, 97(686), 545-576.
- Fabrizio, M.C., Pessutti, J.P., Manderson, J.P., Drohan, A.F., Phelan, B.A. (2005). Use of the Historic Area Remediation Site by black sea bass and summer flounder. U.S. Dep. Commer., Northeast Fish. Sci. Cent. Ref. Doc. 05-06; 95 p. Available from: National Marine Fisheries Service, 166 Water Street, Woods Hole, MA 02543-1026.
- Fabrizio, M. C., Manderson, J. P., & Pessutti, J. P. (2013). Habitat associations and dispersal of black sea bass from a mid-Atlantic Bight reef. *Marine Ecological Progress Series*, 482, 241-253. <https://doi.org/10.3354/meps10302>
- Fabrizio, M. C., Manderson, J. P., & Pessutti, J. P. (2014). Habitat associations and dispersal of black sea bass from a mid-Atlantic Bight reef. *Marine Ecological Progress Series*, 482, 241-253. <https://doi.org/10.3354/meps10302>
- Fenner, D. P. (1991). Effects of Hurricane Gilbert on coral reefs, fishes and sponges at Cozumel, Mexico. *Bulletin of Marine Science*, 48(3), 719-730.

- Fish, J. F., & Offutt, G. C. (1972). Hearing thresholds from toadfish, *Opsanus tau*, measured in the laboratory and field. *The Journal of the Acoustical Society of America*, 51(4), 1318-1321. <https://doi.org/10.1121/1.1912977>
- Fox, J. and Weisberg, S. (2019). An {R} Companion to Applied Regression, Third Edition. Thousand Oaks CA: Sage.  
URL: <https://socialsciences.mcmaster.ca/jfox/Books/Companion/>
- von Frisch, K. (1938). The sense of hearing in fish. *Nature*, 141, 8-11.
- Frisk, G. V. (2007). Noiseconomics: The relationship between ambient noise levels in the sea and global economic trends. *Scientific Reports*, 437(2).  
<https://doi.org/10.1038/srep00437>
- Froese, R. and D. Pauly, Editors. 2000. FishBase 2000: concepts, design and data sources. ICLARM, Los Baños, Laguna, Philippines. 344 p.
- Gardner, T. A., Côté, I. M., Gill, J. A., Grant, A., & Watkinson, A. R. (2005). Hurricanes and Caribbean coral reefs: Impacts, recovery patterns, and role in long-term decline. *Ecology*, 86(1), 174-184.
- Gill, A., Huang, Y., Spencer, J., & Gloyne-Philips, I. (2012). *Electromagnetic Fields Emitted by High Voltage Alternating Current Offshore Wind Power Cables and Interactions with Marine Organisms*. Electromagnetics in Current and Emerging Energy Power Systems Seminar, London, UK.
- Ginis, I. (2002). Tropical cyclone-ocean interactions. *Atmosphere-Ocean Interactions, Advances in Fluid Mechanics Series*, 33, 83-114.
- Graves, S., Piepho, H.P., and Selzer, L. (2015). multcompView: Visualizations of Paired Comparisons. R package version 0.1-7. <https://CRAN.R-project.org/package=multcompView>
- Gunn, W. W. H., & Crocker, A. M. (1951). Analysis of unusual bird migration in North America during the storm of April 4-7, 1947. *The Auk*, 68(2), 139-163.
- Halvorsen, M. B., Casper, B. M., Woodley, C. M., Carlson, T. J., & Popper, A. N. (2012). Threshold for onset of injury in Chinook salmon from exposure to impulsive pile driving sounds. *PLoS One*, 7(6).
- Harmelin-Vivien, M. L. (n.d.). The effects of storms and cyclones on coral reefs: A review. *Journal of Coastal Research*, (12), 211-231.
- Hawkins, A. D., & Johnstone, D. F. (1978). The hearing of the Atlantic Salmon, *Salmo salar*. *Journal of Fish Biology*, 13, 655-673.



- Hawkins, A. D., Pembroke, A. E., & Popper, A. N. (2015). Information gaps in understanding the effects of noise on fishes and invertebrates. *Reviews in Fish Biology and Fisheries*, 25, 39-64. <https://doi.org/10.1007/s11160-014-9369-3>
- Hawkins, A. D., & Popper, A. N. (2017). A sound approach to assessing the impact of underwater noise on marine fishes and invertebrates. *ICES Journal of Marine Science*, 74(3), 635-651. <https://doi.org/10.1093/icesjms/fsw205>
- Heinselman, M. L. (1973). Fire in the virgin forests of the Boundary Waters Canoe Area, Minnesota. *Quaternary Research*, 3, 329-382. [https://doi.org/10.1016/0033-5894\(73\)90003-3](https://doi.org/10.1016/0033-5894(73)90003-3)
- Heupel, M. R., Simpfendorfer, C. A., & Hueter, R. E. (2003). Running before the storm: Blacktip sharks respond to falling barometric pressure associated with Tropical Storm Gabrielle. *Journal of Fish Biology*, 63, 1357-1363. <https://doi.org/10.1046/j.1095-8649.2003.00250.x>, available online at <http://www.blackwell-synergy.com>
- Higgs, D. M., Souza, M. J., Wilkins, H. R., Presson, J. C., & Popper, A. N. (2001). Age- and size-related changes in the inner ear and hearing ability of the adult zebrafish (*Danio rerio*). *Journal of the Association for Research in Otolaryngology*, 3, 174-184. <https://doi.org/10.1007/s101620020035>
- Hildebrand, J. A. (2009). Anthropogenic and natural sources of ambient noise in the ocean. *Marine Ecology Progress Series*, 395, 5-20. <https://doi.org/10.3354/meps08353>
- Holland, G., & Bruyère, C. L. (2014). Recent intense hurricane response to global climate change. *Climate Dynamics*, 42, 617-627. <https://doi.org/10.1007/200382-013-1713-0>
- Holling, C. S. (1973). Resilience and stability of ecological systems. *Annual Review of Ecology and Systematics*, 4, 1-23.
- Holt, D. E., & Johnston, C. E. (2011). Hearing sensitivity in two black bass species using the auditory brainstem response approach. *Environmental Biology of Fishes*, 91, 121-126. <https://doi.org/10.1007/s10641-010-9756-0>
- Horodysky, A. Z., Brill, R. W., Fine, M. L., Musick, J. A., & Latour, R. J. (2008). Acoustic pressure and particle motion thresholds in six sciaenid fishes. *Journal of Experimental Biology*, 211, 1504-1511. <https://doi.org/10.1242/jeb.016196>

- Hothorn, T., Bretz, F., and Westfall, P. (2008). Simultaneous Inference in General Parametric Models. *Biometrical Journal* 50(3), 346-363.
- Houghton, R. W., Schlitz, R., Beardsley, R. C., Butman, B., & Chamberlin, J. L. (1982). The Middle Atlantic Bight cold pool: Evolution of the temperature structure during summer 1979. *Journal of Physical Oceanography*, 12, 1019-1029.
- Huang, P., Sanford, T. B., & Imberger, J. (2009). Heat and turbulent kinetic energy budgets for surface layer cooling induced by the passage of Hurricane Frances (2004). *Journal of Geophysical Research*, 114(C12023), 1-14. <https://doi.org/10.1029/2009JC005603>
- Hyndman R. J., Khandakar Y. (2008). "Automatic time series forecasting: the forecast package for R." *Journal of Statistical Software*, 26(3), 1-22. <http://www.jstatsoft.org/article/view/v027i03>.
- Hyndman R., Athanasopoulos G., Bergmeir C., Caceres G., Chhay L., O'Hara-Wild M., Petropoulos F., Razbash S., Wang E., Yasmeeen F. (2019). *forecast: Forecasting functions for time series and linear models*. R package version 8.9, <http://pkg.robjhyndman.com/forecast>.
- Jackson, J. B. C., & Hughes, T. P. (1985). Adaptive strategies of coral reef invertebrates: Coral reef environments that are regularly disturbed by storms and by predation often favor the very organisms most susceptible to damage by these processes. *American Scientist*, 73(3), 265-274.
- Jury, S. H., Howell, W. H., & Watson, W. H., III. (1995). Lobster movement in response to a hurricane. *Marine Ecology Progress Series*, 119, 305-310.
- Kastelein, R. A., van der Heul, S., Verboom, W. C., Jennings, N., van der Veen, J., & de Haan, D. (2008). Startle response of captive North Sea fish species to underwater tones between 0.1 and 64 kHz. *Marine Environmental Research*, 65, 369-377. <https://doi.org/10.1016/j.marenvres.2008.01.001>
- Kaufman, L. S. (1983). Effects of Hurricane Allen on reef fish assemblages near Discovery Bay, Jamaica. *Coral Reefs*, (2), 43-47.
- Kelly, J. C., & Nelson, D. R. (1975). Hearing thresholds of the horn shark, *Heterodontus francisci*. *The Journal of the Acoustical Society of America*, 58(4), 905-909. <https://doi.org/10.1121/1.380742>
- Kennelly, S. J. (1987). Physical disturbances in an Australian kelp community. I. Temporal effects. *Marine Ecology Progress Series*, 40, 145-153.

- Kenyon, T. N., Ladich, F., & Yan, H. Y. (1998). A comparative study of hearing ability in fishes: The auditory brainstem response approach. *Journal of Comparative Physiology A*, *182*, 307-318.
- Knutson, T. R., Tuleya, R. E., & Kurihara, Y. (1998). Simulated increase of hurricane intensities in a CO<sub>2</sub>-warmed climate. *Science*, *279*, 1018-1020.
- Kojima, T., Ito, H., Komada, T., Taniuchi, T., & Akamatsu, T. (2005). Measurement of auditory sensitivity in common carp *Cyprinus carpio* by the auditory brainstem response technique and cardiac conditioning method. *Fisheries Science*, *71*, 95-100.
- Kojima, T., Suga, T., Kusano, A., Shimizu, S., Matsumoto, H., Aoki, S., . . . Taniuchi, T. (2010). Acoustic pressure sensitivities and effects of particle motion in red sea bream *Pagrus major*. *Fisheries Science*, *76*, 13-20. <https://doi.org/10.1007/s12562-009-0194-x>
- Kritzler, H., & Wood, L. (1961). Provisional audiogram for the shark, *Carcharhinus leucas*. *Science*, *133*(3463), 1480-1482.
- Kunc, H. P., McLaughlin, K. E., & Schmidt, R. (2016). Aquatic noise pollution: Implications for individuals, populations, and ecosystems. *Proceedings of the Royal Society B*, *283*. <https://doi.org/10.1098/rspb.2016.0839>
- Ladich, F., & Yan, H. Y. (1998). Correlation between auditory sensitivity and vocalization in anabantoid fishes. *Journal of Comparative Physiology A*, *182*, 737-746.
- Ladich, F. (1999). Did auditory sensitivity and vocalization evolve independently in otophysan fishes. *Brain, Behavior, and Evolution*, *53*, 288-304.
- Ladich, F., & Popper, A. N. (2004). Parallel evolution in fish hearing organs. *Evolution of the Vertebrate Auditory System*, *22*, 95-127.
- Lassig, B. R. (1983). The effects of a cyclonic storm on coral reef fish assemblages. *Environmental Biology of Fishes*, *9*(1), 55-63.
- Leatherland, J. F. (1982). Environmental physiology of the teleostean thyroid gland: A review. *Environmental Biology of Fishes*, *7*(1), 83-110.
- Lechner, W., & Ladich, F. (2008). Size matters: Diversity in swimbladders and Weberian ossicles affects hearing in catfishes. *Journal of Experimental Biology*, *211*, 1681-1689. <https://doi.org/10.1242/jeb.016436>

- Lee, S. B., M. Li, and F. Zhang (2017), Impact of sea level rise on tidal range in Chesapeake and Delaware Bays, *J. Geophys. Res. Oceans*, 122, 3917–3938, doi:10.1002/2016JC012597.
- Lentz, S., Shearman, K., Anderson, S., Plueddemann, A., & Edson, J. (2003). Evolution of stratification over the New England shelf during the coastal mixing and optics study, August 1996-June 1997. *Journal of Geophysical Research*, 108(C1), 1-14. <https://doi.org/10.1029/2001JC001121>
- Lentz, S. J. (2007). Seasonal variations in the circulation over the Middle Atlantic Bight Continental Shelf. *Journal of Physical Oceanography*, 38, 1486-1500.
- Lentz, S. J. (2017). Seasonal warming of the Middle Atlantic Bight Cold Pool. *Journal of Geophysical Research: Oceans*, 122, 941-954. <https://doi.org/10.1002/2016JC012201>
- Li, Y., & Xue, H. (2002). Air-sea interactions during the passage of a winter storm over the Gulf Stream: A three-dimensional coupled atmosphere-ocean model study. *Journal of Geophysical Research*, 107(C11), 1-13. <https://doi.org/10.1029/2001JC001161>
- Lin, N., Emanuel, K., Oppenheimer, M., & Vanmarcke, E. (2012). Physically based assessment of hurricane surge threat under climate change. *Nature Climate Change*, 2, 462-467. <https://doi.org/10.1038/NCLIMATE1389>
- Loftus, A. J., & Stone, R. B. (2007, June). *Artificial reef management plan for Maryland* (Maryland Environmental Service Contract No. 06-07-58).
- López de Lacalle, J. (2019). tsoutliers: Detection of outliers in time series. R package version 0.6-8. <https://CRAN.R-project.org/packages=tsoutliers>
- Lovell, J. M., Findlay, M. M., Moate, R. M., Nedwell, J. R., & Pegg, M. A. (2005). The inner ear morphology and hearing abilities of the Paddlefish (*Polyodon spathula*) and the Lake Sturgeon (*Acipenser fulvenscens*). *Comparative Biochemistry and Physiology*, 142, 286-296.
- Lovell, J. M., Findlay, M. M., Nedwell, J. R., & Pegg, M. A. (2006). The hearing abilities of the silver carp (*Hypophthalmichthys molitrix*) and bighead carp (*Aristichthys nobilis*). *Comparative Biochemistry and Physiology*, 143, 286-291. <https://doi.org/10.1016/j.cbpa.2005.11.015>
- Lugli, M., Yan, H. Y., & Fine, M. L. (2003). Acoustic communication in two freshwater gobies: The relationship between ambient noise, hearing thresholds and sound spectrum. *Journal of Comparative Physiology A*, 189, 309-320. <https://doi.org/10.1007/s00359-003-0404-4>

- Mann, D. A., Hastings, M. C., & Popper, A. N. (1998). Detection of ultrasonic tones and simulated dolphin echolocation clicks by a teleost fish, the American shad (*Alosa sapidissima*). *The Journal of the Acoustical Society of America*, *104*(1), 562-568. <https://doi.org/10.1121/1.423255>
- Mann, D., Higgs, D., Tavalga, W., & Souza, M. J. (2001). Ultrasound detection by clupeiform fishes. *The Journal of the Acoustical Society of America*, *109*(6), 3048-3054.
- Mann, D. A., Cott, P. A., Hanna, B. W., & Popper, A. N. (2007). Hearing in eight species of northern Canadian freshwater fishes. *Journal of Fish Biology*, *70*, 109-120. <https://doi.org/10.1111/j.1095-8649.2006.01279.x>
- Maruska, K. P., Boyle, K. S., Dewan, L. R., & Tricas, T. C. (2007). Sound production and spectral hearing sensitivity in the Hawaiian sergeant damselfish, *Abudefduf abdominalis*. *Journal of Experimental Biology*, *210*, 3990-4004. <https://doi.org/10.1242/jeb.004390>
- Maryland Department of Natural Resources. (n.d.). *MARI/Ocean City Reef Foundation Reefs*. Retrieved from [https://dnr.maryland.gov/fisheries/Documents/MARIOC04209postersize\\_with\\_coordinates\\_web.pdf](https://dnr.maryland.gov/fisheries/Documents/MARIOC04209postersize_with_coordinates_web.pdf)
- McCauley, R. D., Fewtrell, J., Duncan, A. J., Jenner, C., Jenner, M.-N., Penrose, J. D., & 4 others. (2000). Marine seismic surveys: A study of environmental implications. *APPEA Journal*, 692-708.
- McCauley, R. D., Fewtrell, J., & Popper, A. N. (2003). High intensity anthropogenic sound damages fish ears. *The Journal of the Acoustical Society of America*, *113*(1), 1-5. <https://doi.org/10.1121/1.1527962>
- McCormick, C. A., & Popper, A. N. (1984). Auditory sensitivity and psychophysical tuning curves in the elephant nose fish, *Gnathonemus petersii*. *Journal of Comparative Physiology A*, *155*, 753-761.
- McDonald, M. A., Hildebrand, J. A., & Wiggins, S. M. (2006). Increases in deep ocean ambient noise in the Northeast Pacific west of San Nicolas Island, California. *The Journal of the Acoustical Society of America*, *120*(2), 711-718. <https://doi.org/10.1121/1.2216565>
- McPhaden, M. J., Foltz, G. R., Lee, T., Murty, and 5 others (2009). Ocean-atmosphere interactions during Cyclone Nargis. *EOS Transactions American Geophysical Union*, *90*(7), 53-60.

- Mercer, L. P., & Moran, D. (1989). *Species profile: Life histories and environmental requirements of coastal fishes and invertebrates (South Atlantic)* (Biological Report No. 82 11.99).
- Michener, W. K., Blood, E. R., Bildstein, K. L., Brinson, M. M., & Gardner, L. R. (1997). Climate change, hurricanes and tropical storms, and rising sea level in coastal wetlands. *Ecological Applications*, 7(3), 770-801.
- Moser, J., & Shepherd, G. R. (2009). Seasonal distribution and movement of black sea bass (*Centropristis striata*) in the Northwest Atlantic as determined from a mark-recapture experiment. *Journal of Northwest Atlantic Fishery Science*, 40, 17-28.
- Mumby, P. J. (1999). Bleaching and hurricane disturbances to populations of coral recruits in Belize. *Marine Ecology Progress Series*, 190, 27-35.
- Musick, J. A., & Mercer, L. P. (1977). Seasonal distribution of black sea bass (*Centropristis striata*), in the Middle Atlantic Bight with comments on the ecology and fisheries of the species. *Transactions of the American Fisheries Society*, 106(1), 12-25. [https://doi.org/10.1577/1548-8659\(1977\)106<12:SDOBSB>2.0.CO;2](https://doi.org/10.1577/1548-8659(1977)106<12:SDOBSB>2.0.CO;2)
- Myrberg, A. A., & Spires, J. Y. (1980). Hearing in damselfishes: An analysis of signal detection among closely related species. *Journal of Comparative Physiology A*, 140, 135-144.
- National Research Council. (2003). *Ocean noise and marine mammals*. Washington D.C., USA: The National Academies Press. <https://doi.org/10.17226/10564>.
- Nedwell, J. R., Edwards, B., Turnpenny, A. W. H., & Gorden, J. (2004, September). *Fish and marine mammal audiograms: A summary of available information* (Subacoustech Report No. 534R0214).
- Nelson, D. R. (1967). Hearing thresholds, frequency discrimination, and acoustic orientation in the lemon shark, *Negaprion brevirostris* (poey). *Bulletin of Marine Science*, 17(3), 741-768.
- Nowacek, D. P., Clark, C. W., Mann, D., Miller, P. J. O., Rosenbaum, H. C., Golden, J. S., . . . Southall, B. L. (2015). Marine seismic surveys and ocean noise: Time for coordinated and prudent planning. *Frontiers in Ecology and the Environment*, 13(7), 378-386. <https://doi.org/10.1890/130286>
- O'Brien, M. H. P. (2019). TelemetryR. R package version 0.9.4. <https://rdrr.io/github/mhpob/TelemetryR/>

- Offut, G. C. (1974). Structures for the detection of acoustic stimuli in the Atlantic codfish, *Gadus morhua*. *The Journal of the Acoustical Society of America*, 56(2), 665-671.
- Öhman, M. C., Sigray, P., & Westerberg, H. (2007). Offshore windmills and the effects of electromagnetic fields on fish. *Ambio*, 36(8), 630-633.
- Onuf, C. P., & Quammen, M. L. (1983). Fishes in a California coastal lagoon: Effects of major storms on distribution and abundance. *Marine Ecology Progress Series*, 12, 1-14.
- Oxman, D. S., Barnett-Johnson, R., Smith, M. E., Coffin, A., Miller, D. L., Josephson, R., & Popper, A. N. (2007). The effect of vaterite deposition on sound reception, otolith morphology, and inner ear sensory epithelia in hatchery-reared Chinook salmon (*Oncorhynchus tshawytscha*). *Canadian Journal of Fisheries and Aquatic Science*, 64, 1469-1478.  
<https://doi.org/10.1139/F07-106>
- Parmentier, E., Colleye, O., & Mann, D. (2009). Hearing ability in three clownfish species. *Journal of Experimental Biology*, 212, 2023-2026.  
<https://doi.org/10.1242/jeb.030270>
- Parmentier, E., Mann, K., & Mann, D. (2011). Hearing and morphological specializations of the mojarra (*Eucinostomus argenteus*). *Journal of Experimental Biology*, 214, 2697-2701. <https://doi.org/10.1242/jeb.058750>
- Petraltis, P. S., Latham, R. E., & Niesenbaum, R. A. (1989). The maintenance of species diversity by disturbance. *The Quarterly Review of Biology*, 64(4), 393-418.
- Petterson, J. S., Stanley, L. D., Glazier, E., & Philipp, J. (2006). A preliminary assessment of social and economic impacts associated with Hurricane Katrina. *American Anthropologist*, 108(4), 643-670.
- Pinheiro J, Bates D, DebRoy S, Sarkar D, R Core Team (2018). *nlme: Linear and Nonlinear Mixed Effects Models*. R package version 3.1-137, <URL: <https://CRAN.R-project.org/package=nlme>>.
- Poggendorf, D. (1952). Die absoluten hörschwellen des zwerglhwelses (*Amiurus nebulosus*) und beiträge zur physik des Weberschen apparates der Ostariophysen. *Zeitschrift für vergleichende Physiologie*, 34, 222-257.
- Popper, A. N. (1970). Auditory capacities of the Mexican blind cave fish (*Astyanax jordani*) and its eyed ancestor (*Astyanax mexicanus*). *Animal Behavior*, 18, 552-562.

- Popper, A. N., & Coombs, S. (1982). The morphology and evolution of the ear in Actinopterygian fishes. *American Zoologist*, 22, 311-328.
- Popper, A. N., & Fay, R. R. (1993). Sound detection and processing by fish: Critical review and major research questions. *Brain, Behavior and Evolution*, 41, 14-38.
- Popper, A. N., Smith, M. E., Cott, P. A., Hanna, B. W., MacGillivray, A. O., Austin, M. E., & Mann, D. A. (2005). Effects of exposure to seismic airgun use on hearing of three fish species. *The Journal of the Acoustical Society of America*, 117(6), 3958-3971. <https://doi.org/10.1121/1.1904386>
- Popper, A. N., & Hastings, M. C. (2009). The effects of human-generated sound on fish. *Integrative Zoology*, 4, 43-52. <https://doi.org/10.1111/j.1749-4877.2008.00134.x>
- Popper, A. N., & Fay, R. R. (2011). Rethinking sound detection by fishes. *Hearing Research*, 273, 25-36. <https://doi.org/10.1016/j.heares.2009.12.023>
- Popper, A. N., Hawkins, A. D., Fay, R. R., Mann, D. A., Bartol, S., Carlson, T. J., . . . Tavalga, W. N. (2014). *Sound exposure guidelines for fishes and sea turtles: A technical report prepared by ANSI-Accredited Standards Committee S3/SC1 and registered with ANSI* (Technical Report No. 2196-1212). Acoustical Society of America.
- Popper, A. N., & Hawkins, A. D. (2018). The importance of particle motion to fishes and invertebrates. *The Journal of the Acoustical Society of America*, 143(1), 470-488. <https://doi.org/10.1121/1.5021594>
- Popper, A. N., & Hawkins, A. D. (2019). An overview of fish bioacoustics and the impacts of anthropogenic sounds on fishes. *Journal of Fish Biology*, 94, 692-713. <https://doi.org/10.1111/jfb.13948>
- Popular wreck dives along our Delaware and Maryland coast. (n.d.). Retrieved from Aqua Ventures Online website: <http://www.aquaventuresonline.com/wrecks.html>
- Pörtner, H. O. (2001). Climate change and temperature-dependent biogeography: Oxygen limitation of thermal tolerance in animals. *Naturwissenschaften*, 88, 137-146. <https://doi.org/10.1007/s001140100216>
- Pörtner, H. O. (2002). Climate variations and the physiological basis of temperature dependent biogeography: Systemic to molecular hierarchy of thermal tolerance in animals. *Comparative Biochemistry and Physiology Part A*, 132, 739-761.



- Ramcharitar, J., & Popper, A. N. (2004). Masked auditory thresholds in sciaenid fishes: A comparative study. *The Journal of the Acoustical Society of America*, *116*(3), 1687-1691. <https://doi.org/10.1121/1.1771614>
- Ramcharitar, J. U., Higgs, D. M., & Popper, A. N. (2006). Audition in sciaenid fishes with different swim bladder-inner ear configurations. *The Journal of the Acoustical Society of America*, *119*(1), 439-443. <https://doi.org/10.1121/1.2139068>
- Rasmussen, L. L., Gawarkiewicz, G., Owens, W. B., & Lozier, M. S. (2005). Slope water, Gulf Stream, and seasonal influences on southern Mid-Atlantic Bight circulation during the fall-winter transition. *Journal of Geophysical Research*, *110*, 1-16. <https://doi.org/10.1029/2004JC002311>
- Rigby R. A., & Stasinopoulos D. M. (2005). Generalized additive models for location, scale and shape, (with discussion). *Applied Statistics*, *54*, 507-554.
- Robins, C. R. (1957). Effects of storms on the shallow-water fish fauna of southern Florida with new records of fishes from Florida. *Bulletin of Marine Science in the Gulf and Caribbean*, *7*(3), 266-275.
- Rood, S. B., Goater, L. A., Mahoney, J. M., Pearce, C. M., & Smith, D. G. (2007). Floods, fire, and ice: Disturbance ecology of riparian cottonwoods. *Canadian Journal of Botany*, *85*, 1019-1032. <https://doi.org/10.1139/B07-073>
- Rosen, D. E., & Greenwood, P. H. (1970). Origin of the Weberian apparatus and the relationship of the Ostariophysan and Gonorynchiform fishes. *American Museum Novitates*, (2428).
- Russell V. L. (2016). Least-Squares Means: The R Package lsmeans. *Journal of Statistical Software*, *69*(1), 1-33. doi:10.18637/jss.v069.i01
- Sackett, D. K., Able, K. W., & Grothues, T. M. (2007). Dynamics of summer flounder, *Parlichthys dentatus*, seasonal migrations based on ultrasonic telemetry. *Estuarine Coastal and Shelf Science*, *74*, 119-130. <https://doi.org/10.1016/j.ecss.2007.03.027>
- Sarà, G., Dean, J. M., Amato, D. D., Buscaino, and 7 others (2007). Effect of boat noise on the behavior of bluefin tuna *Thunnus thynnus* in the Mediterranean Sea. *Marine Ecology Progress Series*, *331*, 243-253.
- Scholz, K., & Ladich, F. (2006). Sound production, hearing and possible interception under ambient noise conditions in the topmouth minnow *Pseudorasbora parva*. *Journal of Fish Biology*, *69*, 892-906. <https://doi.org/10.1111/j.1095-8649.2006.01168.x>

- Schulz-Mirbach, T., Metscher, B., & Ladich, F. (2012). Relationship between swim bladder morphology and hearing abilities- A case study on Asian and African cichlids. *PLOS One*, 7(8).  
<https://doi.org/10.1371/journal.pone.0042292>
- Secor, D. H. (2015). *Migration ecology of marine fishes*. Baltimore, MD: John Hopkins University Press.
- Secor, D. H., Zhang, F., O'Brien, M. H.P., & Li, M. (2019). Ocean destratification and fish evacuation caused by a Mid-Atlantic tropical storm. *ICES Journal of Marine Science*, 1-12. <https://doi.org/10.1093/icesjms/fsx241>
- Sedberry, G. R., & Van Dolah, R. F. (1984). Demersal fish assemblages associated with hard bottom habitat in the South Atlantic Bight of the USA. *Environmental Biology of Fishes*, 11(4), 241-258.
- Shepherd, G. R., & Terceiro, M. (1994, August). *The summer flounder, scup, and black sea bass fishery of the Middle Atlantic Bight and Southern New England waters* (NOAA Technical Report NMFS No. 122). Seattle, WA: US Department of Commerce.
- Sisneros, J. S., Popper, A. N., Hawkins, A. D., & Fay, R. (2015). Audio evoked potential audiograms compared with behavioral audiograms in aquatic animals. *Advances in Experimental Medicine and Biology*, 875, 1049-1056.
- Skalski, J. R., Pearson, W. H., & Malm, C. I. (1992). Effects of sounds from a geophysical survey device on catch-per-unit-effort in a hook-and-line fishery for rockfish (*Sebastes spp.*). *Canadian Journal of Fisheries and Aquatic Sciences*, 49, 1357-1365.
- Slabbekoorn, H., Bouton, N., van Opzeeland, I., Coers, A., ten Cate, C., & Popper, A. N. (2010). A noisy spring: The impact of globally rising underwater sound levels on fish. *Trends in Ecology and Evolution*, 25(7), 419-427.  
<https://doi.org/10.1016/j.tree.2010.04.005>
- Solis, D., Perruso, L., del Corral, J., Stoffle, B., & Letson, D. (2013). Measuring the initial economic effects of hurricanes on commercial fish production: the US Gulf of Mexico grouper (Serranidae) fishery. *Natural Hazards*, 66, 271-289. <https://doi.org/10.1007/s11069-012-0476-y>
- Sousa, W. P. (1984). The role of disturbance in natural communities. *Annual Review of Ecology, Evolution, and Systematics*, 15, 353-391.

- Steimle, F. W., & Figley, W. (1996). The importance of artificial reef epifauna to black sea bass diets in the Middle Atlantic Bight. *North American Journal of Fisheries Management*, 16, 433-439.
- Steimle, F. W., & Zetlin, C. (2000). Reef habitats in the Middle Atlantic Bight: Abundance, distribution, associated biological communities, and fishery resource use. *Marine Fisheries Review*, 6(2), 24-42.
- Stenberg, C., Støttrup, J. G., van Deurs, M., Berg, and 5 others (2015). Long-term effects of an offshore wind farm in the North Sea on fish communities. *Marine Ecology Progress Series*, 528, 257-265. <https://doi.org/10.3354/meps11261>
- Strobbe, F., McPeck, M. A., De Block, M., & Stoks, R. (2011). Fish predation selects for reduced foraging activity. *Behavioral Ecology and Sociobiology*, 65, 241-247. <https://doi.org/10.1007/s00265-010-1032-y>
- Sturrock, A. M., Trueman, C. N., Darnaude, A. M., & Hunter, E. (2012). Can otolith elemental chemistry retrospectively track migrations in fully marine fishes? *Journal of Fish Biology*, 81, 766-795. <https://doi.org/10.1111/j.1095-8649.2012.03372.x>
- Sutton, G. H., & Barstow, N. (1990). Ocean-bottom ultralow frequency (ULF) seismo-acoustic ambient noise: 0.002 to 0.4 Hz. *The Journal of the Acoustical Society of America*, 87, 2005-2012. <https://doi.org/10.1121/1.399328>
- Syms, C., & Jones, G. P. (1999). Scale of disturbance and the structure of a temperate fish guild. *Ecology*, 80(3), 921-940.
- Tavolga, W. N., & Wodinsky, J. (1963). Auditory capacities in fishes: Pure tone thresholds in nine species of marine teleosts. *Bulletin of the American Museum of Natural History*, 126, 172-240.
- Thomsen, F., Lüdemann, K., Kafemann, R., & Piper, W. (2006, July). *Effects of offshore wind farm noise on marine mammals and fish*. Hamburg, Germany: Cowrie.
- Underwood, A. J. (1999). Physical disturbances and their direct effect on an indirect effect: Responses of an intertidal assemblage to a severe storm. *Journal of Experimental Marine Biology and Ecology*, 232, 125-140.
- Vabø, R., Olsen, K., & Huse, I. (2002). The effect of vessel avoidance of wintering Norwegian spring spawning herring. *Fisheries Research*, 58, 59-77.

- Vasconcelos, R. O., Amorim, M. C. P., & Ladich, F. (2007). Effects of ship noise on the detectability of communication signals in the Lusitanian toadfish. *Journal of Experimental Biology*, *210*, 2104-2112.  
<https://doi.org/10.1242/jeb.004317>
- Vermaire, J. C., Pisaric, M. F. J., Thienpont, J. R., Mustaphi, C. J. C., Kokelj, S. V., & Smol, J. P. (2013). Arctic climate warming and sea ice declines lead to increased storm surge activity. *Geophysical Research Letters*, *40*, 1386-1390.  
<https://doi.org/10.1002/grl.50191,2013>
- Wahlberg, M., & Westerberg, H. (2005). Hearing in fish and their reaction to sounds from offshore wind farms. *Marine Ecology Progress Series*, *288*, 295-309.
- Waide, R. B. (1991). Summary of the response of animal populations to hurricanes in the Caribbean. *Biotropica*, *23*(4), 508-512.
- Walsh, W. J. (1983). Stability of a coral reef fish community following a catastrophic storm. *Coral Reefs*, *2*, 49-63.
- Wardle, C. S., Carter, T. J., Urquhart, G. G., Johnstone, A. D. F., Ziolkowski, A. M., Hampson, G., & Mackie, D. (2001). Effects of seismic airguns on marine fish. *Continental Shelf Research*, *21*, 1005-1027.
- Wauer, R. H., & Wunderle, J. M., Jr. (1992). The effect of Hurricane Hugo on bird populations on St. Croix, U.S. Virgin Islands. *The Wilson Bulletin*, *104*(4), 656-673.
- Weilgart, L. (2018, May). *The impact of ocean noise pollution on fish and invertebrates*. OceanCare.
- Wenz, G. M. (1962). Acoustic ambient noise in the ocean: Spectra and sources. *The Journal of the Acoustical Society of America*, *34*(12), 1936-1956.
- Werner, E. E., & Peacor, S. D. (2003). A review of trait-mediated indirect interactions in ecological communities. *Ecology*, *84*(5), 1083-1100.
- White, P. S., & Jentsch, A. (2001). The search for generality in studies of disturbance and ecosystem dynamics. *Progress in Botany*, *62*, 399-450.
- Williams, A. H. (1984). The effects of Hurricane Allen on Back Reef populations of Discovery Bay, Jamaica. *Journal of Experimental Marine Biology and Ecology*, *75*, 233-243.
- Wilson, J. D., & Makris, N. C. (2006). Ocean acoustic hurricane classification. *The Journal of the Acoustical Society of America*, *119*(1), 168-181.  
<https://doi.org/10.1121/1.2130961>

- Wilson, J. D., & Makris, N. C. (2008). Quantifying hurricane destructive power, wind speed, and air-sea material exchange with natural undersea sound. *Geophysical Research Letters*, 35, 1-5. <https://doi.org/10.1029/2008GL033200>
- Witman, J. D. (1987). Subtidal coexistence: Storms, grazing, mutualism, and the zonation of kelps and mussels. *Ecological Monographs*, 57(2), 167-187.
- Wright, K. J., Higgs, D. M., Cato, D. H., & Leis, J. M. (2010). Auditory sensitivity in settlement-stage larvae of coral reef fishes. *Coral Reefs*, 29, 235-243. <https://doi.org/10.1007/s00338-009-0572-y>
- Wysocki, L. E., & Ladich, F. (2005). Hearing in fishes under noise conditions. *Journal of the Association for Research in Otolaryngology*, 6, 28-36. <https://doi.org/10.1007/s10162-004-4043-4>
- Wysocki, L. E., Codarin, A., Ladich, F., & Picciulin, M. (2009). Sound pressure and particle acceleration audiograms in three marine fish species from the Adriatic Sea. *The Journal of the Acoustical Society of America*, 126(4), 2100-2107. <https://doi.org/10.1121/1.3203562>
- Yan, H. Y., & Curtsinger, W. S. (2000). The otic gasbladder as an ancillary auditory structure in a mormyrid fish. *Journal of Comparative Physiology A*, 186, 595-602. <https://doi.org/10.1007/s003590000114>
- Yan, H. Y., Fine, M. L., Horn, N. S., & Colón, W. E. (2000). Variability in the role of the gasbladder in fish audition. *Journal of Comparative Physiology A*, 186, 435-445. <https://doi.org/10.1007/s003590050443>
- Zhang, F., Li, M., Ross, A. C., Lee, S. B., & Zhang, D.-L. (2017). Sensitivity analysis of Hurricane Arthur (2014) storm surge forecasts to WRF physics parameterizations and model configurations. *Weather and Forecasting*, 32, 1745-1764. <https://doi.org/10.1175/WAF-D-16-0218.1>